



HAL
open science

Global connections between aeolian dust, climate and ocean biogeochemistry at the present day and at the last glacial maximum

B A Maher, J M Prospero, D Mackie, D. Gaiero, P P Hesse, Yves Balkanski

► To cite this version:

B A Maher, J M Prospero, D Mackie, D. Gaiero, P P Hesse, et al.. Global connections between aeolian dust, climate and ocean biogeochemistry at the present day and at the last glacial maximum. Earth-Science Reviews, 2009, 99 (1-2), pp.61-97. 10.1016/j.earscirev.2009.12.001 . hal-02870475

HAL Id: hal-02870475

<https://hal.science/hal-02870475>

Submitted on 17 Jun 2020

HAL is a multi-disciplinary open access archive for the deposit and dissemination of scientific research documents, whether they are published or not. The documents may come from teaching and research institutions in France or abroad, or from public or private research centers.

L'archive ouverte pluridisciplinaire **HAL**, est destinée au dépôt et à la diffusion de documents scientifiques de niveau recherche, publiés ou non, émanant des établissements d'enseignement et de recherche français ou étrangers, des laboratoires publics ou privés.

1 **Global connections between aeolian dust, climate and ocean biogeochemistry at the present**
2 **day and at the last glacial maximum.**

3

4 B. A. Maher^{a*}, J.M. Prospero^b, D. Mackie^c, D. Gaiero^d, P.P. Hesse^e, Y. Balkanski^f

5

6 ^a Centre for Environmental Magnetism & Palaeomagnetism, Lancaster Environment Centre,
7 University of Lancaster, LA1 4YQ, UK

8

9 ^b Marine and Atmospheric Chemistry & The Cooperative Institute for Marine and Atmospheric
10 Studies, Rosenstiel School of Marine and Atmospheric Science, University of Miami, 4600
11 Rickenbacker Causeway, Miami FL 33149, USA

12

13 ^c Department of Chemistry, University of Otago, Dunedin, New Zealand

14

15 ^d Centro de Investigaciones Geoquímicas y Procesos de la Superficie, Facultad de Ciencias
16 Exactas Físicas y Naturales, Universidad Nacional de Córdoba, Avda. Vélez Sársfield 1611,
17 X5016CGA – Córdoba, Argentina

18

19 ^e Department of Environment and Geography, Macquarie University, NSW 2109, Sydney,
20 Australia

21

22 ^f Laboratoire des Sciences du Climat et de l'Environnement, l'Orme des Merisiers, 91191 Gif
23 sur Yvette Cedex, France.

24

25

26 *Corresponding author b.maher@lancs.ac.uk, tel. +44 1524 510268, fax +44 1524 510269

27

28

29

30 **Abstract**

31 Palaeo-dust records in sediments and ice cores show that wind-borne mineral aerosol ('dust') is
32 strongly linked with climate state. During glacial climate stages, for example, the world was
33 much dustier, with dust fluxes two to five times greater than in interglacial stages. However, the
34 influence of dust on climate remains a poorly quantified and actively changing element of the
35 Earth's climate system. Dust can influence climate directly, by the scattering and absorption of
36 solar and terrestrial radiation, and indirectly, by modifying cloud properties. Dust transported to
37 the oceans can also affect climate via ocean fertilization in those regions of the world's oceans
38 where macronutrients like nitrate are abundant but primary production and nitrogen fixation are
39 limited by iron scarcity. Dust containing iron, as fine-grained iron oxides/oxyhydroxides and/or
40 within clay minerals, and other essential micronutrients (e.g. silica) may modulate the uptake of
41 carbon in marine ecosystems and, in turn, the atmospheric concentration of CO₂. Here, in order
42 to critically examine past fluxes and possible climate impacts of dust in general and iron-bearing
43 dust in particular, we consider present day sources and properties of dust, synthesise available
44 records of dust deposition at the last glacial maximum (LGM); evaluate the evidence for changes
45 in ocean palaeo-productivity associated with, and possibly caused by, changes in aeolian flux to
46 the oceans at the LGM; and consider the radiative forcing effects of increased LGM dust
47 loadings.

48

49 **Keywords:** aerosols, dust, climate change, palaeoclimatology, radiative forcing, iron
50 fertilisation.

51 1. *Introduction*

52 Palaeo-dust records show that wind-borne mineral aerosol (here referred to as 'dust') is strongly
53 linked with climate state. Studies of dust in sediments and ice cores show that dust
54 concentrations and fluxes have changed greatly in association with changes in climate, for
55 example, in the transitions from glacial to interglacial regimes. During glacial climate stages, the
56 world was much dustier, with dust fluxes two to five times greater than in interglacial stages (e.g.
57 Kohfeld and Harrison, 2001). However, the influence of dust on climate remains a poorly
58 quantified and actively changing element of the Earth's climate system. We know from present-
59 day studies that dust can influence climate directly, by changing the radiative properties of the
60 atmosphere through the scattering and absorption of solar and terrestrial radiation, and indirectly,
61 by acting as ice nuclei (Sassen et al., 2003) and modifying cloud properties which, in turn, can
62 impact both the radiative balance of the Earth and the hydrological cycle (Arimoto, 2001). Dust
63 transported to the oceans can also affect climate indirectly, by supplying elements such as Fe, an
64 essential micronutrient in enzymes essential to photosynthesis (Martin et al., 1991);
65 phytoplankton in about 40% of the world ocean are Fe-limited (Moore et al., 2002). Thus, dust
66 delivery to the ocean can modulate the uptake of carbon in marine ecosystems and, in turn, the
67 atmospheric concentration of CO₂.

68

69 Dust not only can affect climate, but the generation and transport of dust is itself extremely
70 sensitive to climate. At the present day, the most obvious link is with aridity – the globally
71 dominant sources of dust are all located in arid or semi-arid regions. Global model estimates of
72 present-day dust mobilization rates are poorly constrained, reflecting the scarcity of temporal and
73 spatial data coverage, and range between ~ 1 and 3.5 Pg yr⁻¹ (e.g. Tanaka and Chiba, 2006;
74 Zender et al., 2003; Engelstaedter et al., 2006); optimized multi-model estimates yield a range of
75 1.5 to 2.6 Pg yr⁻¹ (Cakmur et al., 2006). Estimates of deposition to the oceans range from about
76 0.3 to 2 Pg yr⁻¹ (Zender et al., 2004; Mahowald et al., 2005). Human activities can have an
77 impact on dust mobilization but here too estimates are poorly constrained and range from 0 to 50
78 % of global dust emissions (e.g. Tegen et al., 2004; Mahowald et al., 2004; Yoshioka et al.,
79 2005).

80

81 As recorded in sediments and ice cores, there have been large and systematic variations in dust
82 loading in the past. The large changes in dust emissions and transport seen from the palaeo-dust
83 record may reflect a variety of processes: changes in sources and source conditions; changes in
84 vegetative cover; sub-aerial erosion of emergent continental shelves; deflation from periglacial
85 deposits; variations in wind speed and gustiness; changed wind patterns linking sources to
86 deposition areas; changes in deposition along the dust transport path. In order to interpret the
87 palaeo-record and to anticipate future changes in climate, we need to have a better understanding
88 of the factors that affect dust mobilization and its subsequent climatic impacts.

89

90 The complex linkages between climate and the dust generation-transport process on glacial-
91 interglacial time scales is illustrated in figure 1. There are many processes that can affect the dust
92 cycle either directly or indirectly under any specific climate scenario. The relative importance of
93 any specific process can change dramatically when shifting from one climate state to another –
94 e.g., during glacial stages, low sea levels expose coastal sediments and glacial action can produce
95 unvegetated, unconsolidated deposits all of which can become major sources of dust. A major
96 driver in the Earth's climate system is atmospheric CO₂. Figure 1 shows how dust transport to the
97 oceans could conceivably modify ocean productivity and atmospheric CO₂ and the consequent
98 impacts on other climate variables including the dust cycle. One major objective of
99 palaeoclimatology is to use the dust record in ice cores and sediments, coupled with our
100 knowledge of Earth surface processes today, to improve our understanding of these linkages in
101 the current climate state and to use this information to better interpret the Earth's past climate
102 history.

103

104

105 For the future, dust cycle models predict large changes in aeolian transport from the continents to
106 the oceans over coming centuries, in response to anthropogenic climate change (e.g. Mahowald
107 et al., 2006). In order to anticipate the effects of future changes in dust emissions, it is important
108 to identify the impacts of past and present-day dust flux changes in terms of feedbacks with
109 regard to radiative forcing of dust aerosols and any ocean fertilization and resultant productivity-
110 driven changes in atmospheric CO₂.

111

112 Here, in order to examine past fluxes and possible climate impacts of dust in general and iron-
113 bearing dust in particular, we synthesise available records of dust deposition at the last glacial
114 maximum (LGM); evaluate the evidence for changes in ocean palaeo-productivity associated
115 with, and possibly caused by, changes in aeolian flux to the oceans at the LGM; and consider the
116 radiative forcing effects of increased LGM dust loadings. We begin by presenting an overview of
117 global dust processes and the state of our knowledge about these processes.

118

119 Figure 1

120

121 2. Present-Day Global Dust Processes and Distributions

122 2.1 Dust source processes.

123 Dust mobilization is a highly complex process that is a function of many atmospheric, soil, and
124 terrain properties (Goudie, 2008). Consequently the detachment, entrainment and transport of
125 dust are highly variable both spatially and temporally. Dust generation is mostly associated with
126 strong and/or gusty winds with the emitted flux varying as the third or fourth power of wind
127 speed. The necessary wind fields to uplift dust can be generated by a wide range of local
128 meteorological conditions. In particular, surface heat fluxes that induce convective activity can
129 lead to dust generation (Engelstaedter and Washington, 2007), e.g., haboobs (Williams, 2008).

Deleted: ranging from synoptic-scale systems

Deleted: to smaller scale convective processes

130 Terrain features can strongly modulate emission rates (Washington et al., 2005; Koren et al.,
131 2007). Particle detachment is inhibited by any element which increases surface roughness, e.g.
132 vegetation, snow cover and surface armouring (by pebbles, stones or by salt crusts). Soil
133 moisture plays a critical role by affecting particle cohesion along with cementation by salt
134 content and soil structure. Dust emission thus tends to be favoured in arid or semi-arid areas,
135 with annual rainfall $< \sim 250$ mm p.a. (Prospero et al., 2002; Washington et al., 2003), little or no
136 vegetation cover and strong, long-fetch winds.

Deleted: ¶

137 Many of the most intense present-day dust sources are associated with deep alluvial deposits laid
138 down in the Pleistocene and Holocene (Prospero et al., 2002). Direct detachment and
139 entrainment by the wind of particles (especially fine particles, $< 20 \mu\text{m}$, PM_{20}) appears
140 subordinate to the effects of saltation (fig. 2); the impacts of sand-sized grains and/or aggregates
141 on their downward trajectory cause 'sandblasting' - the emission of finer dust grains from the
142 surface and/or from the original saltating aggregate (e.g. Gillette, 1978; Shao et al., 1993; Sow et

146 al., 2009). Thus the dust mobilization process and the resulting properties of the deflated dust can
147 be extremely sensitive to a wide range of environmental variables (including, for example, land
148 use change (Tegen et al., 1995)). The complexity of these processes potentially makes dust a
149 good proxy for climate variability but also makes the dust record difficult to interpret.

150

151 Figure 2.

152

153 2.2. Global dust sources and transport.

154 Much of our knowledge of the large-scale transports of dust is based on remotely sensed data,
155 primarily from satellites. While there is an extensive literature of the directly measured
156 concentrations and physical properties of dust, these are mostly too isolated in time and space to
157 provide a coherent picture of dust transports. However, such measurements, when coupled with
158 remote sensing data, can provide a compelling and informative picture of global dust transport.
159 Satellites have come to play a dominant role in aerosol research (Kaufman et al., 2002). At
160 present there is a large variety of sensors and platforms that provide information on aerosol
161 concentrations and on some aspects of their physical properties - e.g., size, radiative absorption,
162 polarization (Dubovik et al, 2008) - and also on the altitude distribution of these properties (e.g.,
163 Liu et al., 2008).

164

165 Satellite measurements of aerosol optical depth (AOD) with NOAA Advanced Very High
166 Resolution Radiometer (AVHRR) provide a global picture of aerosol transport over the oceans
167 (Fig. 3a; Husar et al., 1997). Over land, the most active dust source regions are detected with the
168 Total Ozone Mapping Spectrometer (TOMS) absorbing aerosol product (Fig. 3b; Prospero et al.,
169 2002). More recently, Shepanski et al. (2007) identified the regions where dust source is
170 activated using three different infrared channels of the Meteosat Second Generation (MSG)
171 instrument. This analysis is based on the frequency of dust generation but does not allow to
172 retrieve the magnitude of the flux resulting from the episodes. Analyzing dust emission flux or
173 evaluating dust mass requires a careful analysis of dust optical depth retrieved over deserts by
174 the MISR (Multiangle Imaging SpectroRadiometer) instrument, together with information on the
175 vertical distribution of dust retrieved from CALIPSO (Cloud-Aerosol Lidar and Infrared
176 Pathfinder Satellite Observation). Shepanski et al. (2009) were able to retrieve information on

Deleted: ¶

Formatted: Font: Times New Roman, 12 pt

Formatted: Font: Times New Roman

178 [the diurnal cycle of dust emissions over Western Africa. Sixty five percents of dust source](#)
179 [activation was found to occur in early morning from 0600–0900 UTC, well before the hours](#)
180 [when the surface latent heat fluxes become important.](#)

181

182 It is clear from Figure 3 that at the present day the northern hemisphere is far more ‘dusty’ than
183 the southern hemisphere. This statement is based largely on *in situ* aerosol measurements made
184 in different ocean regions (e.g. Duce et al., 1991; Prospero, 1996a; Prospero et al., 1989) and on
185 satellite products such as shown in Figure 3. Satellite AOD distributions (fig. 3a) show large
186 areas of high AOD over the oceans; the distribution of these plume-like features is clearly linked
187 to continental sources. The largest and most persistent plumes (fig. 3a) emanate from arid
188 regions in North Africa, the Middle East and Asia; the aerosols in these plume regions typically
189 contain high concentrations of dust (e.g., Husar et al., 1997; Duce et al., 1991; Prospero, 1996;
190 Prospero et al., 1989). These plumes can be directly linked to dust sources on the continents
191 using the TOMS satellite (fig. 3b), one of the few sensors that can effectively sense aerosols over
192 land (Herman et al., 1997).

193

194 It is notable that the major source regions (Fig. 3a and b; Table 1) are concentrated within a
195 broad ‘dust belt’ that extends from the west coast of North Africa eastward to the Pacific coast of
196 China. The timing of maximum dust emissions varies across this dust belt. In North Africa,
197 maximum dust transport occurs in boreal summer, with dust transported across the
198 Mediterranean to Europe and the Middle East (Moulin et al., 1998) and across the Atlantic to the
199 Caribbean (Prospero and Lamb, 2003), the southeastern United States (Perry et al., 1997;
200 Prospero, 1999), and the midlatitude western North Atlantic (Arimoto et al., 1995). There is also
201 considerable transport in the winter with dust carried into South America (Prospero, 1981). In the
202 Middle East, activity peaks in the late spring/summer and is at a minimum in the winter. Over
203 the Indian subcontinent, activity peaks in the spring and decreases in the summer with the onset
204 of the southwest monsoon. In Asia, dust activity peaks strongly in the boreal spring.

205

206 Of the major dust sources, North Africa is by far the strongest, contributing ~ 40-60 % of global
207 dust emissions (e.g. Prospero, 1996b; Ginoux, 2001). For example, the so-called Sahara–Sahel
208 ‘dust corridor’ extends over ~ 4000 km from Chad to Mauritania and emits very large volumes

209 of dust over the Atlantic Ocean (Moreno et al., 2006). Within this broad ‘corridor’, specific
210 sources stand out as ‘hot spots’ of activity. Most notable is the Bodele Depression, Chad, the
211 world’s most persistently intense dust source at present day, responsible for an estimated ~ 15-20
212 % of North African emissions (Washington et al., 2006). While the Bodele stands out as a unique
213 source on a global scale, much of North Africa serves as an effective dust source. Indeed, much
214 of North Africa is frequently covered by a dust pall during much of the year. A large region of
215 intense and frequent dust activity lies in Mali, Mauritania and southern Algeria (Prospero et al.,
216 2002; Goudie and Middleton, 2006). Many of the most active sources are associated with
217 drainage systems from the Ahaggar Mountains. This region is probably more representative
218 generally of arid region dust sources and source processes, with many types of sources
219 contributing to the dust emissions: i.e., old alluvial deposits, playas, dried lakes and wadis.
220 Another area of dust activity lies in Tunisia and Northeast Algeria, greatest activity occurring in
221 association with an extensive system of salt lakes and dry lakes in the lowlands south of the Tell
222 Atlas Mountains. Major dust activity also occurs in the eastern Libyan desert in a region marked
223 with an interconnected a chain of wadis (Wadi al-Farigh, Wadi al Hamim). Other active sites are
224 found in Egypt, Sudan and the flanks of the Ethiopian Highlands.

225

226 The other major source regions of the Northern Hemisphere are the Arabian peninsula (~10-20
227 % of global emissions, Table 1) and central and eastern Asia (~15-20 %). For the Arabian
228 peninsula, two major active areas extend along the eastern side of the peninsula along the Persian
229 Gulf, and along the Oman coastal margins (fig. 3), comprising coastal sabkhas and dissected
230 wadi systems, respectively (Goudie and Middleton, 2006). The lower Tigris-Euphrates basin,
231 from north of Baghdad to the Persian Gulf, also provides a summer peak in dust activity, sourced
232 from an immense alluvial plain. Very high concentrations of dust and pollution-derived species
233 are found over the Arabian Sea early in the year (fig. 3a) carried by the winter monsoon and the
234 action of systems moving from the North (Verma et al., 2007). Dust is carried from sources in
235 the eastern Sahara and in northwest India (including the Thar Desert) and Pakistan.

236 Concentrations of dust and pollutant species drop sharply across the inter-tropical convergence
237 zone and with the onset of the southwest (summer) monsoon (Savoie et al., 1987; Krishnamurti
238 et al., 1998) and demonstrate the effectiveness of the inter-tropical convergence zone in blocking
239 the transport of aerosols to the southern hemisphere.

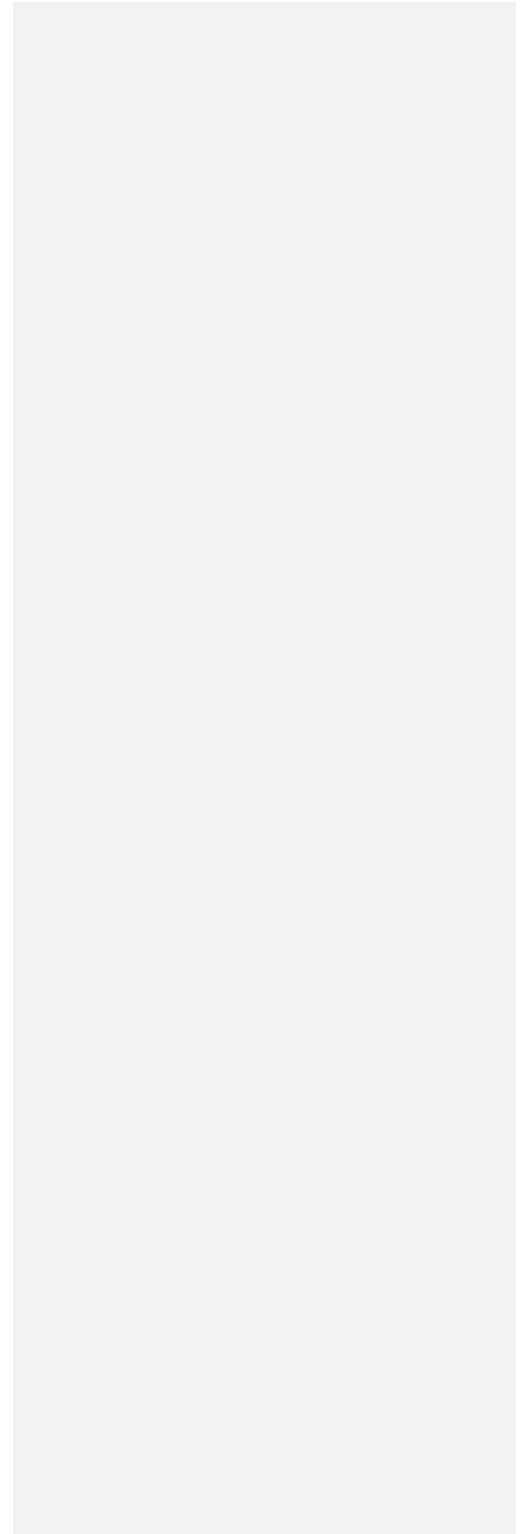
240

241 In eastern Asia, dust sources - mostly in China - are extremely active in the boreal spring. Very
242 large quantities of dust (often mixed with high concentrations of pollutants) are carried out of
243 China eastward, across the coastal waters, and over Korea and Japan where the dust is such a
244 persistent phenomenon, noted in many centuries of historical records, that it is given a name,
245 'kosa' – yellow dust (Kar and Takeuchi, 2004). Asian dust is routinely observed in relatively
246 high concentrations at stations in the central North Pacific (Prospero et al., 1989). The strong
247 seasonal dust cycle and the trans-Pacific extent of the transport can be seen in figure 3a.
248 Although there are many active dust sources in China (Prospero et al., 2002; Goudie and
249 Middleton, 2006; Wang et al., 2004), several stand out in satellite images: the Tarim Pendi basin
250 (containing the Taklimakan Desert; central Inner Mongolia Plateau and the Gobi Desert); the
251 Hexi Corridor and the Loess Plateau; and western Inner Mongolian Plateau. The Tarim Pendi
252 basin, which receives very little rainfall (50-100 mm a year along its periphery and ~ 10 mm in
253 the central regions), is most active from February through May. The Gobi desert, located east of
254 the Tarim Basin on the Mongolian Plateau, is a major dust source at present. Every spring,
255 spectacular dust storms can be seen generated over the Gobi; similar to many dust events in
256 North Africa, the most active sources cover a relatively small area of the surface in effect acting
257 as 'point' sources. Gobi dust outbreaks can be followed n satellite imagery as they move across
258 the Pacific to North America (Husar et al., 2001). The Loess Plateau extends over ~440,000 km²
259 and is covered with loess with depths ranging from typically ~100 m to as much as 350 m
260 (Maher et al., 2008). The Loess Plateau is unique in the global dust picture in that it is the only
261 loess region that serves as a highly active dust source at the present day. These loessic soils are
262 now susceptible to enhanced deflation because of the intense agricultural activity in this region
263 (Wang et al., 2004). While various estimates exist as to the quantitative effects of human
264 activities in dust mobilization (*see Section 1*), it is clear that of all the major dust sources, the
265 Asian sources are those where humans could be having a major effect on emissions, although
266 this is still a matter of considerable debate (Wang et al., 2006).

267

268 Figure 3 a and b

269



270 For the southern hemisphere, contemporary dust sources have been mapped by Prospero et al.
271 (2002) using TOMS data. Australia, South America and southern Africa each have localized
272 areas of dust emissions. However, there is little evidence of major and sustained dust activity in
273 these regions. Although there are few measurements of aerosols over the southern oceans, these
274 show much lower concentrations than over the northern oceans (e.g., Prospero et al., 1989; Baker
275 et al., 2006; Wagener et al., 2008). Measurements of AOD (e.g. Fig. 3a) made by a wide variety
276 of satellite systems (Zhu et al., 2007) fail to detect substantial aerosol plume effects that can be
277 attributed to dust sources. This may partly reflect some under-estimation by TOMS due to
278 difficulties of dust detection in cloudy conditions (e.g. Gassó and Stein, 2007). However,
279 compilations of satellite aerosol event imagery contain many hundreds of examples of dust
280 plumes, the overwhelming majority of which are linked to Northern Hemisphere sources (see,
281 for example: <http://visibleearth.nasa.gov/>; <http://rapidfire.sci.gsfc.nasa.gov/gallery/>). In stark
282 contrast, model results (IPCC, 2001a; Li et al., 2008) often identify emission of large dust
283 plumes from Australia (comparable to those sourced from NW Africa). Ground-truthing of
284 either the remotely sensed or modelled data is severely constrained by the lack of modern dust
285 data. For example, while the ModelE dust component of the GISS Global Circulation Model
286 (Cakmur et al., 2006) is constrained by data from 96 individual sites, only 18 of those are in the
287 southern hemisphere (and of these, 13 were measured during a historic low for dust emissions
288 from Australia (Mackie et al., 2008). The main Australian source is the Lake Eyre basin (Bullard
289 et al., 2008), followed by the Murray-Darling basin, both comprising extensive river systems,
290 floodplains and dunefields (Bullard and McTainsh, 2003). There are two main dust transport
291 paths, one to the northwest and one to the southeast (Bowler, 1976). Although the southeast path
292 is often described as crossing the Tasman Sea (and Australian dust is often reported in New
293 Zealand, e.g. Marx et al., 2005), individual events are variable and can contribute sediment
294 further south, to the Southern Ocean and southwest Pacific (McGowan et al., 2000; McTainsh et
295 al., 2005; Shao et al., 2007). Iron is a conspicuous component of Australian soils and dust storms
296 (Taylor et al., 1983; McTainsh, 1989; Mackie et al., 2008) but the concentrations and mineralogy
297 of Antipodean long range transport (LRT) dusts are poorly known. From magnetic
298 measurements, modern dusts from eastern Australia and the palaeo-dust contained within
299 Tasman Sea sediments contain fine-grained haematite/goethite, which varies directly with the
300 concentration of the mineral dust fraction (Hesse, 1997). New Zealand appears to be an

301 insignificant source of dust at the present day (Prospero et al, 2002), unsurprising as prevailing
302 trans-Tasman winds are to the east (McGowan et al., 2000).

303

304 Although southern Africa has some significant dust sources (notably the Etosha, Namibia and
305 Magkadikgadi, NE Botswana, pans; Prospero et al., 1992; Washington et al. 2003), it is not a
306 major exporter of dust. Iron-rich South African dust that enters the ocean is largely (> 90 %)
307 deposited in the S. Indian Ocean (e.g. Piketh et al., 2000) along latitude ~ 35 °E with only ~ 4 %
308 entering the S. Atlantic (Garstang et al., 1996) Some work (Stuut et al. 2005) points to deflation
309 of silt-rich (> 20 µm) dust to the southwest into the South Atlantic, but it is unknown if this is
310 then transported into the higher latitudes.

311 For South America, the southern region is spanned by a continuous band of arid or semi-arid
312 terrains extending from the Peruvian to the Patagonian coast (the 'Diagonal àrida'/*arid*
313 *diagonal*). Based on TOMS data, Prospero et al. (2002) identified three main dust sources in
314 southern S. America which overlap most of this *arid diagonal*: the Puna (22-26 °S)/Altiplano
315 (15-22 °S) Plateau, central-west Argentina (27-35 °S) and Patagonia (39-52 °S). Preferential
316 emission sources appear linked to large dry lakes (Puna/Altiplano), thousands of small enclosed
317 basins (Patagonia) and extensive alluvial fans (central-west Argentina). Patagonia is strongly
318 influenced by the southern hemisphere westerlies. Patagonian-sourced dust is estimated to supply
319 ~90 % (~ 30 g m⁻² a⁻¹) of the present day sediment flux to the SW Atlantic from S. America
320 (Gaiero et al. 2003). In the high arid plateau (Puna/Altiplano) of the central Andes, the climate is
321 mostly governed by the subtropical jet stream and dust emitted from this area can be directly
322 injected into the tropospheric winds. Both wind systems can produce eastward dust transport and
323 deposition to proximal areas like the Pampas and the nearby Atlantic Ocean or, distally, to the
324 Southern Ocean or the East Antarctic Plateau. The characteristics of present day Patagonian dust
325 are relatively well known (Gaiero et al., 2003; Gaiero et al., 2004; Gaiero et al., 2007). Clay-size
326 fractions are dominated by the clay mineral, smectite. The chemical/isotopic composition of dust
327 reflects the contribution of Jurassic and Quaternary explosive volcanism (Gaiero et al., 2007).
328 Dust deposition rates vary from ~5 g m⁻² a⁻¹ at the Patagonian coast, ~28 g m⁻² a⁻¹ (Gaiero et al.,
329 in prep.) at the Central Pampa (33 °S); and ~26 g m⁻² a⁻¹ for the southern Pampa (39 °S) regions
330 (Ramsperberger et al., 1998; Gaiero et al., 2003).

331

332 Major dust sources require not only the operation of efficient dust deflation and transport
333 processes but also a replenishment of dust supply, through active weathering and comminution
334 of parent materials. TOMS (fig. 3b) shows a clear association of dust sources with specific types
335 of terrains and environments. All major sources in figure 2b are located in arid regions (annual
336 rainfall $< \sim 200\text{--}250$ mm) and centered over topographical lows or on lands adjacent to strong
337 topographical highs. Although the source regions themselves are arid or hyper-arid, fluvial action
338 is evident everywhere by the presence of ephemeral rivers and streams, alluvial fans, playas, and
339 saline lakes. Furthermore, even presently arid source areas have had a relatively recent pluvial
340 history. The association of dust sources with water features is consistent with our understanding
341 of the processes involved in the production of fine particles through weathering (Pye, 1989;
342 Smalley et al., 2005). Fluvial and chemical weathering processes appear much more efficient in
343 the production of small particles (i.e., particles $< \sim 10$ μm diameter) than are aeolian processes
344 (i.e. grinding and impaction). Subsequently, through fluvial action, small particles are carried to
345 depositional basins or alluvial plains where, after drying, they are subject to deflation by wind.
346 Thus, precipitation totals and timing are important both in the (low-lying) area of emission and in
347 any adjacent, dust-supplying highlands. TOMS shows a remarkably consistent association of
348 dust sources with playas and associated terrain environments [Prospero et al., 2002], such as the
349 alluvial fans that ring the basins in which the playas are found (Reheis et al., 1995). The playa is
350 the ultimate receptacle of almost all the fine-grained sediments eroded within a basin over a
351 geological time period, thus they are storehouses of fine, dry, unconsolidated (and thus wind-
352 erodible) sediments often in amounts far in excess of production rates in the present climate. An
353 important characteristic of other major dust sources is the presence of deep and extensive alluvial
354 deposits. During pluvial phases, these basins were flooded and thick layers of sediment were
355 deposited which are now exposed. Many of the most active TOMS sources were flooded during
356 the Pleistocene - Holocene. The prime example is the Bodele Depression in Chad, the largest
357 source of long-range dust in the world (Warren et al., 2007).

358 Thus, the most productive dust-source environments at the present day are the result of the
359 complex interplay between climate, terrain and geological history. In order to understand the
360 linkages between climate, dust production, and transport, we must understand in detail how these
361 features interact.

362

363 Over the past decade, global circulation models and chemical transport models have come to
364 play an important role in understanding dust-climate relationships. At present, there are over a
365 dozen models that simulate the dust cycle, represent its optical properties and predict dry and wet
366 deposition over the global domain (Textor et al., 2006). However, the accuracy of global aerosol
367 models is limited by uncertainties in aerosol emission source characteristics, in our knowledge of
368 atmospheric transport and removal processes and also errors in the meteorological data
369 assimilated into the model computations. Thus there can be large differences among the outputs
370 of the various models and, in the absence of aerosol measurements over large areas of the Earth,
371 it is difficult to select the "best" model. Regardless of these shortcomings, most of the currently
372 reported dust budget values are based on transport models (e.g. Werner et al., 2002; Luo et al.,
373 2003; Zender et al., 2003 and 2004; Ginoux et al., 2004; Mahowald et al., 2005; Cakmur et al.,
374 2006; Miller et al., 2006; Tanaka and Chiba, 2006; Li et al., 2008).

375

376 *3. Dust impacts on climate.*

377 *3.1 Dust as a source of bioavailable iron*

378 Dust may play a critical, indirect role in climate change, through biogeochemical interactions
379 (e.g. via iron or other essential element fertilization of ocean and/or terrestrial ecosystems) and
380 chemical interactions with ozone and sulphur cycles (Cwiertny et al., 2008; Chin et al., 2000). In
381 the case of ocean fertilization, dust containing iron, as fine-grained iron oxides/oxyhydroxides
382 and/or within clay minerals, and other essential micronutrients (e.g. silica) may play a significant
383 role for those regions of the world's oceans where macronutrients like nitrate are abundant but
384 primary production and nitrogen fixation is limited by iron scarcity. Hence, as formalised by
385 Martin et al. (1990, 1991), the efficiency of the 'biological pump' is low and there is significant
386 potential for enhanced export production and drawdown of atmospheric CO₂. The Southern
387 Ocean and the equatorial and northwestern subarctic Pacific are the major high nitrate, low
388 chlorophyll (HNLC) areas, totalling some 30-50 % of the world ocean (Moore et al., 2004;
389 Aumont et al., 2003). Diatoms are the key phytoplankton group for formation of algal blooms in
390 such areas and are strongly iron-limited. Additionally, in tropical and subtropical regions, iron
391 deficiency may also limit phytoplankton growth in subtropical gyres (Johnson et al., 1997;
392 Sedwick et al., 2005) and nitrogen fixation by the diazotrophs (Falkowski, 1997; Moore et al.,
393 2006). Supply of iron-bearing dust may thus directly and indirectly limit primary productivity for

394 large portions of the world ocean (Moore and Doney, 2007), affecting biological carbon export at
395 the global scale (Moore and Braucher, 2008).

396

397 Consistently higher dissolved iron concentrations (>1 nM) are observed for ocean areas below
398 major dust plumes (Sarhou et al., 2003). The 'iron hypothesis' (Martin, 1990) suggests that past
399 increases in aeolian, iron-bearing dust supply to the surface of HNLC ocean waters during
400 glacial stages relieved iron limitation on primary productivity. The resultant increase in the
401 export of biogenic carbon from surface to deep ocean waters (the 'biological pump') caused a
402 decrease in surface ocean $p\text{CO}_2$ that was balanced by an increased drawdown of CO_2 from the
403 atmosphere. The details of this process, and the possible magnitude of its effects on the global
404 carbon cycle, are the subject of much international debate (e.g. Honda et al., 2006; Maher and
405 Dennis, 2001; Moore and Doney, 2007).

406

407 The sensitivity of HNLC regions to increased iron supply has been demonstrated by a series of
408 artificial mesoscale iron fertilization experiments in the HNLC regions (e.g. Boyd et al., 2007;
409 Coale et al., 2004; Coale et al., 1996). The common outcomes to these experiments were the
410 expansion of phytoplankton standing stocks, with distinct population shifts to large diatom
411 species, and resultant drawdown in atmospheric CO_2 (deBaar et al., 2008; Tsuda et al., 2003). It
412 has been difficult to quantify export production via subsurface storage of carbon (rather than
413 subsequent re-release from the ocean mixed layer). For the NW Pacific SEEDS experiment,
414 drawdown of atmospheric carbon was estimated at ~ 150-1500 C atoms per iron atom added
415 (Tsuda et al., 2003). The most recent experiment was also the largest (Lohafex, 2009), with 6
416 tonnes of dissolved iron added to a 300 km² ocean patch in the southwest Atlantic sector of the
417 Southern Ocean. However, whilst there was a doubling of (non-diatom) phytoplankton biomass
418 within the first two weeks, increased grazing pressure of zooplankton prevented further
419 development of the algal bloom, with only minor amounts of carbon being removed from the
420 ocean surface layer as a result.

421

422 Based on these magnitudes of export production, and taking into account the rather low fractions
423 of iron estimated to be bioavailable from mineral dust (e.g. Baker et al., 2006a), modelled
424 glacial-stage changes in atmospheric CO_2 resulting from dust-driven iron fertilisation range from

425 ~ 20 % (Bopp et al., 2003) to > 50 % (Watson et al., 2000) of the total interglacial-glacial change
426 of ~ 100 ppmv. However, extrapolation of the artificial iron enrichment experiments to estimate
427 past carbon sequestration may be unrealistic given their short duration and use of unfeasibly
428 large and rapid iron additions, which lead to loss of most (80 – 95 %) of the iron added during
429 the enrichment experiments (Bowie et al., 2001). More realistic estimates of carbon sequestration
430 may be derived from analysis of a recent (Nov. 2004 – Feb. 2005), natural phytoplankton bloom
431 in the Southern Ocean (Blain et al., 2007). This natural event was driven by indirect iron supply
432 from upwelling of bottom waters (Lefevre and Watson, 1999; Maher and Dennis, 2001), rather
433 than direct aeolian iron supply. $p\text{CO}_2$ measurements of the surface waters showed that the bloom
434 was an important CO_2 sink, with mean $p\text{CO}_2$ drawdown 2–3 x higher than that observed for the
435 artificial Southern Ocean iron experiments, probably reflecting the longer duration of the natural
436 bloom. Carbon sequestration efficiency was estimated to be at least 10 times higher than that
437 estimated from the artificial experiments. The higher sequestration efficiency of the natural
438 bloom has been attributed to its more complete and longer-lasting development, aided by slow
439 and continuous natural additions of iron (and eventually other required macro-nutrients), from
440 adjacent deep water supply (Blain et al., 2007). These results indicate first that aeolian supply of
441 iron to the oceans, both directly and indirectly (i.e. deposited elsewhere and subsequently
442 dissolved and transported), may have been significant in palaeo-ocean and atmospheric CO_2
443 changes. Second, the HNLC oceans may presently be, and previously have been, more sensitive
444 to aeolian iron supply than has been indicated to date by the artificial experiments. However,
445 the SOIREE experiment (Boyd and Abraham, 2001) showed that the photosynthetic competency
446 of iron-limited Southern Ocean phytoplankton increased only when the concentration of
447 dissolved iron exceeded a threshold value of ~0.2 nM, i.e. ~ 2 x twice the ambient $[\text{Fe}]_{\text{dissolved}}$
448 value. Deposition of dust can thus increase the iron inventory of surface waters without
449 stimulating a phytoplankton bloom (Boyd et al., 2009). Previous reports of correlation between
450 dust events and remotely observed increases in surface water chlorophyll (e.g. Gabric et al.,
451 2002; Shaw et al., 2008) need to be evaluated with respect to a physiologically realistic lag time
452 between the increase in dust/iron supply and phytoplankton response (Boyd et al., 2004). For
453 example, whilst Shaw et al. (2008) attributed a bloom in waters of the Great Barrier Reef Lagoon
454 (<50 km from mainland) coastal to a large dust storm (the largest in over 40 years), Mackie
455 (2009) pointed out that the time ($\ll 1$ day) between dust deposition and observations of

456 chlorophyll increase precluded dust as a causal agent. In response, Shaw et al. (2009) suggested
457 that smaller dust events before the large dust storm were responsible. However, in waters so
458 close to the coast, subject to numerous such small dust events, it is unlikely that iron limitation
459 would develop in any case.

460

461 An assumption of many of the dust-cycle and iron supply models is that atmospheric input of
462 bioavailable iron to the surface ocean varies linearly with dust loading. Present day field
463 collection and dust leaching studies (Sedwick et al., 2007; Baker & Jickells, 2006; Jickells et al.,
464 2005) indicate that it is critical to identify the nature (mineralogy), source (e.g. size distribution)
465 and transport history of the dust, in order to evaluate the possible proportion of bioavailable iron
466 carried within the terrigenous dust loading (Baker and Jickells, 2006; Baker and Croot, 2009). A
467 diverse range of dissolution experiments has been reported for a range of iron-bearing
468 aluminosilicates and iron oxides (e.g. Journet et al., 2008), potential source soils (e.g. Visser et
469 al., 2003) and increasing numbers of natural dust samples (e.g. Spokes et al., 1994; Baker et al.,
470 2006b; Desboeufs et al., 2005; Mackie et al., 2005). Generally low but spatially variable iron
471 solubilities appear the norm, i.e. < 0.6 % (e.g. Baker et al., 2006b; Journet et al., 2008). At or
472 close to source areas, soil mineralogy appears to be the key influence on iron solubility. For
473 example, for some African sources, higher solubilities (0.3 %) were displayed by iron-bearing,
474 smectite-rich dust from the central Sahara and lower values (0.1 %) by illite/haematite/goethite-
475 rich dust from the western Sahara and the Sahel (Journet et al., 2008). Conversely, at areas
476 remote from major dust sources, and associated with decreased dust concentrations, increased
477 levels of iron solubility have been reported, and ascribed to progressive particle fining with long
478 range transport (e.g. Baker and Croot, 2009). However, as discussed below, the particle size of
479 LRT dust appears to stabilise rather than become progressively finer. Other factors of likely
480 significance for iron solubility include enhancement of fine particle reactivity during the
481 transport process, especially related to ligand formation and surface adsorption and/or desorption
482 processes. Depending on ambient pH, iron-hydroxyl groups at iron oxide surfaces can achieve
483 negative surface charge by dissociation ($\text{Fe-OH} \rightarrow \text{FeO}^- + \text{H}^+$) or association ($\text{FeOH} + \text{H}^+ \rightarrow$
484 FeOH^{2+}) of protons (e.g. Cornell and Schwertmann, 2003; Taylor et al., 1983). For the iron
485 oxides/ hydroxides, the zero point of charge (zpc, i.e. where there are equal concentrations of
486 surface FeO^- and FeOH^{2+}) varies between ~ pH 5 - 8. Similar pH-dependence of surface and

487 inter-layer charge is displayed by the clay minerals, but with much lower zpc values, from < pH
488 2-3 for smectite to pH 2 – 4.5 for kaolinite . Below the zpc, negatively-charged adsorbates, such
489 as natural organic matter, can subsequently be retained at or near the mineral surface. Such
490 adsorption may play a key role both in reducing particle scavenging and increasing iron
491 solubility in the marine environment. Iron reduction can result from photolysis of Fe^{3+} -
492 complexed with bacterially-produced siderophores (Barbeau et al., 2001) complexes. The
493 solubilised Fe^{2+} could then undergo direct biological uptake, be re-oxidised to Fe^{3+} and/or
494 subjected to subsequent complexation. Recent reports suggest that Fe-reducing compounds, such
495 as dimethyl sulphide, might interactively be released from iron-deficient phytoplankton
496 (Johansen and Key, 2006), although the iron compound modelled in this study was ferrihydrite,
497 the most microcrystalline and reactive of the soil oxyhydroxides. It is clear that large
498 uncertainties presently remain regarding the biogeochemistry of iron complexation, release,
499 uptake and scavenging in the marine environment (Baker and Croot, 2009).

500

501 The interpretation of Fe solubility in aerosol samples is complicated at the present day by the
502 possible presence of Fe derived from anthropogenic sources, in particular, combustion processes,
503 both industrial and biomass burning. Measurements on Bermuda (Sedwick et al., 2007) show
504 that air masses from North American air typically contain relatively low concentration of aerosol
505 iron ($0.5 \text{ nmol Fe m}^{-3}$) but the fractional solubility is very high, 19 %. In contrast dust-laden
506 African air masses contained relatively high concentrations of aerosol iron ($27.8 \text{ nmol Fe m}^{-3}$)
507 but the fractional solubility was low, only 0.44 %. The net result is that the quantity of soluble Fe
508 derived from the aerosols was the same in both cases. The finest particle size fraction yielded the
509 highest solubility for both aerosol types. Model results (Luo et al., 2008) suggest that
510 combustion-derived iron can account for as much as 50 % of the total iron deposited in some
511 regions. However, over the open ocean it is usually less than 5 % of the total iron although close
512 to the East Asian continent in the North Pacific values can be as high as 30 %.

513

514 The observation of increased iron solubility associated with low dust concentrations would imply
515 proportionally enhanced supply of bioavailable iron to ocean areas distal from dust sources
516 (notably, the Southern Ocean) and less to high dust flux areas (Baker and Croot, 2009). The
517 nature of the causal link between dust concentration and solubility requires further evaluation, in

518 order for robust incorporation of varying values of iron solubility of dust into global models of
519 iron flux (e.g. Fung et al., 2000; Bopp et al., 2003). Most models for dust-iron processes use a
520 single uniform value for iron solubility from dust but a recent report of 2-3 % solubility of iron
521 from glacial flour compared to <1 % for arid soils (Schroth et al., 2009) provides a new variable
522 for models to incorporate. The impacts of ocean acidification, likely to modify aerosol and iron
523 solubilisation processes, also require evaluation (Breitbarth et al., 2009).

524

525 *3.2 Dust impacts on climate: radiative effects.*

526 *3.2.1 Dust particle size*

527 Dust size distributions in ocean sediments and ice cores are often used as a measure of dust
528 generation and transport dynamics. The size distributions of dust particles also have a critical
529 influence on the direct and indirect climate impact of dust (see below) and they are also a major
530 uncertainty in dust modelling. Most of the long-traveled dust mass is located in the size range
531 under about 20 μm diameter (e.g. Arimoto et al., 1997), with a mass median diameter of $\sim 1.5 -$
532 $3 \mu\text{m}$ (Balkanski et al., 1995; Reid et al., 2003). Particles in this size range can remain suspended
533 in the troposphere for days to weeks, and be carried over great distances ($\gg 1000 \text{ km}$) before
534 being removed from the atmosphere by deposition processes. Asian dust, for example, has been
535 shown to contribute to dust samples spanning western to eastern China (Gao et al., 1992), the
536 Yellow Sea (Gao et al., 1997), Japan and Korea (e.g. Park et al., 2005), the Pacific Ocean (e.g.
537 Duce et al., 1980; Rea et al., 1985; Uematsu et al., 1985). More distally, it has a significant
538 impact on air quality in the western United States (VanCurren and Cahill, 2002); and is a major
539 source of dust in Greenland ice cores (Bory et al., 2003). North African dust is carried in great
540 quantities to the Amazon basin (Swap et al., 1992), into the Caribbean (Prospero and Lamb,
541 2003) and the southeastern (Prospero, 1999), eastern and northeastern US (Perry et al., 1997).
542 The first challenge for improving data on dust particle size distributions, whether at present day
543 or for the palaeo-record, is the need for expanded geographic and temporal coverage. The second
544 requires instrumental convergence. Across the modern and palaeo-data aerosol communities,
545 particle size tends to be measured using different instruments. For ice and sediment cores, for
546 example, particle size analyses are most frequently derived from instruments using the Coulter
547 Principle (such as the Coulter Multisizer). In contrast, the atmospheric community uses a wide
548 range of instruments that are based on different physical principles, i.e., the mobility of aerosols

549 in electric fields, the optical properties of aerosols, aerosol aerodynamic properties. These
550 instruments yield widely disparate results even when making measurements on identical dust
551 aerosol populations, including African dust (e.g. Reid et al., 2003).

552

553 Notwithstanding this instrumental caveat, modern aerosol size data suggest evolution of the
554 modal diameters for long range transport (LRT, i.e. > 1000 km) dust to a rather invariant range
555 of ~ 3 to 3.5 μm diameter, in contrast to values obtained in or near source regions, which tend to
556 cluster at ~ 5 μm diameter (Sviridenkov et al., 1993; Arimoto et al., 1997, Moore et al., 2004;
557 Maring et al., 2003). For example, dust measured on the Canary Islands (300 km from the N.
558 African coast) and in Puerto Rico (5000 km to the west) shows very similar particle size
559 distributions for the < 7 μm size range (fig. 4a). Larger particles (> ~ 7-8 μm diameter) do
560 display between-event differences, due to their preferential removal during atmospheric
561 transport.

562

563 Similarly, in surface sediments along a 3600 km-long, west-east transect of the North Pacific, a
564 transect lying ~ 4000-8000 km downwind from the E. Asian source areas (i.e. distal from any
565 possible non-aeolian terrigenous sources), the median dust grain size barely changes, at ~ 2.8 μm
566 to 2.4 μm (Janecek, 1985). More recent atmospheric sampling campaigns also suggest a size
567 range of ~ 1- 3 μm for LRT particles in this region (e.g. Zhao et al., 2003). A simple empirical
568 model, which sets the vertical velocity of dust particles equal to the Stokes gravitational settling
569 velocity minus an upward velocity of ~0.33 cm s^{-1} , accurately predicts changes in dust size
570 distribution during atmospheric transport (Maring et al., 2003). Thus it appears that some
571 atmospheric process or processes partially counteract gravitational settling along long transport
572 pathways. It should also be noted that the transport of giant, >75 μm , grains of dust for up to
573 10,000 km has been reported (e.g. Pitty, 1968; Betzer et al., 1988, Middleton et al., 2001) and
574 can not be explained in terms of simple Stokes type settling. The presence of long-lived, long-
575 travelled dust concentrations within the atmosphere remains an unresolved challenge to our
576 understanding of LRT processes.

577

578 Such relative observed invariance of dust size also suggests some degree of constancy in dust
579 mineralogy, morphology and size at the regional scale (e.g. fig. 4a), in turn indicating that source

580 soils or sediments are a factor in controlling dust particle size, in addition to wind speed and/or
581 in-transport processing (Grini and Zender, 2004). In this scenario, dust properties remain
582 consistent when the sources also remain constant, but can be expected to change if and when the
583 source areas change. Wang et al. (2007) report similar conclusions for modern dusts sourced
584 from NW China. The dust grain size distributions vary from source to source but are generally
585 trimodal, with the first peak for particles $> 11 \mu\text{m}$, the second for particles $4.7 - 7 \mu\text{m}$, the third
586 for sub-micrometre particles ($< 0.43 \mu\text{m}$). These distributions remain essentially the same for any
587 one source whether under dust storm or non-dust storm conditions. As noted by Wake and
588 Mayewski (1994), distinctive variations have been observed in the particle number- and mass-
589 size distributions of dusts collected from different geographic regions, including Europe (e.g.
590 Junge, 1963), the Sahara (Schutz and Jaenicke, 1974), the Swiss Alps (Wagenbach and Geis,
591 1987), Colorado and Texas (Patterson and Gillette, 1976), Tajikistan (Gomes and Gillette, 1993)
592 and Greenland (Steffensen, 1985, 1997).

593 These observational data do not support the wind speed dependence of LRT dust particle size
594 (fig. 4b) reported experimentally by Alfaro et al. (1998) and by observation by Sow et al. (2009).
595 These studies indicate enhancement of very fine ($< 2 \mu\text{m}$) particles with increased wind speeds
596 and surface shear velocity (u^*), as a result of ‘sandblasting’ by saltating grains. *Within* an
597 erosional event, however, the dust size distribution appears relatively insensitive to measured
598 changes of u^* . This apparent conflict may reflect a dissonance between the typically long u^*
599 averaging time (15 mins) and significantly shorter response times of the dust emission processes
600 (Sow et al., 2009). Engelstaedter et al. (2007), in contrast, use AERONET data to support the
601 conventional view that larger particle sizes reflect stronger, or possibly gustier, winds.

602

603 Figure 4.

604

605 *3.2.2 Dust radiative properties: effective particle size and mineralogy.*

606 In terms of radiative effects (RE), atmospheric dust can both scatter and absorb incoming solar
607 and outgoing long-wave radiation (direct RE), which alters the energy balance of the atmosphere
608 (IPCC 2001b; IPCC 2007), and can in turn produce changes in atmospheric circulation (Miller
609 and Tegen, 1998) and cloud cover (Perlwitz and Miller, 2009). The effect of dust absorptivity is
610 to produce warming of the atmosphere, locally or regionally, and cooling of the surface. The

611 effect of scattering is to produce more widespread cooling, the result of increased upwards
612 radiance. Dust also plays an important role in cloud microphysics, particularly with regard to
613 numbers of cloud condensation and ice nuclei, thus influencing the formation and lifetime of
614 clouds (indirect RE), which in turn influences the planetary albedo (e.g. Spracklen et al., 2008).
615 Estimates from dust-cycle models of the net top of atmosphere direct RE currently span both
616 negative and positive values, ranging from -0.6 to $+0.4 \text{ Wm}^{-2}$ (IPCC 2007). This uncertainty in
617 both sign and amplitude of dust radiative forcing at the present day reflects both the complexity
618 of dust distribution (including its vertical distribution, interaction with clouds, the albedo of the
619 underlying surface) and poor understanding of the scattering/absorptivity of dust particles, in
620 turn related to poorly known dust concentrations, mineralogy, particle size, and shape (e.g.
621 Nousiainen, 2009). These latter properties vary regionally, depending on the source materials
622 (soils, dry lake beds, ephemeral channels etc); and for any population of grains within a parcel of
623 entrained dust, they also vary interdependently. Mineral dusts typically consist of an internal
624 mixture of mineral species (and particle morphologies), often including quartz, clay minerals,
625 iron oxides and calcium carbonate (Claquin et al., 1999), each with their own optical properties
626 (Sokolik and Toon, 1999). Platy clay mineral particles, for example have different optical
627 properties than equidimensional silicates (Nousiainen et al., 2009). Recent estimates in radiative
628 forcing computations indicate that assuming that dust particles are homogenous spheres causes
629 roughly as large an error as that associated with the uncertainties in refractive index (Kahnert et
630 al., 2007). The latter has previously been considered the dominant source of uncertainty in dust
631 optical properties. The radiative behaviour of dust particles also depends on their effective
632 particle size, i.e. in relation to the wavelength under consideration. Thus, particles with diameters
633 of around $0.5 - 1 \mu\text{m}$ are effective in scattering solar radiation (fig. 5), relatively unaffected by
634 particle shape or surface roughness effects. Such effects become increasingly important for
635 wavelength-scale and larger particles (Nousiainen, 2009), including therefore those within the \sim
636 $1.5 - 3 \mu\text{m}$ size range (i.e. the reported mass median diameter for LRT dust, as above).

637

638 Figure 5

639 Another poorly quantified potential control on dust absorptivity is the presence of iron oxides/
640 oxyhydroxides, as so-called 'free iron', i.e. often as discrete, sub-micrometre particles (figure 6),
641 or as surface coatings on quartz grains, and, more rarely, iron oxide-clay aggregates (Sokolik and

642 Toon, 1999). Only where soil pH is low will iron oxide grains carry sufficient positive charge,
643 and/or the clay particles carry sufficient negative charge, to interact with each other (Cornell and
644 Schwertmann, 2003).

645

646 Figure 6.

647

648 Haematite and goethite occur as minor soil components ($< \sim 5\%$ by mass) on a global scale,
649 reflecting the near-surface weathering of Fe^{2+} -containing primary (lithogenic) minerals by
650 hydrolysis and oxidation. Given that they occur in minor concentrations, both these minerals
651 have a disproportionate radiative impact, displaying large absorbing potential at shorter
652 wavelengths (Alfaro et al., 2004; Sokolik and Toon, 1999; Balkanski et al., 1997). The
653 mineralogy and concentration of iron oxides in dusts is dominantly controlled by the source soil
654 hydrology and mineralogy (Schwertmann and Taylor, 1977), subsequently by any erosional
655 processes of grain aggregation and/or disaggregation, and finally, by any particle size changes
656 during transport (e.g. Zhang et al., 2005). Establishing mineralogical linkages between potential
657 sources and airborne dust is likely to be most robust when based on particle size-specific
658 comparisons between the clay and fine silt fractions of source soils/ sediments and the fine and
659 coarse mode of sampled dust (Maher et al., 2009; Sokolik and Toon, 1999). Compared with its
660 'parent' soil, dust is likely to be biased towards smaller, less dense, and flatter (large surface-
661 area-to-volume ratio) particles (Nousiainen, 2009). Haematite and goethite tend to be associated
662 with fine ($\ll 10\mu\text{m}$, i.e. fine silt and clay-sized) particles, with long residence times (i.e. days) in
663 the atmosphere and thus potentially long transport paths.

664 Haematite has been identified as a significant absorber in terms of dust radiative properties
665 (especially when present as sub-micrometre grains, fig. 6b and c). It is very stable, is the end
666 product of the dehydroxylation of all iron oxyhydroxides and is thus prevalent in warmer and
667 drier regions and increasingly limited in occurrence pole-wards of latitudes $\sim 40^\circ \text{N}$ and S
668 (Cornell and Schwertmann, 2003). For modern dusts from arid and semi-arid regions (Claquin et
669 al., 1999), haematite content varies between 0.6 to 3.4 % (by volume). The iron oxyhydroxide,
670 goethite, is less restricted in its distribution. Although the red coloration of many soils and dusts
671 often reflects the presence of haematite (highly pigmenting when it occurs as sub-micrometre
672 grains), goethite is often volumetrically the more important. In the loess and palaeosols of the

673 Chinese Loess Plateau, for example, the wt % of goethite is 2–3 x higher than that of haematite
674 (Balsam et al., 2007; Ji et al., 2004). Similar dominance of goethite has been reported for a
675 limited number of dust source samples from the Sahara and the Sahel (Lafon et al., 2006). The
676 presence of goethite can lead to large differences in the wavelength dependence of the single
677 scattering albedo (Sokolik and Toon, 1999). The evenness of distribution of goethite in the soil
678 matrix and resultant dusts is also likely to maximize its absorptivity. Inclusion of goethite in dust
679 modelling thus seems essential, given its near-ubiquity in source soils.

680

681 Direct RE forcing by dust appears to result in cooling over much of the Earth's surface (fig. 7,
682 and e.g. Perlwitz et al., 2001; Zhu et al., 2007). Conversely, over bright surfaces (such as
683 deserts), dust can exert significant warming effects. For example, discrepancies between
684 measured and modelled outgoing radiation over cloud-free, desert areas of north Africa indicate
685 that dust may exert a long wave radiation forcing as great as 50 Wm^{-2} in the monthly mean at
686 1200 U TC (Haywood et al., 2005). Similarly, for the 'great Indian desert' (Thar) area, warming
687 of the lower atmosphere from dust absorptivity (greatest during the winter season) has been
688 estimated at $0.7\text{--}1.2 \text{ K day}^{-1}$ (Moorthy et al., 2007). Due to direct and indirect RE, dust can
689 regulate and interact with the heat sources and sinks of monsoonal regions, altering the
690 monsoonal water budget (Lau and Kim, 2006). A further complication arises from increased
691 emissions of anthropogenic, carbonaceous aerosols, which have reduced the global annual
692 average single scattering albedo; aerosol at present day is estimated to be approximately twice as
693 absorbing as that in preindustrial conditions (Myhre, 2009).

694

695 Given the potential impacts of effective particle size and iron mineralogy, improved modelling of
696 dust optical properties at solar wavelengths can only be achieved with improved data on present
697 and past regional variations in aerosol size and shape distributions, and in iron oxide
698 concentrations, mineralogies and mixing state. Given that haematite and goethite occur mostly in
699 minor concentrations, their quantification in dusts and sediments requires from any method of
700 analysis the capacity to analyse to low concentrations (i.e. below the detection levels of x ray
701 diffraction, for example). Diffuse reflectance spectrometry and environmental magnetic methods
702 offer potential in this regard, these measurements responding selectively to the iron oxide-

703 specific signals of colour and magnetic properties, respectively (Arimoto et al., 2002; Balsam et
704 al., 2007; Maher et al., 2007; Watkins et al., 2007).

705

706 Figure 7.

707

708 4. *The palaeo-dust record for the last glacial maximum.*

709 4.1 *Dust fluxes, size distributions, mineralogy.*

710 Glacial/interglacial changes in the flux and particle size of dust have been recorded in ice cores
711 and sediment records, both continental (windblown loess, lake sediment and peat records) and
712 marine. Spanning the entire transect from pole to equator to pole, these dust records have shown
713 that dust flux was higher in both hemispheres during past glacial stages (fig. 8). In light of the
714 ongoing debates regarding modern dust supply and transport outlined above, what does the
715 palaeo-dust record represent? Flux changes may record information on changes in the dust
716 supply, reflecting changes at and/or of source area(s). Source areas may have expanded, through
717 glaciogenic action (Mahowald and Muhs, 2006), emergence of continental shelves into the sub-
718 aeral zone (Bigler et al., 2006), and (seasonally-extended) expansion of arid and semi-arid areas
719 (Werner et al., 2002; Tegen et al., 2002). Particle size changes may reflect changes in transport
720 and/or source. Many palaeoclimate studies have used dust size as an indicator of wind strength in
721 source regions (i.e. larger particles indicate stronger palaeo-winds, e.g. Rea 1995) or changes in
722 the transport pathway (smaller particles indicate longer transport pathways, e.g. Lambert et al.,
723 2008). Clearly, these arguments only hold if there is no change in the source size distributions,
724 and no change in the source-sink distance. However, transporting winds may have altered in their
725 trajectory and/or speed or gustiness (*see section 3.2.1*). Transport paths may have been
726 effectively extended or shortened by changes in the degree of rain-out en route (Yung et al.,
727 1996; Ruth et al., 2005; Lambert et al., 2008). Deposition rates on land may have varied in
728 response to changes in vegetation and resultant trapping of dust by increased surface roughness
729 (Marticorena and Bergametti, 1995; Marticorena et al., 1997).

730

731 Rates of dust deposition in sediment records are most often reported (e.g. Kohfeld and Harrison,
732 2001) as aeolian mass accumulation rates (MARs), calculated as:

733

734
$$\text{MAR (g m}^{-2} \text{ a}^{-1}) = \text{LSR} \times \text{DBD} \times f$$

735

736 where LSR = the linear sedimentation rate (calculated as the thickness of the sediment
737 section (m)/ the time taken for the sediment to accumulate (yrs), DBD is the dry bulk
738 density of the sediment (g m⁻³), and *f* is the fraction of the sediment that is of aeolian origin.
739 Figures 9a and 10a show aeolian MARs for the present day and the LGM, respectively, as
740 collated in our updated version ('DIRTMAP3') of the original 'Dust indicators and records of
741 terrestrial and marine palaeo-environments, DIRTMAP' database (Kohfeld and Harrison, 2001).
742 For comparison, figures 9b and 10b show modelled present day and LGM dust fluxes
743 (Mahowald et al., 2006). Here, we discuss LGM deposition rates (as archived in DIRTMAP3);
744 comparisons between these palaeo-data and the model simulations are discussed in section 6.2.

745

746

747 Figure 9.

748

749

750 Figure 10.

751

752

753 4.2. *The continental loess record.*

754 For the terrestrial environment, sequences of loess sediments provide key aeolian archives on
755 every continent. High-resolution loess/palaeosol sequences can provide new understanding of the
756 relation between aerosols and climate (e.g. Maher, 2007): they provide a record of dust
757 accumulation over large continental areas (Kukla, 1987; Thompson and Maher, 1995); they can
758 be dated directly (Roberts, 2008; Roberts and Duller, 2003), to obtain dust flux changes through
759 time; and they provide mineralogical, physical and chemical information on transported dust
760 (e.g. Prins et al., 2008; Sun et al., 2008), which in turn may affect biogeochemical cycles in the
761 ocean. Loess sequences can act both as a sink and a source for aeolian sediments. For example,
762 the Chinese Loess Plateau, the largest Quaternary accumulation of windblown sediment in the
763 world, has been identified by elemental and isotopic characterization as a major dust source for
764 the sedimentary record of the northwest and equatorial Pacific (Rea et al., 1994; Shigemetsu et

765 al., 2007; Ziegler et al., 2008). In turn, the glacial stage units of the Chinese Loess Plateau
766 comprise extremely well-mixed dust sourced most likely by westerly transport from the western
767 Taklimakan Desert and the northern margins of Tibet (e.g. Maher et al., 2009). The controversy
768 over the extent of Tibetan glaciations during past glacial stages, and hence the extent of
769 glaciogenic supply of loess, remains unresolved at present (e.g. Lehmkuhl and Owen, 2005).
770

771 Reflecting the proximal nature of many loess deposits to their sources, loess MARs at the LGM
772 are the highest of any recorded aeolian fluxes (fig. 10a). For North America, for example, last
773 glacial MARs in excess of $6,700 \text{ g m}^{-2} \text{ a}^{-1}$ have been recorded from loess sections in central
774 Nebraska (Roberts et al., 2003). Provenance information indicates that these extremely high
775 deposition rates reflect increased sediment supply resulting from desiccation and expansion of
776 areas of the Great Plains, rather than from glacial production of silt-sized particles (Aleinikoff et
777 al., 2008). In light of MARS typically ranging from ~ 100 s to 1000 s $\text{g m}^{-2} \text{ a}^{-1}$, and
778 notwithstanding their proximal and thus coarser-grained nature, loess transport on such a scale
779 inevitably incurred deflation and entrainment of large volumes of finer particles ($< 10 \mu\text{m}$), of
780 potentially significant radiative impact. For the central Nebraskan region, for example, PM_{10}
781 MARs range from ~ 500 to $> 900 \text{ g m}^{-2} \text{ a}^{-1}$; such high rates of fine particle flux suggested to have
782 caused prolonged post-LGM cooling in the central N. American region (Roberts et al., 2003).
783 Elsewhere in N. America, loess was supplied from glacial sediment sources, downwind from the
784 Rocky Mountains, and close to rivers issuing from the southern margins of the Late Wisconsin
785 ice sheet. Significant loess accumulations span areas of Iowa, Illinois and Kansas; further north
786 and west, parts of Idaho, Wyoming, Alaska and the Yukon peninsula (fig. 10a).
787

788 For the Eurasian region of the northern hemisphere, a swathe of loess girdles Eurasia from west
789 to east (fig. 10a), reflecting dust supply both from expanded glaciogenic and arid/semi-arid
790 sources. For the European zone, loess MARs typically range from ~ 200 to $600 \text{ g m}^{-2} \text{ a}^{-1}$ for the
791 last glacial stage, with some 'hotspots' of deposition reported, e.g. for the Nussloch site,
792 Germany ($> 2000 \text{ g m}^{-2} \text{ a}^{-1}$, Rousseau et al., 2002) and Paks in Hungary ($> 1000 \text{ g m}^{-2} \text{ a}^{-1}$,
793 Frechen et al., 1997). Extending eastwards over the Russian steppe, loess MARs have a similar
794 range ($\sim 200 - 700 \text{ g m}^{-2} \text{ a}^{-1}$), rates then increase towards Tajikistan ($\sim 1700 \text{ g m}^{-2} \text{ a}^{-1}$, Frechen
795 and Dodonov, 1998) and into the loess sequences of China. Across the Chinese Loess Plateau,

796 the increase in MARs during the last glacial stage, as estimated from median MARs across the
797 region, is of the order of up to $\times 5$, i.e. $\sim 300 \text{ g m}^{-2} \text{ a}^{-1}$ compared to an estimated $65 \text{ g m}^{-2} \text{ a}^{-1}$ for
798 the last interglacial stage ($\sim 125 \text{ ka}$, MIS5e) (Kohfeld and Harrison, 2003). However, the range
799 of LGM MARs estimated for the Loess Plateau spans < 100 to $> 1000 \text{ g m}^{-2} \text{ a}^{-1}$. In common with
800 most of the world's loess sequences, major spatial and temporal (sub-millennial) variability of
801 these glacial-stage increases in dust flux have been reported (e.g. Zhang et al., 2002). In terms of
802 mineralogy, quartz ($\sim 35 \%$), feldspars ($\sim 20 \%$), clay minerals (25 %, illite and illite-smectite)
803 and calcite (12 %) make up the very well-mixed loess (Jeong et al., 2008). Magnetic analyses
804 additionally quantify the presence of minor amounts of haematite and goethite ($\sim 1 \%$); the grain
805 size of the haematite in the interbedded palaeosols is distinctively sub-micrometre, and confers
806 the reddish hues to these soils (Maher, 2007).

807

808 Figure 11

809

810 A characteristic feature of many loesses is their trimodal particle size distribution, with
811 overlapping coarse and fine size modes (fig. 11, and e.g. Wang et al., 2006; Machalett et al.,
812 2008; Lim and Matsumoto, 2008). For the Chinese Loess Plateau, particle size end members
813 have been identified (Prins et al., 2007) comprising a 'sandy loess' component (modal size $63 \mu\text{m}$)
814 a 'silty loess' (modal size $37 \mu\text{m}$), and a 'clayey loess' (modal size $22 \mu\text{m}$). The two
815 coarser end members are thought to reflect saltation and suspension of 'local' coarse dust during
816 dust storms in spring; the finer end member inferred to represent higher level transport by
817 background and dust storm supply. For these sequences, increases in the proportion of coarse
818 particles has been interpreted as an increase in wind speed and thus of more intense winter
819 monsoon circulation (e.g. Xiao et al., 1995; Maher and Hu, 2006). The increased glacial-stage
820 MARs are also associated with increased particle size. At Luochuan, central Loess Plateau, for
821 example, the median diameter of aeolian quartz particles is $\sim 15 \mu\text{m}$ for the last glacial stage
822 sediments compared with $\sim 6 - 9 \mu\text{m}$ for the Holocene (fig. 12; Xiao et al., 1992). These paired
823 increases in fluxes and particle size may indicate both expanded source areas and increased wind
824 speeds, possibly coupled with a shortened transport path. Asian dust is and has been a major
825 component of the sedimentary record of the Pacific Ocean (*see section 4.3*). Downwind of the
826 Loess Plateau, present day estimates of dust flux range from ~ 6 to 12×10^6 tons of Asian dust

827 transported annually to the central North Pacific. Larger quantities are probably deposited over
828 the western North Pacific, closer to the Asian sources (Uematsu et al., 1983).

829

830 Figure 12

831

832 For the southern hemisphere, significant loess accumulations exist in South America and New
833 Zealand (fig. 10a). For the South American continent, the loess sequences of the Argentinian
834 pampas (the central Argentinian plains) cover $\sim 1.0 \times 10^6$ km², with an average thickness of ~ 30 -
835 40 m, thus comprising the largest loess accumulation in the southern hemisphere. Many of these
836 sequences have yet to be analysed in detail; age control is limited for the Tezanos Pinto
837 Formation, traditionally considered to represent the last glacial stage but possibly extending to \sim
838 145 ka (Kemp et al., 2004). Estimated/adjusted MARs for the Pampas for the LGM are thus
839 scarce but range from 45-145 g m⁻² a⁻¹ (Krohling and Iriondo, 1999, cited in Mahowald et al.,
840 2006). Primary sources of these aeolian sediments are linked directly or indirectly to the Andean
841 region and the *arid diagonal* located to the west. In general, the composition of the Argentine
842 loess mirrors the mineralogical and chemical composition of Andean rocks (Gaiero, 2007).
843 Reflecting a dominant Patagonian dust source, the southern loess deposits (~ 36 -38 °S) have
844 similar chemical and isotopic composition and a dominance of smectite, with illite present in
845 smaller amounts (Gaiero et al., 2004). This contrasts with the clay mineralogy of northern loess
846 deposits (~ 26 -28 °S), dominated (Schellenberger and Veit, 2006) by illite (70–85 %), followed
847 by smectite (10–25 %). Between the northern and southern loesses, illite slightly dominates the
848 mineralogical composition of loess, while the coastal plains (Buenos Aires province) exhibit an
849 approximately equal mixture of smectite, illite and kaolinite (Zarate, 2003). The loess deposits
850 are coarse-textured. In the southern Pampas, the average sand–silt–clay content is 44 %, 26 %
851 and 24 %, respectively, the maximum sand content (mostly very fine sand) being ~ 80 % (Bidart,
852 1996). Magnetic properties of loess from this area indicate the presence of detrital magnetite and
853 titanomagnetite as the main ferromagnesian minerals (Orgeira et al., 2009). Northern loess
854 deposits show fairly uniform particle size (silt loam) averaging 14 % sand, 74 % silt, and 12
855 % clay. 80 % of the iron in the sediment is in paramagnetic minerals; ~ 20 % of the iron is in
856 hematite (~ 1.6 % of the sediment's mass), and $\ll 1$ % of the total iron is present as
857 magnetite/maghemite (~ 0.1 % of the sediment's total mass) (Carter-Stiglitz et al., 2006).

858 Elsewhere in the southern hemisphere, loess occurs most extensively in New Zealand, notably in
859 the lowlands surrounding formerly glaciated areas of the South Island (Eden and Hammond,
860 2003). Glacial and floodplain sources have dominated dust production in New Zealand; its loess
861 deposits are thicker (or possibly better documented) than in the S. American Pampean region, for
862 example. Locally, Holocene loess has accumulated up to several metres thickness and very thick
863 (> 10s m) LGM accumulations have been documented (Berger et al. 2002). MARs for the LGM
864 range between 70 to 150 g m⁻² a⁻¹ (Eden and Hammond, 2003). Most of the New Zealand loess is
865 quartz- and feldspar-rich. Glacially-derived loess deposits are strongly weathered (Marx et al.,
866 2005), being clay-poor but mica-rich and relatively coarse-grained compared to dust derived
867 from arid lands (McGowan et al., 2005).

868 Loessic sediments occur to more limited extents in other southern hemisphere countries. The
869 'parna' of southeastern Australia, for example, is characterised by low supply and deposition
870 rates; it dominantly comprises illite and kaolinite, carbonate and silt-sized quartz particles (e.g.
871 Summerell et al., 2000). Accumulation rates measured at a 3m loess section in the highlands
872 west of Sydney were relatively unchanged from 50-10 ka, at between 28 - 45 g m⁻² a⁻¹ (Hesse et
873 al., 2003).

874

875 *4.3. The palaeo-dust record of HNLC regions in the Pacific.*

876 As discussed above, the dust-generating regions of E. Asia appear to have expanded and
877 contracted across a range of glacial/periglacial and arid zone environments during the LGM. In
878 turn, these source changes have produced major changes in dust flux and dust characteristics to
879 the downwind continental sequences of the Chinese loess and palaeosols, and thence onwards to
880 the northwestern and equatorial Pacific.

881

882 For the northwest and the equatorial Pacific regions, there are globally important questions
883 regarding the possible causal role of changes in ocean biogeochemistry and export production
884 (carbon sequestration, i.e. biomass permanently removed from the carbon cycle) during the
885 glacial and interglacial stages of the Quaternary. The importance of understanding the influence
886 of aeolian-supplied Fe can be illustrated by recent fertilization experiments in the northwest
887 region of the Pacific, where iron-enrichment experiments led to the greatest expansion yet
888 observed of phytoplankton standing stocks, together with shifts to dominance of large centric

889 diatoms (Tsuda et al., 2003; de Baar et al., 2005). These two features suggest that the NW Pacific
890 Ocean may be particularly sensitive to iron fertilization. With regard to export production (i.e.
891 subsurface storage, rather than re-release from the ocean mixed layer), the drawdown of
892 atmospheric carbon resulting from this experiment is estimated at ~ 150-1500 C atoms per iron
893 atom added (*see section 3.1*; de Baar et al., 2008). The controversial question of whether changes
894 in palaeo-dust fluxes have caused past changes in ocean productivity in the NW Pacific is also
895 outlined here. Unequivocal identification of palaeo-productivity changes in the Pacific remains
896 challenging in light of: differing approaches to determining sediment fluxes; varying rates of
897 formation and dissolution of individual biogenic components (e.g. carbonate and opal; Honjo et
898 al., 1995); and varying interpretations of radionuclide (e.g. ^{230}Th) and organic degradation
899 products (e.g. biogenic barite). Combined, these issues have resulted in difficulties in quantifying
900 and integrating different biological products and hence total marine export production. As
901 discussed below, different proxies and different approaches to age models have resulted in
902 differing interpretations of glacial-interglacial changes in palaeo-productivity.

903

904 *4.3.1. Northwest Pacific dust fluxes*

905 Reported as one of the best records of aeolian flux from the NW Pacific, core V21-146 from the
906 Shatsky Rise (37.7°N 163°E) was retrieved from an elevated core site which lies beneath the
907 loess-transporting westerlies and provides a robust $\delta^{18}\text{O}$ record for age control (Hovan et al.,
908 1989, 1991). These Shatsky Rise sediments display increased dust fluxes (~ x 3.5, i.e. from ~ 2
909 to 7 $\text{g m}^{-2} \text{a}^{-1}$) during glacial stages, and indicate a direct link between intervals of accelerated
910 continental deposition of loess and enhanced dust flux to the open ocean. Variations in aeolian
911 grain size in the Shatsky Rise (fig. 13) show forcing at Milankovitch orbital frequencies, but
912 coarser grains (median diameter ~ 8 μm) show some association both with interglacial stages (at
913 the 100 ka frequency) and with low tilt and maximal precession, i.e. associated with glaciations
914 (Rea, 1994). Gravity core H3571 was recovered from the Hess Rise (34.9 °N 179.7 °E) some
915 1500 km to the east of the Shatsky Rise site and ~ 3000 km from the Chinese mainland. This
916 record also displays higher dust fluxes during glacial stages, of similar magnitude to the V21-146
917 record. However, these two records show significant differences in the timing and magnitude of
918 their dust flux maxima; V21-146 has maximal fluxes at the LGM, for example, while H3571
919 displays only moderate flux values (~ 5.5 $\text{g m}^{-2} \text{a}^{-1}$) at this time.

920 Tracing Asian dust around its entire northern hemisphere trajectory, the Chinese loess, Pacific
921 deep-sea record and Greenland ice cores all display large and rapid changes both in dust flux and
922 particle size from interglacial into glacial climate stages (fig. 12). It is notable too that large dust
923 flux changes are also evident *within* glacial stages, on sub-millennial timescales. The relative
924 significance of changes in source (e.g. stronger and/or more frequent dust emission events)
925 compared with changes in transport efficiency (e.g. shorter transit times and/or reduced rain-out
926 en route) has been the subject of debate (e.g. Nilson and Lehmkuhl, 2001; Ruth, 2005; Lambert
927 et al., 2008; Fischer et al., 2007). For the North-Greenland Ice Core Project (NGRIP) core, at the
928 distal end of this transport path, the dust source is thought from isotopic evidence to have
929 remained 'constant' through glacial and interglacial stages, i.e. the Taklimakan and Tengger/Mu
930 Us deserts of W. China and Inner Mongolia, respectively (Svensson et al., 2000; Bory et al.,
931 2003), though this is poorly expressed by models (e.g. Andersen et al., 1998). Given stationary
932 sources, the evidence for increased dust flux all along the transport pathway, i.e. from the
933 proximal Chinese loess sequences (e.g. Xiao et al., 1999; Ding et al., 2002), and across the mid-
934 latitude Pacific (e.g. Hovan et al., 1991; Kawahata et al., 2000) does indicate stronger and/or
935 more frequent winds at source (Ruth, 2005). This conclusion requires careful examination,
936 however. Care is needed in linking the more proximal loess sequences with the distal Pacific
937 record. First, from air mass back-trajectory analysis, present day (coarse, ~ 2- 20 μm) dust
938 supply to the Loess Plateau appears dominantly controlled by ambient (non-dust storm)
939 northwesterly surface winter winds (Zhang et al., 1999). This is in contrast to the (fine-grained)
940 LRT dust, which is uplifted during springtime dust storms from sources such as the western
941 Taklimakan Desert (Bory et al., 2003) and carried by the westerly jet at upper levels (~ 5- 8 km)
942 before descending towards the northeasterly trade winds, to the south and east of the subtropical
943 high (Zhang et al., 1999). In contrast, during glacial stages, the dust source for both the LRT dust
944 and the Loess Plateau appears, on multi-proxy elemental and magnetic grounds, to have been the
945 same, dominantly the western desert and Tibetan Plateau regions (Maher et al., 2009; Torii et al.,
946 2001). Second, in terms of particle size, glacial-interglacial variations of particle size along the
947 proposed dust trajectory - from the East Asian deserts to the Loess Plateau to the NW Pacific to
948 Greenland - present some complications. For the Loess Plateau and for NGRIP, glacial stages are
949 associated with increased particle size (fig. 12). Glacial stages in the NGRIP dust record are
950 characterized by particles > 1.6 μm in diameter; interglacials by particle sizes ~ 1 μm .

951 For the NW Pacific (Shatsky Rise), in contrast, finer sizes (median diameter $\sim 3 \mu\text{m}$) have been
952 reported for glacial stages and coarser sizes ($5 \mu\text{m}$) during interglacials (e.g. Hovan et al., 1991),
953 whilst data collated by Zhang et al. (2007) show no clear glacial-interglacial trend (fig. 13).

954

955 Figure 13

956

957 *4.3.2. Equatorial Pacific dust fluxes*

958 Until recently, consistency of glacial-interglacial records of dust flux has been difficult to obtain
959 for the equatorial Pacific, reflecting the confounding effects of sediment redistribution by bottom
960 water currents (e.g. Mitchell and Lyle, 2005) and inputs of volcanically-derived aerosols
961 (Olivarez and Owen, 1991). Critically, glacial to interglacial aeolian fluxes estimated from
962 oxygen isotope-derived age models have varied both in sign and magnitude (e.g. Rea, 1994;
963 Murray et al., 1995). Development of the ^{230}Th normalization method (Bacon, 1984; Francois et
964 al., 1991; Francois et al., 2004) may provide a means (Lyle et al., 2007; Broecker, 2008) to
965 calculate truly aeolian MARS. This method is based on the assumption that the rain-out rate of
966 particulate ^{230}Th sinking to the sea bed is equivalent to the known rate of ^{230}Th production by
967 ^{234}U decay in the overlying water column. MARS are calculated by dividing the production rate
968 of ^{230}Th in the water column by the concentrations of scavenged ^{230}Th in the sediment. In
969 tandem, terrigenous dust fluxes have been estimated for these sediments by using the ratio of
970 ^{232}Th and ^{230}Th as a proxy for dust flux. ^{232}Th is dominantly sourced from continental dust
971 sources (its concentration in volcanogenic materials, for example, is an order of magnitude
972 lower), it is almost insoluble in seawater, and is not subjected to any post-depositional redox-
973 related change. Differences in dust provenance have so far been reported to exert relatively little
974 effect on measured ^{232}Th concentrations, falling within 1 ppm of the upper continental crustal
975 average of 10.7 ppm (Anderson et al., 2006). For an increasing number of sediment cores
976 spanning the equatorial Pacific, recent studies making use of these techniques consistently
977 demonstrate increased dust fluxes during glacial stages, with dust fluxes up to 2.5 x higher
978 during the last glacial stage (Anderson et al., 2006; McGee et al., 2007, Winckler et al., 2008).
979 Dust fluxes decrease from west to east, and towards the south, where northern and equatorial
980 South American dust sources may contribute (Anderson et al., 2006), compared to the
981 dominantly Asian-sourced aerosol towards the north (Ziegler et al., 2009). These new data

982 indicate a coherent response by dust generation and transport processes, from the equator to the
983 South Pole, to glacial/interglacial climate changes through the late Pleistocene (fig. 14). The
984 gradient in dust flux values from north to south across the equator may change through time in
985 response to changes in the latitudinal position and/or the intensity of the intertropical
986 convergence zone (Rea, 1994; Rea and Hovan, 1995; McGee et al., 2007; Ziegler et al., 2008).
987 As noted by Anderson et al. (2006) and Winckler et al. (2008), the observed equatorial Pacific
988 glacial flux increase (up to x 2.5 higher) is very different from modelled dust fluxes for this
989 region. For example, while earlier models (Mahowald et al., 1999, Reader et al. 1999) produced
990 unrealistically large LGM flux increases (LGM/modern ratios ranging between 12 and 105),
991 more recent simulations result in disproportionately low LGM fluxes and also a west to east
992 *increase* in flux (Mahowald et al., 2006).

993

994 Figure 14

995

996

997 *4.4. The palaeo-dust record of the HNLC ocean regions: Antarctic ice cores and Southern*
998 *Ocean.*

999 *4.4.1. Antarctic ice cores*

1000 Some of the longest, most detailed palaeo-dust records have been retrieved from the Antarctic
1001 polar region. Our interpretation of this paleo-record would be greatly facilitated by
1002 measurements of present-day dust transport. Unfortunately, there are remarkably few dust data in
1003 the Southern Hemisphere and, consequently, a major problem in quantifying LGM/modern dust
1004 flux ratios for the wider Southern Ocean region is the paucity of data with which to assess
1005 present day dust fluxes from any of the S. hemisphere land masses (*section 2.2*). Dust fluxes
1006 recorded in Antarctic ice cores show that across the southern polar region dust flux was ~ 30 x
1007 higher during the LGM (fig. 15). The reasons for this very large increase in dust at the LGM can
1008 be multiple. Source regions over Patagonia were certainly extended due to drier conditions and
1009 the decrease in sea-level that left exposed wide continental regions. In addition, the transport
1010 paths could have been changed and the wet deposition is likely to have been considerably
1011 reduced. These factors taken in combination or seldom can explain the differences seen in the
1012 deposition fluxes in the ice cores (Yung et al., 1996).

1013

1014 Figure 15

1015

1016 The growing number of ice cores retrieved from the Antarctic plateau provide long, undisturbed
1017 dust and climate records (extending back over eight glacial cycles) representing not only the
1018 Southern Ocean region but also sectoral differences (fig. 16) within that region (Fischer et al.,
1019 2007). High resolution dust flux records can be compared between several locations, including
1020 Vostok (78° 28'S 106° 48'E) (Petit et al., 1999) and the two EPICA sites (EPICA community
1021 members, 2006), Dome C (EDC, 75°06'S, 123°21'E, in the Indian Ocean sector) and at Kohnen
1022 station in Dronning Maud Land (EDML: 75°00'S, 00°04'E), and Talos Dome (72° 48'S 159°
1023 06'E; Delmonte et al., 2009). For all these cores, the dust profiles are extremely similar both in
1024 terms of total dust flux and the magnitude of the glacial/interglacial changes (Fischer et al., 2007;
1025 Lambert et al., 2008) with high dust fluxes during glacial stages; up to 30 x higher compared
1026 with the Holocene and earlier interglaciations. At EDC, total dust fluxes range from ~ 0.4 mg m⁻²
1027 a⁻¹ at the Holocene to 12 mg m⁻² a⁻¹ during glacial maxima. Tight coupling of the dust and
1028 climate records is especially evident during cold intervals of glacial stages (i.e. when $\delta D > \sim 425$
1029 ‰, Lambert et al., 2008). Episodes of warming are linked with reduced dust fluxes; for instance,
1030 each of the Antarctic isotopic maxima (EPICA community members, 2006) is associated with a
1031 decline in dust fluxes at both the EDC and EDML sites (Fischer et al., 2007), indicating
1032 synchronous changes in the dust source regions (e.g. reduced dust supply and/or reduced wind
1033 speeds).

1034

1035 Figure 16.

1036

1037 Comparison of the EDML and EDC records identifies that the flux of non-sea salt calcium (i.e.
1038 as a mineral dust proxy) was 3 x higher at the EDML, Atlantic sector site; this higher flux is
1039 attributed to its greater proximity to S. American dust sources (Fischer et al., 2007). Debate is
1040 ongoing with regard to the relative influences of glacial-interglacial changes in source strength
1041 and changes in dust transport processes (especially atmospheric residence time and transport
1042 rate) on rates of dust deposition at Antarctica (e.g. see Fischer et al., 2007 compared with
1043 Lambert et al., 2008). If source strength has been the major influence, then glacial dust fluxes to

1044 the Atlantic sector of the Southern Ocean, lying between the S. American sources and the
1045 Antarctic region, should approach those observed in Antarctica (*see section 4.4.2*).

1046

1047 An additional if subtle complication arises with reported regional differences dust particle size
1048 around the different Antarctic sectors (Delmonte et al., 2004). In terms of dust particle size, the
1049 mass-size distribution of aeolian particles in east Antarctica is well sorted around a mean mass
1050 diameter of 2 μm , the largest particle diameter is $\sim 5 \mu\text{m}$, and the contribution of particles < 0.7
1051 μm contributes $< \sim 10\%$ of the total mass (Delmonte et al., 2004b). However, during glacial
1052 stages, smaller particles were deposited at the EDC site, in contrast to Vostok and Dome B,
1053 where increased particle size has been reported during glacial stages (Petit et al., 1982; Delmonte
1054 et al. 2004).

1055

1056 Provenancing of the Antarctic dust by magnetic (Maher, 2009), elemental (Marino et al., 2008)
1057 and isotopic, Sr and Nd, techniques (e.g. Grousset et al., 1992; Basile et al., 1997) is still being
1058 refined, in order to extend the range of well-characterised potential source areas. As noted by
1059 Mahowald et al. (1999), no potential source area can be discounted or verified if it has not been
1060 sampled and characterised. It is also essential to take into account particle size effects on
1061 mineral, elemental and isotopic signatures (figure 17a and b and e.g. Delmonte et al., 2004;
1062 2009). For dust both at Vostok and EDC, the isotopic fields are almost identical (within the
1063 ranges $0.708 < {}^{87}\text{Sr}/{}^{86}\text{Sr} < 0.711$ and $-5 < \epsilon \text{Nd} (0) < +5$), indicating a common dust source across
1064 the East Antarctic region. So far, around 60 potential source areas samples from S. America (33
1065 samples), New Zealand (15), Australia (22), southern Africa (6) and the Antarctic Dry Valleys
1066 (6) have been subjected to isotopic analysis of their fine size fractions ($< 5 \mu\text{m}$), encompassing
1067 loess and loess-like deposits, silts and sands, fluvio-glacial sediments, soils, moraines (Delmonte
1068 et al., 2004, 2007, 2009) and glacial lacustrine deposits (Sugden et al., 2009). At present, those
1069 potential source areas showing partial overlap with the glacial stage ice core dusts are S.
1070 America, New Zealand, the Antarctic Dry Valleys (fig. 17), and some Australian areas (Lake
1071 Eyre). The overlap with Australian-sourced samples increases for interglacial stage samples
1072 (Revel-Rolland et al., 2006; Delmonte et al., 2007; 2009; Marino et al., 2008).

1073

1074 Figure 17.

1075

1076 So far, the consensus has been that Patagonia, and possibly the Puna Altiplano area, have been
1077 the major glacial dust sources for the Antarctic ice records (Gaiero, 2007; Delmonte et al., 2007).
1078 Satellite observations identify these hypothesized source regions as prominent present-day dust
1079 sources (*see fig. 3b, section 2.2*). Lowered glacial-stage sea level rendered Patagonia twice as
1080 large as today and glacial activity was extensive; this region was most likely an intense dust
1081 source during the LGM and previous glacial stages (e.g. Iriondo, 2000; Sugden et al., 2009).
1082 There is no published continental record of Quaternary dust accumulation from Patagonia,
1083 reflecting the high potential for wind erosion and poor geomorphic conditions for sediment
1084 accumulation. Rather, loess accumulation was concentrated further to the north and east in the
1085 pampas of Argentina (e.g. around $\sim 30^{\circ}\text{S}$, $\sim 60^{\circ}\text{W}$). Age control for these loess sequences has
1086 not been well established yet, but MARs at the LGM are estimated at between ~ 45 and 145 g
1087 $\text{m}^{-2} \text{a}^{-1}$ (Krohling and Iriondo, 1999). Evidence for direct links between the Antarctic records of
1088 dust deposition and activating sources within the Patagonian region comes from chronological
1089 and isotopic data on glacial outwash sediments fringing the Straits of Magellan (Sugden et al.,
1090 2009). During the last glaciation, an Andean ice sheet developed between latitudes 44°S and 55
1091 $^{\circ}\text{S}$. Outlet glaciers flowing eastwards from this ice sheet debouched into large outwash plains,
1092 with meltwater eventually draining into the S. Atlantic Ocean. When the outlet glaciers advanced
1093 to terminate directly at the outwash plains around the (then emergent) Magellan Straits, large
1094 amounts of glacial dust were supplied and available for uplift and transport by intensified
1095 westerly winds. Conversely, when the glaciers terminated in proglacial lakes, the dust supply
1096 was effectively ‘switched off’. Isotopic analysis (Sr, Nd) of the finest fraction ($<5 \mu\text{m}$) of
1097 Magellan glacial lacustrine sediments indicates that they may have been one of the sources of the
1098 Antarctic dust during glacial stages (Sugden et al., 2009). Correlation between the dated
1099 sequence of Patagonian glacial activity and the Antarctic (Dome C) dust peaks is good, although
1100 anomalies do occur (e.g. the ice core dust peak at 30 ka has no glacial correlative in Patagonia;
1101 and the dated sediments are lacustrine, possibly indicative of periods of glacial retreat rather than
1102 advance). Rapid retreat of the glaciers can account for the observed rapid decreases in dust flux
1103 during deglaciation. Notably, the deglacial decline in Antarctic dust flux precedes the reduction
1104 in sea ice in the Southern Ocean, the warming of the Southern Ocean and the deglacial rise in sea
1105 level (Sugden et al., 2009; Fischer et al., 2007; Wolff et al., 2006). One problem with this

1106 proposed glacial outwash dust source is the key and characteristic presence of leaf wax-derived
1107 n-alkanes in the intervening sedimentary record of the Southern Ocean (*see section 4.4.2*); the
1108 presence of vegetation might suggest a more low-lying source area (e.g. the emergent coastal
1109 shelf) rather than a glacial/periglacial source.

1110

1111 *4.4.2. The Southern Ocean dust record*

1112 It has so far proved difficult to quantify the flux of dust across the Southern Ocean, and thence to
1113 Antarctica, during past glacial stages. Glacial stage sediments are characterised by increased
1114 lithogenic MARs in all three sectors of the Southern Ocean but these sedimentary records have
1115 diverse terrigenous contributions, including iceberg-rafted debris, current-transported sediment
1116 and aeolian dust (Diekmann, 2007). As with the Pacific sedimentary record, significant lateral
1117 transport of sediment by strong bottom water currents has affected the Southern Ocean records.
1118 There are presently very few integrative studies which have used a range of independent proxies
1119 to establish robust lithogenic and aeolian MARs, and identify glacial/interglacial changes in
1120 export production. Martínez-García et al. (2009) present multiproxy-derived estimates of dust
1121 and iron supply, and marine productivity, over the last 1.1My from a deep-sea sediment record
1122 (PS2489-2, ODP Site 1090) located in the subantarctic South Atlantic (fig. 18). The initial age
1123 model for this composite sedimentary record was obtained by oxygen isotope analysis of benthic
1124 foraminifera (prior to tuning by correlation between the sediment sea surface temperature record
1125 and the EDC temperature record). Using $^{232}\text{Th}:$ ^{230}Th as a proxy for dust flux (in combination
1126 with other terrigenous tracers, including long-chain n-alkanes derived from leaf waxes), these
1127 authors report dust fluxes varying from $\sim 1 \text{ g m}^{-2} \text{ a}^{-1}$ ($\sim 50 \text{ mg m}^{-2} \text{ a}^{-1}$ of iron) for interglacial
1128 periods, to $\sim 5\text{-}7 \text{ g m}^{-2} \text{ a}^{-1}$ ($\sim 250 \text{ mg m}^{-2} \text{ a}^{-1}$ of iron) for glacial stages (fig. 18). Assuming the dust
1129 source to be S. America, these estimates thus indicate up to 7 x increase in the source strength for
1130 this region. This magnitude of change contrasts with the x 20-25 increase in dust flux recorded
1131 by the Antarctic ice cores (Lambert et al., 2008). These data suggest that increased dust source
1132 strength, due to increased (possibly glacially-driven) dust supply and/or higher wind speeds,
1133 might be less significant for the recorded Antarctic dust fluxes than increased efficiency of long
1134 range transport, due to shorter transit times and/or less rain-out en route.

1135

1136 Figure 18

1137

1138 In terms of dust source, whilst very few dust flux data exist for either the present day or the LGM
1139 for this region, present day dust fluxes seem very low (*see section 2.2*). Hence, it is probable that
1140 sources additional to present-day southern S. American source areas were active during the last
1141 glacial period. Recent research does indicate that southern S. America was the most important
1142 LGM dust source for this region, as evidenced by the dominant overlap of isotopic compositions
1143 of sediments from the Pampean loess (Gaiero, 2007), the Southern Ocean (Walter et al., 2000)
1144 and the Antarctic dust (Delmonte et al., 2008). Modelling (Krinner and Genthon, 2003; Lunt &
1145 Valdes, 2002) and mineralogical studies (Gaiero, 2007; Delmonte et al., 2008) indicate that ~ 80
1146 % of dust reaching the Antarctic Plateau during cold periods was derived from Patagonia. Less
1147 clear is the contribution of southern S. American materials to the South Atlantic Ocean. On
1148 isotopic grounds, glacial sediments from the north Scotia Sea seem dominated by a southernmost
1149 Patagonian source (Walter et al., 2000). However, compared with the potential southern S.
1150 American sources, sediments from the Atlantic sector of the Southern Ocean (~41 °S, 14 °W)
1151 display notably higher chlorite content (Diekmann, 2007). Total detrital MARs for this region
1152 are ~15 g m⁻² a⁻¹ for the last interglacial stage (MIS 5, ~ 125 ka) and ~120 g m⁻² a⁻¹ for the LGM
1153 (Walter et al., 2000), but the aeolian contribution to these figures is not known.

1154

1155 For the other S. hemisphere land masses, the Murray-Darling basin was a major Australian dust
1156 source in the LGM, exporting dust towards the south and southeast (Hesse, 1994; Hesse and
1157 McTainsh, 2003). With dust storm frequency ~ 50 % higher (McTainsh and Lynch, 1996), the
1158 LGM flux of Australian dust to the mid-Tasman Sea (160 °E, 40 °S) is estimated at ~ 3 x
1159 Holocene levels (Hesse, 1994). An additional LGM sediment source was the ancestral Lake Eyre
1160 basin (Dulhunty, 1982). Australian dust may have been a long-term contributor to the Southern
1161 Ocean and the southwest Pacific (Stancin et al., 2006, 2008) but the record is obscured by poor
1162 carbonate preservation in the deep Southern Ocean basins and reworking of sediments by strong
1163 Antarctic circum-polar circulation. In terms of particle size, LGM dust transported to the Tasman
1164 Sea from Australia (Hesse and McTainsh, 1999) comprises a minor coarse silt component
1165 (modal diameter 20-25 µm) and dominant fine silt and clay (< 4 µm). Compared to the present
1166 day, there is little change either in the mode or the size of the coarser particles, indicating little
1167 change in the strength of the zonal westerlies over Australia at the LGM. The palaeo-dust

1168 contained within Tasman Sea sediments contains fine-grained haematite/goethite, the
1169 concentration of which varies directly with the dust concentration (Hesse, 1997). Thus, the flux
1170 of fine-grained haematite/goethite to the Southern Ocean and southwest Pacific and from
1171 Australia was greater in the LGM and previous glacials than in the Holocene and previous
1172 interglacials. (The volumetric flux of these minerals, however, has yet to be determined).
1173 Although New Zealand appears to be an insignificant source of dust to the Pacific sector of the
1174 Southern Ocean today (Prospero et al., 2002; fig. 3), it represents a (poorly documented) potential
1175 contributor of dust to the palaeo-Southern Ocean. Given its significant terrestrial accumulations
1176 of loess, New Zealand may have been a significant source of dust to the southwest Pacific and
1177 Southern Ocean at least during glacial intervals of the Late Quaternary. While the geochemical
1178 fingerprint of New Zealand dust overlaps glacial and interglacial Vostok dust signatures (figure
1179 16; Delmonte et al., 2004, 2009), it is likely that New Zealand, like Australia, contributes more
1180 to the Pacific than other sectors of the Southern Ocean. It is notable that New Zealand's Taupo
1181 volcano has been excluded as a potential aerosol source for the Antarctic ice cores from Dome C
1182 ($75^{\circ}06'S$ $123^{\circ}21'E$) and Vostok ($78^{\circ}28'S$ $106^{\circ}46'E$), on the basis of its relatively high SiO_2
1183 content (Narcisi et al., 2005). The absence of Taupo-sourced tephra from the last 200 ka of the
1184 Antarctic ice cores suggests that dust transport from the New Zealand/Australian region to
1185 Antarctica is inefficient (Delmonte et al., 2004; Narcisi et al., 2005). Yet Taupo volcanic dust has
1186 been found in Greenland ice cores (Zielinski et al., 1996); it seems unusual that there could have
1187 been no transmission of dust, at least to subantarctic Southern Ocean waters, given the extreme
1188 size of some eruptions. For example, in an eruption dated at ~ 26.5 ka, Taupo emitted $\sim 1.4 \times 10^{18}$
1189 g of tephra (Mason et al., 2004), i.e. 1000 x the current global dust flux.

1190

1191 Given the current scarcity of present day or palaeo-dust flux and provenance data for the
1192 southern S. hemisphere region, model simulations remain to be validated. For the LGM,
1193 modelling of southern hemisphere dust deposition (e.g. Lunt and Valdes, 2002) suggests up to 15
1194 x greater flux of South American dust in the Atlantic sector of the Southern Ocean (compared
1195 with up to 7 x flux as reported by Martinez-Garcia et al., 2009), and > 90 % contribution of S.
1196 American dust to deposition in the Atlantic and Indian Ocean sectors. In the Lunt & Valdes
1197 (2002) study, the modelled LGM flux of Australian dust exceeds the S. American value
1198 (presumably reflecting the greater area of the Australian continent) but the Australian dust is

1199 dispersed over the entire Pacific sector of the Southern Ocean (Lunt and Valdes, 2002). Other
1200 modelled fluxes (Mahowald et al., 1999, 2006) indicate LGM/modern ratios in the Southern
1201 Ocean ranging from 0.5 to 2 (with dust sources as modelled for the present day) and 20 to 50
1202 (with modelled expansion in dust sources at the LGM).

1203

1204 *5. Palaeo-productivity changes during the LGM in the HNLC regions*

1205 *5.1. Northwestern and equatorial Pacific.*

1206 In the context of iron fertilization, did the measured LGM enhancement of flux of Asian dust
1207 overcome iron limitation in the HNLC regions of the northwestern and equatorial Pacific,
1208 resulting in significant drawdown of atmospheric CO₂? Export production has previously been
1209 reported to have been globally higher during the LGM, with just one exception, the Southern
1210 Ocean (Kohfeld et al., 2005). Some studies have identified an association between glacial
1211 climate stages and increased productivity in the Pacific Ocean. For example, for core H3571
1212 from the NW Pacific, biogenic opal and organic carbon were both reported to have increased
1213 during glacial stages (Kawahata et al., 2000). Similarly, for sediments retrieved from the eastern
1214 equatorial Pacific, Pedersen (1983) identified peak sedimentary organic carbon content (C_{org}) in
1215 association with the LGM. This study used the iodine:C_{org} ratio to rule out enhanced preservation
1216 as a causal factor and thus ascribed the peak C_{org} to a significant increase in productivity during
1217 the LGM. Using biogenic barite fluxes as a palaeo-productivity indicator and conventional
1218 stratigraphically-derived MARs, Paytan et al. (1996) also identified ~ 2 x higher export
1219 production during glacial stages for central and eastern equatorial Pacific cores.

1220

1221 More recent studies reporting increased glacial stage export production, in the western equatorial
1222 and subarctic Pacific, include those of Zhang et al. (2007) and Amo and Minagawa (2003),
1223 respectively. Zhang et al. (2007), using a mixture of micropalaeontological and foraminiferal
1224 isotopic ($\delta^{13}\text{C}$) proxies from Hole 807A (Ontong Java Plateau, 3°36.42N, 165°37.49E), find that
1225 productivity has been greater during glacial stages and has gradually increased since MIS13 (~
1226 530 ka). They also find correlation between their palaeoproductivity record and the dust flux
1227 record in northwestern Pacific core V21-146 (37°N 163°E), from the Shatsky Rise (Hovan et al.,
1228 1991). Zhang et al. (2007) thus suggest that dust transported from East Asia may be significant
1229 for enhancement of biological productivity in the western equatorial Pacific during glacial times.

1230 Similarly, Amo and Minagawa (2003) estimated temporal changes of organic carbon fluxes
1231 during the last 130 ka from marine and terrigenous sources for sediments at the Shatsky Rise
1232 (33.3 °N, 159 °E). In contrast with the minor input of terrestrially-derived carbon, C_{marine} was
1233 estimated at > 86% of the total organic carbon for the whole core, reaching highest accumulation
1234 rates (9.2 mg C cm⁻² ka⁻¹) in the LGM, and next highest rates in earlier glacial periods. From
1235 their alkenone-derived SST reconstructions, Amo and Minagawa (op. cit.) show that although
1236 cold sea surface temperatures (SSTs) prevailed at their Shatsky Rise site throughout MIS 2-4 (~
1237 20 – 7- ka), export production peaked at the LGM, when aeolian dust flux to the site was also at
1238 a maximum. It should be noted that both this study and that of Zhang et al. (2007) use
1239 conventional $\delta^{18}\text{O}$ -derived chronologies for calculation of MARs.

1240

1241 However, recent work on equatorial Pacific sediments has contradicted these findings. Revising
1242 their previous conclusions, Paytan et al. (2004) reported that with normalisation of sediment
1243 accumulation rates using ²³⁰Th, the apparent glacial increases in Pacific productivity either
1244 disappeared or even reversed. They conclude that higher rates of biogenic flux during glacial
1245 stages result not from greater export production but from increased lateral influx of sediment,
1246 transported by bottom water currents. This problem of sediment focusing appears to be
1247 widespread across the equatorial Pacific region, as indicated by ratios in excess of 1 for
1248 $\frac{^{230}\text{Th}_{\text{measured}}}{^{230}\text{Th}_{\text{expected}}}$ (water column production). In another approach, using calcite
1249 accumulation rates (excess ²³⁰Th-normalised and corrected for dissolution), Loubere et al. (2004)
1250 also estimated significantly reduced export production in the eastern equatorial Pacific (from 0.1
1251 to 3.1 °S and 84.65 – 95.65 °W) at the LGM, i.e. ~ 30-50 % lower than during the Holocene.
1252 They attribute this reduction to lowered nutrient supply from the Southern Ocean via the
1253 equatorial undercurrent. This magnitude of productivity reduction is echoed by Bradtmiller et
1254 al.'s (2006) analysis of ²³⁰Th normalized opal fluxes and ²³¹Pa:²³⁰Th ratios in eleven equatorial
1255 Pacific cores; Holocene opal burial rates those of the late glacial period by 35 %. Rather than
1256 systematic reduction in productivity during glacial stages, Anderson et al. (2008) report that
1257 ²³⁰Th-normalized barite fluxes (equatorial core, TT013-PC72, 140 °W) exhibit no clear glacial–
1258 interglacial pattern of variability (fig. 19). Similarly, whilst acknowledging the absence of any
1259 ‘ideal’ palaeo-productivity proxy, Ziegler et al. (2008) identify no relationship between enhanced
1260 flux of Asian dust and ocean productivity, estimating similar export production rates at the LGM

1261 as at present day (for five equatorial cores retrieved at 140 °W). Nor do they find any relationship
1262 between palaeo-productivity and potential Fe supply by upwelling from the equatorial
1263 undercurrent.

1264

1265 For the subarctic, northwestern Pacific (ODP 882, 50.3 °N, 167.5 °E), Jaccard et al. (2005) report
1266 reduced export production during glacial stages (defined using a $\delta^{18}\text{O}$ -derived age model), based
1267 on use of 'biogenic barium' as a palaeoproductivity proxy (i.e. sedimentary barite concentrations
1268 normalized by detritally-sourced aluminium). They attribute this glacial stage reduction in
1269 productivity to increased glacial ocean stratification, and reduced nutrient supply from
1270 upwelling. Their findings are supported by Shigemitsu et al. (2007) who report increased aeolian
1271 fluxes of loess during glacial stages but reduced marine productivity for another western
1272 subarctic Pacific core (50°N, 164.9°E) . Similarly, low glacial productivity (succeeded by
1273 increased deglacial productivity) is reported by Gebhardt et al. (2008), using biogenic opal and
1274 chlorins as proxy indicators for another piston core (51.27°N, 167.7 °E) near to ODP Site 882.

1275

1276 At present, therefore, where sedimentation rates have been normalized by excess ^{230}Th , evidence
1277 suggests there has been no enhancement of ocean productivity and export production in the
1278 equatorial Pacific during the last glacial stage (fig.19). For the NW Pacific, varying with choice
1279 of proxy, contradictory evidence currently exists. As suggested by Gebhardt et al. (2008),
1280 productivity changes may have differed in time and space across the open ocean. However,
1281 selection and interpretation of productivity proxies in the Pacific region remain an ongoing issue
1282 and, as noted by Ziegler et al. (2008), it may be problematic to infer a change in total
1283 productivity from a change in any one particular biological component.

1284

1285 Figure 19.

1286

1287 5.2. Southern Ocean.

1288 In terms of export production, Martínez-García et al. (2009) report good correlation between
1289 glacial/interglacial changes in total organic carbon and the estimated fluxes of dust, indicating
1290 enhanced, and possibly dust-related, marine productivity in the subantarctic eastern Atlantic
1291 sector of the Southern Ocean during glacial stages (fig. 18). However, despite the high fluxes of

1292 dust recorded by the Antarctic ice cores during the LGM, glacial increases in TOC appear much
1293 greater during previous glacial stages. For example, while the LGM is characterised by ~ 2 x
1294 increase in TOC, increases of up to ~ 28 x are observed during MIS 10 (~ 360 ka) and earlier
1295 glacial stages. One feature common to all the glacial intervals recorded in this composite record
1296 is that increases in export production (i.e. above the average interglacial value) only occurred
1297 when the ice core record of CO₂ concentration fell below ~ 230 ppmv (i.e. > 50 ppmv lower than
1298 during interglacial stages).

1299

1300 Figure 20

1301

1302 Enhanced export production in the glacial subantarctic has previously been reported, based on a
1303 range of radionuclide proxies, for each sector of the Southern Ocean, but varying spatially across
1304 the sectors (Kumar et al., 1995; Pondaven et al., 2000; Dezileau et al., 2003; Chase et al., 2001,
1305 2003). At the present day, biogenic opal accumulates at similar rates in each sector, in the
1306 permanently open-ocean zone of the southern part of the Antarctic Circumpolar Current (ACC),
1307 with productivity maxima south of the modern Polar Front (fig. 20). During the Last Glacial
1308 Maximum, opal accumulation rates decreased in the southern part of the ACC at similar rates in
1309 all three sectors, and increased at regionally different rates in the northern part of the ACC, with
1310 maxima in the Atlantic sector (Diekmann, 2007). This suggests that limitation on primary
1311 productivity was overcome to a greater extent in the Atlantic than in the Indian and Pacific
1312 sectors (fig. 19). For the LGM, thorium-normalised lithogenic MARs were ~ 4 x higher in the
1313 Atlantic than in the Pacific sector (Chase et al., 2003). Glacigenic and bottom water-transported
1314 sediments are likely, however, to have contributed most of the fine-grained terrigenous material
1315 to this sector (Diekmann, 2007; Maher and Dennis, 2001; Latimer and Filipelli, 2001; Tagliabue
1316 et al., 2009).

1317

1318 Figure 20

1319

1320 *6. Synthesis.*

1321 *6.1 LGM dust fluxes and changes in ocean productivity?*

1322 It is clear from the palaeo-data that dust fluxes to the HNLC regions of the world ocean were
1323 higher during the LGM than at the present day. The key question arises of whether or not these
1324 increased mineral fluxes resulted in significant changes in marine productivity, export production
1325 (i.e. carbon sequestration, biomass that is permanently removed from the carbon cycle) and,
1326 consequently, drawdown of atmospheric CO₂ during the last glacial stage.

1327

1328 As summarized above, a growing body of evidence suggests that there has been no enhancement
1329 of ocean productivity and export production in the equatorial Pacific during the LGM. For the
1330 NW Pacific, the evidence appears contradictory. The differences in data interpretation for this
1331 latter region may reflect heterogeneity in ocean productivity through time and space (Gebhardt et
1332 al., 2008), but choice and understanding of productivity proxy also remain an ongoing issue.
1333 Further, the relationships between productivity and export of carbon remain poorly resolved for
1334 this region. Data reported by Hays (2009), for example, indicate lower productivity at the LGM
1335 than in the Holocene but higher LGM export of carbon due to significant re-organization of the
1336 epipelagic food web, in particular the glacial dominance of more productive, deep-living (> 200
1337 m water depth) radiolarian species (especially *Cycladophora davisiana*), as previously reported for
1338 the Sea of Okhotsk (e.g. Hays and Morley, 2004).

1339

1340 For the Southern Ocean, coupling between dust flux and export production is inferred by
1341 Martinez-Garcia et al. (2009), who note that the observed increase in export production during
1342 glacial stages is non-linear, rising only slowly in early glaciation stages before accelerating to
1343 peak at glacial maxima. They attribute this exponential pattern to dust-driven iron supply, with
1344 dust flux also rising exponentially as global ice volume increases (Ridgwell and Watson, 2002;
1345 Lambert et al., 2008). These data would indicate that dust-forced increases in Southern Ocean
1346 export production can induce significant CO₂ drawdown but only during glacial maxima, and
1347 thus can account for ~ 40 -50 ppmv drawdown of CO₂ (i.e. as much as half of the total
1348 interglacial-glacial change of ~ 100 ppmv). The apparent coherence between the productivity
1349 proxy (alkenones) and the record of change in atmospheric CO₂ is notable (fig. 21c). Intervals
1350 where the relationship between dust flux, productivity and CO₂ break down (e.g. ~ 220 ka) seem
1351 quite rare but may provide some clue to the required additional causal factors in CO₂ drawdown.
1352 The coupling of dust flux and CO₂ in the reverse direction (i.e. glacial to interglacial) is less

1353 clear. Rothlisberger et al. (2004) note that only small CO₂ variations accompanied large
1354 variations in the flux of non-sea salt-Ca²⁺ (as a proxy for dust) during glacial Antarctic warm
1355 events A1 to A4. They estimate that decreased dust deposition to the Southern Ocean during
1356 glacial to interglacial transitions accounts for not more than a 20 ppmv increase in CO₂ (with
1357 changes in the North Pacific adding <8 ppmv CO₂).

1358

1359 As yet, productivity proxies have yet to be quantified; there is no linear relationship between, for
1360 example, the Southern Ocean alkenones concentrations and palaeo-productivity. It is possible,
1361 however, to estimate some upper and lower bounds on the extent of productivity increase needed
1362 to account for the timing and fall in atmospheric CO₂, as recorded in the Antarctic ice cores (Box
1363 1).

1364

1365 Similar calculations can be made for other waters. For example, if the drawdown of CO₂ was
1366 attributable to the HNLC waters of the NW Pacific as well as the Southern Ocean, then at ~15 %
1367 of the global NPP, the estimated glacial changes to NPP and/or pump efficiency would be
1368 proportionally smaller. Regardless of whether interglacial-glacial changes in atmospheric pCO₂
1369 are due to a change in pump efficiency, a change in NPP or a combination of the two, the
1370 simplest case is for pump efficiency in the Southern Ocean to be towards the upper end of the
1371 probable range (i.e. closer to 20 % than to 1 %). Lack of observational data (as opposed to
1372 modelled estimates) prevents further resolution of the terms here and we suggest this is a high-
1373 priority goal for future research.

1374

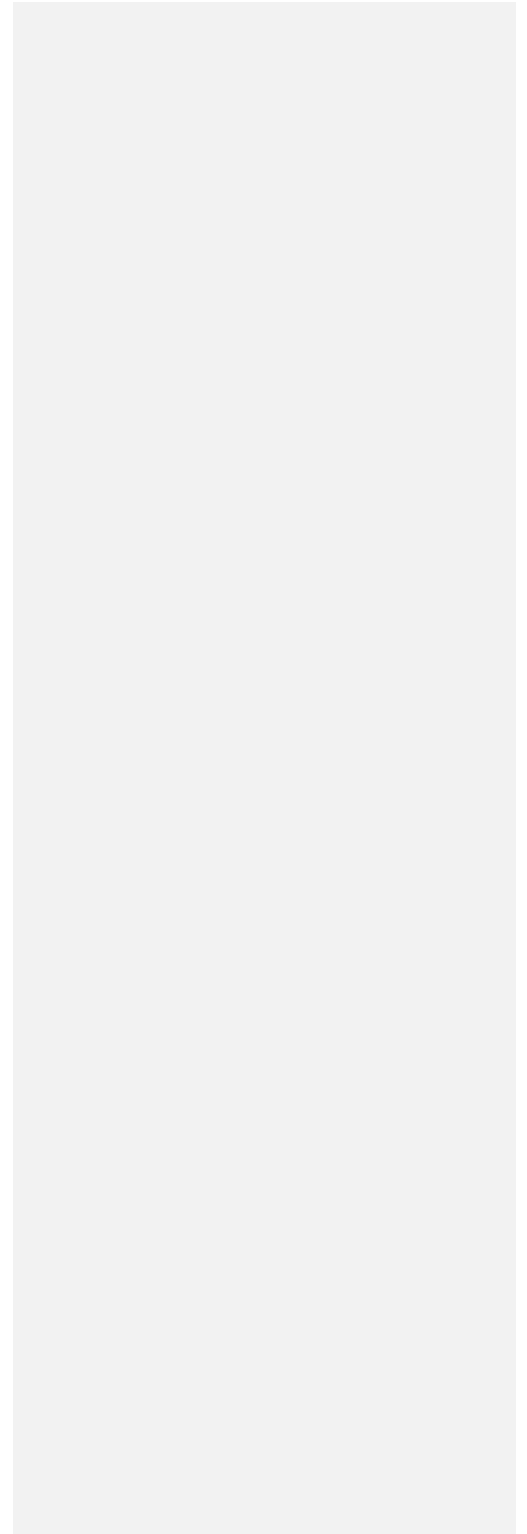
1375 Figure 21.

1376

1377 However, whereas Martinez-Garcia et al. (2009) infer that dust-forced iron fertilization has been
1378 operating in the subantarctic region over at least the last 1.1 My, the spatial distribution of LGM
1379 increases in ocean productivity does clearly vary with sector. LGM opal accumulation rates
1380 increased in the northern part of the ACC but were greatest in the Atlantic sector of the Southern
1381 Ocean, coincident with highest detrital sediment accumulation rates. Rather than of aeolian
1382 origin, much of this terrigenous flux is likely to have been of glaciogenic and/or bottom water-
1383 transported origin (Diekmann, 2007; Maher and Dennis, 2001). Further, even within this sector -

1384 much of which lies directly downwind of the S. American dust source -, it is suggested that areas
1385 of enhanced LGM productivity existed as rather localized 'hotspots' (Anderson et al., 2008), and
1386 that these 'hotspots' may reflect localized iron inputs, such as reactive (i.e. more bioavailable),
1387 nanoparticulate iron from iceberg rafting (Raiswell et al., 2008).

1388



BOX 1: Estimations of changes in net primary productivity and/or efficiency of the biological pump at glacial terminations.

1. Global net primary productivity (NPP) is $\sim 105 \text{ Pg C per year}$, with $\sim 50 \text{ Pg}$ of this in the oceans (e.g. Field et al., 1998). The efficiency of the biological pump is contentious (e.g., Archer and Johnson, 2000; Moore and Doney 2007; Jin et al., 2008); estimates span a wide range from < 1 to 20% of NPP being exported, depending both on the location and definition of 'exported'. Thus, modern carbon export may lie between $0.5 - 10 \text{ Pg C y}^{-1}$.
2. From the onset of glaciations, it takes at least 10,000 years for CO_2 to drop by 100 ppm, such a decrease representing $\sim 220 \text{ Pg carbon}$, or $\sim 0.02 \text{ Pg C y}^{-1}$.
3. Assuming that the decrease in atmospheric CO_2 was due solely to enhanced export from the Southern Ocean, bounding conditions can be established by considering two end member cases. The first end member case (see 4. below) is when NPP changes and pump efficiency is constant; the second end member case (see 5. below) is when NPP is constant and the pump efficiency changes.
4. Modern primary production in the Southern Ocean (waters south of 50°S) is $\sim 2 \text{ Pg C y}^{-1}$ (Arrigo et al., 2008). At the termination of a glacial stage, with a 1% pump efficiency, total export = 0.04 Pg C y^{-1} , i.e. the 'baseline' export of 1% of the modern NPP (2 Pg) = 0.02 Pg C y^{-1} , plus the 0.02 Pg C y^{-1} 'extra export' required to reduce atmospheric CO_2 to its observed glacial value. This would require NPP at the glacial termination to have been 4 Pg C y^{-1} , i.e. a *100 % increase over the modern NPP value*.
5. Conversely, at a glacial termination, with 20% pump efficiency, the total carbon export of $(0.4 + 0.02) \text{ Pg C y}^{-1}$ would have required an NPP of 2.1 Pg C y^{-1} ; i.e. just a *5% increase over modern NPP*.
6. In the case of constant NPP (at 2 Pg C y^{-1}), the total required glacial export in the Southern Ocean of 0.04 Pg C y^{-1} indicates a pump efficiency of 1.3% (a 30% increase over a baseline 1% efficiency), while total export of 1.22 Pg C y^{-1} gives a pump efficiency of 20.3% ($\sim 2 \%$ increase over a baseline 20% efficiency).

1391 In summary, changes in Southern Ocean marine productivity, during the later stages of the LGM,
1392 may have contributed up to half the recorded glacial fall in atmospheric CO₂. These changes may
1393 have been linked directly and causally with increased S. American dust fluxes, but are also likely
1394 to reflect iron supply from other detrital sources.

1395

1396 *6.2 LGM dust fluxes and changes in radiative forcing?*

1397 Dust flux data retrieved from sediment archives (e.g. figs. 8, 10a, 14) demonstrate the major,
1398 global increase in ‘dustiness’ at the LGM, with at least some evidence of coherent MAR
1399 increases between both hemispheres, even at sub-millennial timescales. From the terrestrial loess
1400 sequences in particular, very high dust fluxes indicate marked increases in dust source ‘strength’,
1401 i.e. dust supply increasing due to significant expansion of source areas. Provenance studies of
1402 loess shows that this expansion reflects desiccation and expansion of arid and semi-arid areas
1403 (such as the American Great Plains, the Russian steppe), as well as continental- (northern
1404 hemisphere) and regional-scale (southern hemisphere) glaciation, acting to supply freshly ground
1405 rock particles for deflation and transport at and beyond the ice sheet margins (Hughes, 1992).
1406 Modelling studies also indicate that expansion of dust source areas is required to simulate the
1407 observed LGM fluxes. Using linked terrestrial biosphere, dust source, and atmospheric transport
1408 models to simulate the dust cycle, Mahowald et al. (1999), for example, show that the simulated
1409 increase in high-latitude dustiness requires the expansion of unvegetated areas, especially in the
1410 high latitudes and central Asia. This expansion results from increased aridity and lowered
1411 atmospheric CO₂, indicating the impact of vegetation feedbacks in modulating the atmospheric
1412 dust sources and fluxes. Visual comparison of the LGM modelled and measured dust fluxes (fig.
1413 10), however, shows that while the dust cycle models simulate far-field dust deposition
1414 moderately well, they frequently under-estimate dust loadings close to dust sources, and over the
1415 continents in general, sometimes by up to an order of magnitude. Some of this discrepancy has
1416 been resolved by a twofold approach: firstly, by incorporating dust into a GCM and secondly, by
1417 including in dust cycle models a number of glaciogenic dust sources, designated by inversion
1418 from the palaeo-data (fig. 10b, and Mahowald et al., 2006). An important caveat is that dust
1419 cycle models do not commonly represent particles at the coarser end of the size distribution (> 10
1420 µm). Present day observations of dust are often similarly constrained; many aerosol studies use
1421 cascade samplers with a cut-off at 2 µm. Thus, in making comparisons between model outputs

1422 and dust observations and/or archives (e.g. sediment cores), it is important that size fractions are
1423 matched (e.g. Mahowald et al., 2006). Nevertheless, current dust cycle models have yet to
1424 adequately compute deposition fluxes in regions including or in the vicinity of dust sources (as
1425 above). The converse problem is that the models appear to over-estimate dust fluxes in the
1426 Southern Ocean, where dust deposition (to the Kerguelen Plateau) is up to 2 orders of magnitude
1427 lower than in most current models (Wagener et al., 2008).

1428

1429 Complementing these increases in supply of dust, the enhanced transport of that dust can readily
1430 be invoked, given – for example - that the Southern Ocean westerly winds are likely weaker
1431 and/or shifted equatorward during glacial periods compared to interglacial periods (Toggweiler
1432 et al., 2006). However, enhanced transport can be ascribed not only to more vigorous
1433 atmospheric circulation. Changes in transport path and removal mechanisms are also likely to
1434 have occurred, e.g. reduced rain-out (leading to increased atmospheric residence times),
1435 shortening of trajectory from an expanded source, and/or shifting of the atmospheric jet. Such
1436 transport factors may also have resulted in regional-scale variations in dust particle size,
1437 rendering subsequent inferences of wind speed changes subject to some degree of caution. Based
1438 on changes in dust particle size, LGM increases in wind speed have previously been inferred for
1439 northern and central China, Greenland, NW Africa, southern S. America and Antarctica.
1440 However, more complicated particle size/transport path relationships are evident, for example,
1441 for the dust record of the NW Pacific (despite its ‘intermediate’ position between the Chinese
1442 loess and the Greenland ice cores), and indeed across the Antarctic Plateau.

1443

1444 Intensified cyclonic activity in northern middle latitudes has been modelled for the LGM (e.g.
1445 Shin et al., 2003; Bush and Philander, 1999) although with some southerly displacement ($\sim 3^\circ$)
1446 of the core of the jet. Depending on the reconstructed ice sheet topography (Peltier, 1994), the
1447 Laurentide ice sheet also splits the jet stream in the above-cited models; such a split might have
1448 resulted in a more directly coupled transport path from the Chinese dust sources to the Greenland
1449 ice sheet.

1450

1451 In radiative terms, models have indicated rather different outcomes arising from increased glacial
1452 dust fluxes. For example, enhanced glacial fluxes of dust may have increased albedo resulting in

1453 marked net cooling (Claquin et al. (2003); Mahowald et al. (2006)), in turn reducing
1454 convective intensity and precipitation (Miller et al, 2004), and diminishing poleward transport
1455 of heat and moisture (Ivanochko et al., 2005). In direct contrast, Overpeck et al. (1996) suggested
1456 that high atmospheric dust loadings during glaciations may have resulted in episodic, regional-
1457 scale warming (of the order of ~ 5 °C), downwind of the major Asian and ice-margin dust source
1458 regions. The modelled degree of warming was greater at progressively higher latitudes, reaching
1459 peak values (+2.4 °C) for high-albedo (snow- and ice-covered) areas with high atmospheric dust
1460 loadings. Over such bright surfaces, the effects of dust absorption may dominate those of
1461 scattering, thus reducing short wave backscattering and enhancing long wave radiation (*see*
1462 *section 3.2.2*). The model simulations reported by Overpeck et al. (1996) also show glacial-stage
1463 warming patterns which differ markedly from the pattern of the applied, dust-induced radiative
1464 forcing. These differences likely reflect the interactive role of feedbacks, as atmospheric
1465 pressure, circulation and cloud patterns are altered, in modifying the regional energy balance.
1466 These authors note that these dust-driven radiative impacts may be under-estimated by the
1467 model, given the spatial and temporal variability of flux changes traced by the palaeo-dust
1468 record. Nor did the simulations include the radiative effects of deposited dust on snow and ice,
1469 which may significantly amplify warming effects (Peltier and Marshall, 1995; Krinner et al.,
1470 2006). Sub-millennial variability in dust fluxes may in turn reflect feedback-induced oscillations;
1471 for example, in the case of the Asian region, through modifying land-ocean thermal gradients,
1472 resultant monsoonal intensity and extent and type of vegetation cover in the semi-arid zone.
1473 Similarly, dust-induced warming in the Southern Ocean region may have caused glacial retreat in
1474 the southern S. America dust source areas, cutting off dust supply as glaciers terminated and
1475 deposited sediment in proglacial lakes rather than as unvegetated debris on outwash plains
1476 (Sugden et al., 2009).

1477

1478 Across a range of palaeo-dust records, it appears that dust fluxes peak just prior to
1479 Dansgaard/Oeschger oscillations, before and during Heinrich events, and just before glacial
1480 terminations (Rothlisberger et al., 2002). The Southern Ocean records suggest that up to half of
1481 the glacial-interglacial change in atmospheric CO₂ can be accounted for by dust-driven changes
1482 in marine productivity. It seems possible that radiative forcing by dust can provide an additional

1483 key feedback, producing warming above and beyond the extensive bright surfaces – whether ice
1484 and snow or bare soil and desert - of the glacial world.

1485

1486 *7. Conclusions.*

1487 Dust is important because not only can it affect climate, but the generation and transport of dust
1488 is itself extremely sensitive to climate (fig. 1, fig. 22). For the future, dust cycle models predict
1489 large changes in aeolian transport from the continents to the oceans over coming centuries, in
1490 response to anthropogenic climate change. It is thus important and timely to evaluate the extent
1491 to which changes in dust fluxes and properties may modulate or amplify global warming.

1492 Because spatial and temporal coverage of data on dust properties and emissions is limited at the
1493 present day, most of the currently reported dust budget values are based on transport models. The
1494 utility of these models and simulations is limited by uncertainties in our knowledge and
1495 understanding of dust sources and characteristics, and of atmospheric transport and dust removal
1496 and reaction processes (fig. 22). For example, regional-scale variations in dust composition,
1497 shape, particle size and surface roughness introduce significant uncertainties to the problem of
1498 modelling dust radiative forcing. At present, direct radiative forcing by dust appears to result in
1499 cooling over much of the Earth's surface; bright surfaces (such as deserts and ice and snow) are
1500 the exception, where dust can exert significant warming effects. *Improved modelling of dust*
1501 *optical properties at solar wavelengths can only be achieved with improved data on present and*
1502 *past regional variations in aerosol size and shape distributions, and in iron oxide*
1503 *concentrations, mineralogies and mixing state.*

1504

1505 Other types of dust cycle model are being developed in order to estimate the biogeochemical
1506 effects of dust transport to the oceans, through the supply of otherwise limited nutrients to
1507 marine phytoplankton. For example, an observational dust proxy (ocean surface concentrations
1508 of dissolved aluminium), a biogeochemical element cycling ocean model and a global dust
1509 entrainment and deposition model have recently been used in semi-independent combination to
1510 constrain dust deposition to the oceans (Han et al., 2008). However, even with major recent
1511 expansion of the ocean Al database, the present day spatial and temporal dust proxy coverage
1512 remains inadequate for resolving global dust climatology. This scarcity of data on dust fluxes
1513 and properties is an issue to be addressed with new field campaigns. In the case of ocean Al, new

1514 sampling transects across the Pacific and Indian Oceans (within the CLIVAR and GEOTRACES
1515 programs), will begin to address one aspect of this problem. However, the most robust estimates
1516 of past and present dust fluxes are likely to be achieved only with use of multiple observational
1517 datasets (at optimized spatial resolution) to constrain dust cycle models (Cakmur et al., 2006).
1518 The DIRTMAP3 data (figs. 9a and 10a) clearly delineate those regions which remain severely
1519 under-represented in terms of any observed dust fluxes for the present day and/or the LGM. Such
1520 under-represented sites include much of the southern hemisphere, both terrestrial and marine.
1521 Even for those sites encompassed by DIRTMAP3, very few data exist regarding the key dust
1522 properties associated with the known sources and fluxes. *Enhanced collaboration between the
1523 modelling (radiative and biogeochemical) and data-gathering scientific communities can
1524 optimize design of new field campaigns to obtain key observational data both for the present day
1525 and for past time- (and climate-) slices.*

1526
1527 In order to achieve the required spatial and temporal information on dust fluxes, mineralogy,
1528 particle size and shape, effective and economically-feasible means of analysis are required. In
1529 terms of mineralogy, rapid elemental analysis using x ray-based techniques such as particle
1530 induced x-ray emission (PIXE), x ray fluorescence and automated scanning electron microscopy
1531 (with energy dispersive x ray analysis, e.g. 'QEMSCAN'), continue to evolve in terms of sample
1532 preparation, and lowering of analysis cost. For the iron-bearing components of dust, often
1533 nanoscale in size and present in minor or trace concentrations, non-destructive magnetic methods
1534 may provide both a sensitive and fast means of analysis. Regarding particle size, the first
1535 challenge for improving data on dust particle size distributions, whether at present day or for the
1536 palaeo-record, is the need for expanded geographic and temporal coverage. The second requires
1537 a degree of instrumental convergence between the atmospheric and oceanic communities. In
1538 particular it is notable that in the oceanic and ice-core community particle sizes are commonly
1539 measured with instruments based on the Coulter Principle (such as the Coulter Multisizer); such
1540 instruments are rarely used in aerosol research programs. Thus it is difficult or impossible to
1541 relate the size distributions measured by different research groups.

1542
1543 Not only is this a problem for those measuring dust fluxes but also in turn for the modelling
1544 community. If the cut-off size of the instruments used to measure dust fluxes is poorly defined,

1545 then meaningful comparison subsequently with modelled dust fluxes is also hindered. *Thus, if*
1546 *one wants to say with confidence that a model is able to reproduce the main characteristics of*
1547 *the dust deposition fields at present and during the LGM period, then a strategy for measurement*
1548 *and treatment of dust particle size distributions is needed which is agreed and implemented*
1549 *across both the data-gathering and dust modelling communities.*

1550

1551 *Similarly, just as convergence in analytical methods is at least desirable across the aerosol and*
1552 *palaeo-dust research communities, similar discussions between the aerosol, biological and*
1553 *palaeo-dust communities might aid development of the most appropriate analytical approaches*
1554 *to assessing the solubility and bioavailability of iron-bearing dusts.*

1555

1556 The large changes in dust emissions and transport seen from the palaeo-dust record may reflect a
1557 variety of processes (fig. 22): changes in sources and source conditions; changes in vegetative
1558 cover; sub-aerial erosion of emergent continental shelves; deflation from periglacial deposits;
1559 variations in wind speed and gustiness; changed wind patterns linking sources to deposition
1560 areas; changes in deposition along the dust transport path. For the HNLC regions of the world
1561 ocean, the palaeo-dust record indicates increased dust fluxes at the LGM. The equatorial Pacific,
1562 for example, saw dust fluxes ~ 2.5 x higher during the last glacial stage, with dust fluxes
1563 decreasing from west to east, and towards the south. However, where sedimentation rates have
1564 been normalized by excess ^{230}Th , no enhancement of ocean productivity and export production
1565 has been observed in the equatorial Pacific during the LGM. The deep-sea record of the
1566 northwest Pacific, and the Greenland ice cores, display large and rapid changes both in dust flux
1567 and particle size from interglacial into glacial climate stages. It is notable too that large dust flux
1568 changes are also evident *within* glacial stages, on sub-millennial timescales. Contradictory
1569 evidence currently exists for productivity and export changes at the last glacial stage in the
1570 northwest Pacific region, interpretations vary depending on the type of proxy used and its
1571 interpretation. *More information is needed on the reorganization of marine ecology which results*
1572 *from glacial changes in ocean temperature and subsequent effects on export production.*

1573

1574 Dust flux data remain notably scarce in the southern hemisphere, both for the present day and for
1575 the past. *There is an urgent need for dust flux measurements in the Southern Oceans so that we*

1576 *can improve our understanding of dust processes in this region and to facilitate the development*
1577 *of atmosphere-ocean models.* One practical approach to obtaining improved data coverage at the
1578 present day would be to install air samplers on the commercial and/or research vessels travelling
1579 between the Antipodes, South Africa, Antarctica and on islands in the Southern Ocean. For the
1580 past, the sedimentary record recently reported by Martinez-Garcia et al. (2009) appears to
1581 indicate up to 7 x higher dust flux at the LGM compared with the present day. This is in contrast
1582 to the much larger increase (x 30) recorded by the ice cores of the Antarctic Plateau. In terms of
1583 productivity, the Atlantic sector of the Southern Ocean appears to have responded most to these
1584 increased LGM dust fluxes, with increased export production having occurred slowly during the
1585 early glacial period before rising to a peak at the glacial maximum. This temporal pattern
1586 suggests that dust-forced increases in Southern Ocean export production can induce significant
1587 CO₂ drawdown but only during glacial maxima, and thus can account for ~ 40 -50 ppmv
1588 drawdown of CO₂ (i.e. as much as half of the total interglacial-glacial change of ~ 100 ppmv).
1589 Other drivers must be responsible for the early glacial decrease in atmospheric CO₂, i.e. from ~
1590 280 ppmv during the interglacial stage to the mid-glacial level of ~ 230 ppmv. It is possible to
1591 estimate some upper and lower bounds on the extent of the productivity increase in a) the
1592 Southern Ocean and b) the Southern Ocean and NW Pacific combined, in order to account for
1593 the timing and fall in atmospheric CO₂, as recorded in the Antarctic ice cores. These estimates
1594 suggest that the efficiency of the biological pump in HNLC waters is towards the upper end of
1595 the range (i.e. closer to 20 % than to 1 %).

1596

1597 Finally, it seems clear that enhanced collaboration between the diverse scientific communities -
1598 observational, modelling, biological – can only expedite resolution of the key gaps which exist in
1599 our understanding of dust sources, processes and climate impacts (fig. 22). Targeted and cross-
1600 calibrated collection of field data, both for the present day and past time- and climate-slices,
1601 seems a fundamental imperative. The aim must be to achieve not only robust measurement
1602 and/or estimation of dust fluxes across currently data-sparse regions, but also enhanced
1603 information on dust mineralogy, size, shape and surface roughness. Such data are essential both
1604 to benchmark model simulations and indeed to frame new dust, climate and biogeochemical
1605 models, including transient simulations and mesoscale modelling. *Until we have a good*

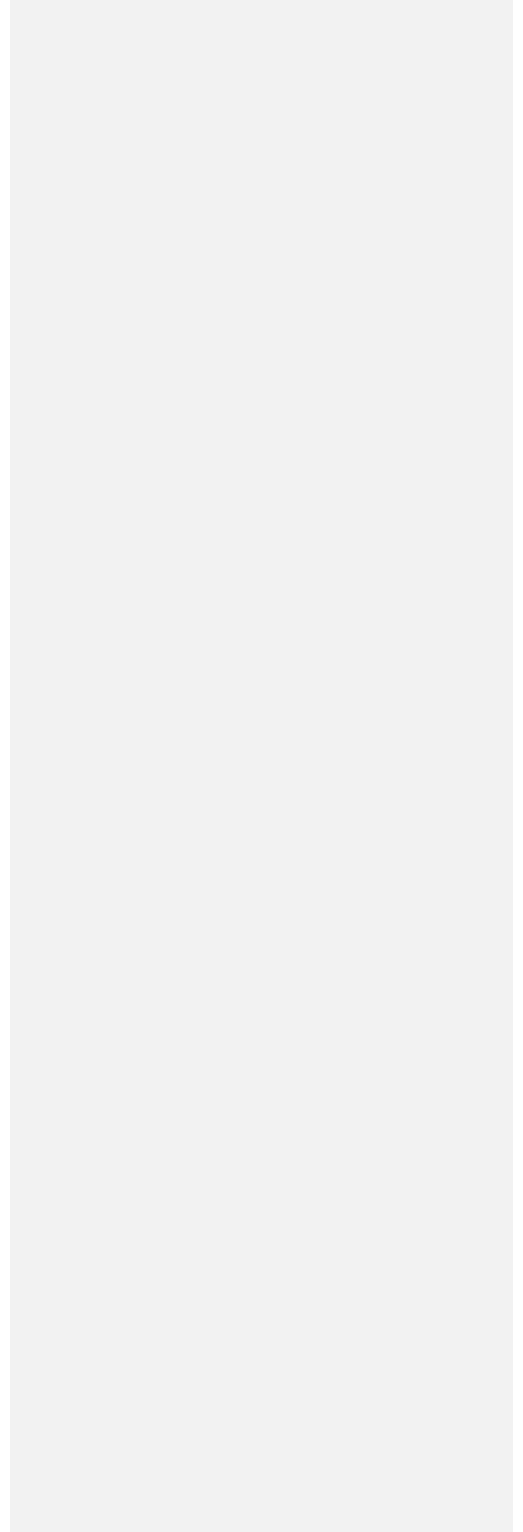
1606 *understanding of present-day processes, we will not be able to adequately address these*
1607 *processes either in the palaeo- record or with regard to the future impacts of dust on climate.*

1608

1609 Acknowledgements.

1610 This paper developed from meetings of the NERC (QUEST) and INQUA-sponsored
1611 ‘DIRTMAP3’ Working Group. BAM gratefully acknowledges support from the Royal Society
1612 (by a Royal Society Wolfson Research Merit Award), DM was supported by a University of
1613 Otago Research Grant awarded to P. Boyd, DMG is a member of the CICyT in Argentina's
1614 CONICET and was supported by IAI, Antorchas, Weizmann Institute, SECyT/UNC and
1615 FONCyT.

1616



1617 References

- 1618 Aleinikoff, J.N., Muhs, D.R., Bettis, E.A., Johnson, W.C., Fanning, C.M. and Benton, R., 2008.
1619 Isotopic evidence for the diversity of late Quaternary loess in Nebraska: Glaciogenic and
1620 nonglaciogenic sources. *Geological Society of America Bulletin*, 120(11-12): 1362-1377.
- 1621 Alfaro, S.C., Gaudichet, A., Gomes, L. and Maille, M., 1997. Modeling the size distribution of a
1622 soil aerosol produced by sandblasting. *Journal of Geophysical Research-Atmospheres*,
1623 102(D10): 11239-11249.
- 1624 Alfaro, S.C., Gaudichet, A., Gomes, L. and Maille, M., 1998. Mineral aerosol production by
1625 wind erosion: aerosol particle sizes and binding energies. *Geophysical Research Letters*,
1626 25(7): 991-994.
- 1627 Alfaro, S.C., Lafon, S., Rajot, J.L., Formenti, P., Gaudichet, A. and Maille, M., 2004. Iron oxides
1628 and light absorption by pure desert dust: An experimental study. *Journal of Geophysical
1629 Research-Atmospheres*, 109(D8): D08208.
- 1630 Amo, M. and Minagawa, M., 2003. Sedimentary record of marine and terrigenous organic matter
1631 delivery to the Shatsky Rise, western North Pacific, over the last 130 kyr. *Organic
1632 Geochemistry*, 34(9): 1299-1312.
- 1633 Andersen, K.K., Armengaud, A. and Genthon, C., 1998. Atmospheric dust under glacial and
1634 interglacial conditions. *Geophysical Research Letters*, 25(13): 2281-2284.
- 1635 Anderson, R.F., Fleisher, M.Q. and Lao, Y., 2006. Glacial-interglacial variability in the delivery
1636 of dust to the central equatorial Pacific Ocean. *Earth And Planetary Science Letters*,
1637 242(3-4): 406-414.

1638 Anderson, R.F., Fleisher, M.Q., Lao, Y. and Winckler, G., 2008. Modern CaCO₃ preservation in
1639 equatorial Pacific sediments in the context of late-Pleistocene glacial cycles. *Marine*
1640 *Chemistry*, 111(1-2): 30-46.

1641 Archer, D.E. and Johnson, K., 2000. A Model of the iron cycle in the ocean. *Global*
1642 *Biogeochemical Cycles*, 14(1): 269-279.

1643 Arimoto, R., Balsam, W. and Schloesslin, C., 2002. Visible spectroscopy of aerosol particles
1644 collected on filters: iron-oxide minerals. *Atmospheric Environment*, 36(1): 89-96.

1645 Arimoto, R., Duce, R.A., Ray, B.J., Ellis, W.G., Cullen, J.D. and Merrill, J.T., 1995. Trace-
1646 Elements in the Atmosphere over the North-Atlantic. *Journal of Geophysical Research-*
1647 *Atmospheres*, 100(D1): 1199-1213.

1648 Arimoto, R., Ray, B.J., Lewis, N.F., Tomza, U. and Duce, R.A., 1997. Mass-particle size
1649 distributions of atmospheric dust and the dry deposition of dust to the remote ocean.
1650 *Journal of Geophysical Research-Atmospheres*, 102(D13): 15867-15874.

1651 Arrigo, K.R., van Dijken, G.L. and Bushinsky, S., 2008. Primary production in the Southern
1652 Ocean, 1997-2006. *Journal of Geophysical Research-Oceans*, 113(C8).

1653 Aumont, O., Maier-Reimer, E., Blain, S. and Monfray, P., 2003. An ecosystem model of the
1654 global ocean including Fe, Si, P colimitations. *Global Biogeochemical Cycles*, 17(2):
1655 1060.

1656 Bacon, M.P., 1984. Glacial to interglacial changes in carbonate and clay sedimentation in the
1657 Atlantic Ocean estimated from Th-230 measurements. *Isotope Geoscience*, 2(2): 97-111.

1658 Baker, A.R. and Croot, P.L., 2009. Atmospheric and marine controls on aerosol iron solubility in
1659 seawater. *Marine Chemistry*, In Press: 10.1016/j.marchem.2008.09.003.

1660 Baker, A.R., French, M. and Linge, K.L., 2006a. Trends in aerosol nutrient solubility along a
1661 west-east transect of the Saharan dust plume. *Geophysical Research Letters*, 33(7):
1662 L07805.

1663 Baker, A.R. and Jickells, T.D., 2006. Mineral particle size as a control on aerosol iron solubility.
1664 *Geophysical Research Letters*, 33(17): L17608.

1665 Baker, A.R., Jickells, T.D., Witt, M. and Linge, K.L., 2006b. Trends in the solubility of iron,
1666 aluminium, manganese and phosphorus in aerosol collected over the Atlantic Ocean.
1667 *Marine Chemistry*, 98(1): 43-58.

1668 Balkanski, Y., Schulz, M., Claquin, T. and Guibert, S., 2007. Reevaluation of Mineral aerosol
1669 radiative forcings suggests a better agreement with satellite and AERONET data.
1670 *Atmospheric Chemistry and Physics*, 7: 81-95.

1671 Balkanski, Y., Schulz, M., Marticorena, B., Bergametti, G., Guelle, W., Dulac, F., Moulin, C.
1672 and Lambert, C.E., 1995. Importance of the source term and of the size distribution to
1673 model the mineral dust cycle. In: S. Guerzoni and R. Chester (Editors), *Impact of African
1674 Dust Across the Mediterranean Conference (ADAM)*. Kluwer Academic Publ, Oristano,
1675 Italy, pp. 69-76.

1676 Barbante, C., Barnola, J.M., Becagli, S., Beer, J., Bigler, M., Boutron, C., Blunier, T.,
1677 Castellano, E., Cattani, O., Chappellaz, J., Dahl-Jensen, D., Debret, M., Delmonte, B.,
1678 Dick, D., Falourd, S., Faria, S., Federer, U., Fischer, H., Freitag, J., Frenzel, A., Fritzsche,

1679 D., Fundel, F., Gabrielli, P., Gaspari, V., Gersonde, R., Graf, W., Grigoriev, D., Hamann,
1680 I., Hansson, M., Hoffmann, G., Hutterli, M.A., Huybrechts, P., Isaksson, E., Johnsen, S.,
1681 Jouzel, J., Kaczmarek, M., Karlin, T., Kaufmann, P., Kipfstuhl, S., Kohno, M., Lambert,
1682 F., Lambrecht, A., Landais, A., Lawer, G., Leuenberger, M., Littot, G., Loulergue, L.,
1683 Luthi, D., Maggi, V., Marino, F., Masson-Delmotte, V., Meyer, H., Miller, H., Mulvaney,
1684 R., Narcisi, B., Oerlemans, J., Oerter, H., Parrenin, F., Petit, J.R., Raisbeck, G., Raynaud,
1685 D., Rothlisberger, R., Ruth, U., Rybak, O., Severi, M., Schmitt, J., Schwander, J.,
1686 Siegenthaler, U., Siggaard-Andersen, M.L., Spahni, R., Steffensen, J.P., Stenni, B.,
1687 Stocker, T.F., Tison, J.L., Traversi, R., Udisti, R., Valero-Delgado, F., van den Broeke,
1688 M.R., van de Wal, R.S.W., Wagenbach, D., Wegner, A., Weiler, K., Wilhelms, F.,
1689 Winther, J.G., Wolff, E. and Members, E.C., 2006. One-to-one coupling of glacial
1690 climate variability in Greenland and Antarctica. *Nature*, 444(7116): 195-198.

1691 Barbeau, K., Rue, E.L., Bruland, K.W. and Butler, A., 2001. Photochemical cycling of iron in
1692 the surface ocean mediated by microbial iron(III)-binding ligands. *Nature*, 413(6854):
1693 409-413.

1694 Basile, I., Grousset, F.E., Revel, M., Petit, J.R., Biscaye, P.E. and Barkov, N.I., 1997. Patagonian
1695 origin of glacial dust deposited in East Antarctica (Vostok and Dome C) during glacial
1696 stages 2, 4 and 6. *Earth And Planetary Science Letters*, 146(3-4): 573-589.

1697 Berger, G.W., Pillans, B.J., Bruce, J.G. and McIntosh, P.D., 2002. Luminescence chronology of
1698 loess-paleosol sequences from southern South Island, New Zealand. *Quaternary Science
1699 Reviews*, 21(16-17): 1899-1913.

1700 Betzer, P.R., Carder, K.L., Duce, R.A., Merrill, J.T., Tindale, N.W., Uematsu, M., Costello,
1701 D.K., Young, R.W., Feely, R.A., Breland, J.A., Bernstein, R.E. and Greco, A.M., 1988.
1702 Long-Range Transport Of Giant Mineral Aerosol-Particles. *Nature*, 336(6199): 568-571.

1703 Bidart, S., 1996. Sedimentological study of aeolian soil parent materials in the Rio Sauce Grande
1704 basin, Buenos Aires Province, Argentina. *Catena*, 27(3-4): 191-207.

1705 Bigler, M., Rothlisberger, R., Lambert, F., Stocker, T.F. and Wagenbach, D., 2006. Aerosol
1706 deposited in East Antarctica over the last glacial cycle: Detailed apportionment of
1707 continental and sea-salt contributions. *Journal Of Geophysical Research-Atmospheres*,
1708 111(D8): D08205.

1709 Blain, S., Queguiner, B., Armand, L., Belviso, S., Bombled, B., Bopp, L., Bowie, A., Brunet, C.,
1710 Brussaard, C., Carlotti, F., Christaki, U., Corbiere, A., Durand, I., Ebersbach, F., Fuda,
1711 J.L., Garcia, N., Gerringa, L., Griffiths, B., Guigue, C., Guillermin, C., Jacquet, S., Jeandel,
1712 C., Laan, P., Lefevre, D., Lo Monaco, C., Malits, A., Mosseri, J., Obernosterer, I., Park,
1713 Y.H., Picheral, M., Pondaven, P., Remenyi, T., Sandroni, V., Sarthou, G., Savoye, N.,
1714 Scouarnec, L., Souhaut, M., Thuiller, D., Timmermans, K., Trull, T., Uitz, J., van Beek,
1715 P., Veldhuis, M., Vincent, D., Viollier, E., Vong, L. and Wagener, T., 2007. Effect of
1716 natural iron fertilization on carbon sequestration in the Southern Ocean. *Nature*,
1717 446(7139): 1070-1074.

1718 Bopp, L., Kohfeld, K.E., Le Quere, C. and Aumont, O., 2003. Dust impact on marine biota and
1719 atmospheric CO₂ during glacial periods. *Paleoceanography*, 18(2): PA1046.

1720 Bory, A.J.M., Biscaye, P.E. and Grousset, F.E., 2003. Two distinct seasonal Asian source
1721 regions for mineral dust deposited in Greenland (NorthGRIP). *Geophysical Research*
1722 *Letters*, 30(4): 1167.

1723 Bowie, A.R., Maldonado, M.T., Frew, R.D., Croot, P.L., Achterberg, E.P., Mantoura, R.F.C.,
1724 Worsfold, P.J., Law, C.S. and Boyd, P.W., 2001. The fate of added iron during a
1725 mesoscale fertilisation experiment in the Southern Ocean. *Deep-Sea Research Part II*,
1726 48(11-12): 2703-2743.

1727 Bowler, J.M., 1976. Aridity In Australia - Age, Origins And Expression In Aeolian Landforms
1728 And Sediments. *Earth-Science Reviews*, 12(2-3): 279-310.

1729 Boyd, P.W. and Abraham, E.R., 2001. Iron-mediated changes in phytoplankton photosynthetic
1730 competence during SOIREE. *Deep-Sea Research Part II-Topical Studies In*
1731 *Oceanography*, 48(11-12): 2529-2550.

1732 Boyd, P.W., McTainsh, G., Sherlock, V., Richardson, K., Nichol, S., Ellwood, M. and Frew, R.,
1733 2004. Episodic enhancement of phytoplankton stocks in New Zealand subantarctic
1734 waters: Contribution of atmospheric and oceanic iron supply. *Global Biogeochemical*
1735 *Cycles*, 18(1): GB1029.

1736 Boyd, P.W., Jickells, T., Law, C.S., Blain, S., Boyle, E.A., Buesseler, K.O., Coale, K.H., Cullen,
1737 J.J., de Baar, H.J.W., Follows, M., Harvey, M., Lancelot, C., Levasseur, M., Owens,
1738 N.P.J., Pollard, R., Rivkin, R.B., Sarmiento, J., Schoemann, V., Smetacek, V., Takeda,
1739 S., Tsuda, A., Turner, S. and Watson, A.J., 2007. Mesoscale iron enrichment experiments
1740 1993-2005: Synthesis and future directions. *Science*, 315(5812): 612-617.

1741 Boyd, P.W., Mackie, D.S. and Hunter, K.A., 2009. Aerosol iron deposition to the surface ocean -
1742 - Modes of iron supply and biological responses. *Marine Chemistry*, In Press: doi:
1743 10.1016.l.marchem.2009.01.008.

1744 Bradtmiller, L.I., Anderson, R.F., Fleisher, M.Q. and Burckle, L.H., 2006. Diatom productivity
1745 in the equatorial Pacific Ocean from the last glacial period to the present: A test of the
1746 silicic acid leakage hypothesis. *Paleoceanography*, 21(4): PA4201.

1747 Breitbarth, E., Achterberg, E. P., Ardelan, M. V., Baker, A. R., Bucciarelli, E., Chever, F., Croot,
1748 P. L., Duggen, S., Gledhill, M., Hassell, M., Hassler, C., Hoffmann, L. J., Hunter, K. A.,
1749 Hutchins, D. A., Ingri, J., Jickells, T., Lohan, M. C., Nielsdottir, M. C., Sarthou, G.,
1750 Schoemann, V., Trapp, J. M., Turner, D. R. and Ye, Y., 2009. Iron biogeochemistry
1751 across marine systems at changing times – conclusions from the workshop held in
1752 Gothenburg, Sweden (14–16 May 2008). *Biogeosciences Discussion*, 6, 6635–6694.

1753
1754 Broecker, W., 2008. Excess sediment Th-230: Transport along the sea floor or enhanced water
1755 column scavenging? *Global Biogeochemical Cycles*, 22(1): GB1006.

1756 Bullard, J., Baddock, M., McTainsh, G. and Leys, J., 2008. Sub-basin scale dust source
1757 geomorphology detected using MODIS. *Geophysical Research Letters*, 35(15): L1504.

1758 Bullard, J.E. and McTainsh, G.H., 2003. Aeolian-fluvial interactions in dryland environments:
1759 examples, concepts and Australia case study. *Progress in Physical Geography*, 27(4):
1760 471-501.

1761 Bullard, J.E., McTainsh, G.H. and Pudmenzky, C., 2007. Factors affecting the nature and rate of
1762 dust production from natural dune sands. *Sedimentology*, 54(1): 169-182.

1763 Bush, A.B.G. and Philander, S.G.H., 1999. The climate of the Last Glacial Maximum: Results
1764 from a coupled atmosphere-ocean general circulation model. *Journal Of Geophysical*
1765 *Research-Atmospheres*, 104(D20): 24509-24525.

1766 Cakmur, R.V., Miller, R.L., Perlwitz, J., Geogdzhayev, I.V., Ginoux, P., Koch, D., Kohfeld,
1767 K.E., Tegen, I. and Zender, C.S., 2006. Constraining the magnitude of the global dust
1768 cycle by minimizing the difference between a model and observations. *Journal Of*
1769 *Geophysical Research-Atmospheres*, 111(D6): D06207.

1770 Carter-Stiglitz, B., Banerjee, S.K., Gourolan, A. and Oches, E., 2006. A multi-proxy study of
1771 Argentina loess: Marine oxygen isotope stage 4 and 5 environmental record from
1772 pedogenic hematite. *Palaeogeography Palaeoclimatology Palaeoecology*, 239(1-2): 45-
1773 62.

1774 Chase, Z., Anderson, R.F. and Fleisher, M.Q., 2001. Evidence from authigenic uranium for
1775 increased productivity of the glacial Subantarctic Ocean. *Paleoceanography*, 16(5): 468-
1776 478.

1777 Chase, Z., Anderson, R.F., Fleisher, M.Q. and Kubik, P.W., 2003. Accumulation of biogenic and
1778 lithogenic material in the Pacific sector of the Southern Ocean during the past 40,000
1779 years. *Deep-Sea Research Part II*, 50(3-4): 799-832.

1780 Chiapello, I., Bergametti, G., Chatenet, B., Bousquet, P., Dulac, F. and Soares, E.S., 1997.
1781 Origins of African dust transported over the northeastern tropical Atlantic. *Journal of*
1782 *Geophysical Research-Atmospheres*, 102(D12): 13701-13709.

1783 Chin, M., Rood, R.B., Lin, S.J., Muller, J.F. and Thompson, A.M., 2000. Atmospheric sulfur
1784 cycle simulated in the global model GOCART: Model description and global properties.
1785 Journal Of Geophysical Research-Atmospheres, 105(D20): 24671-24687.

1786 Chung, C.E., Ramanathan, V., Kim, D. and Podgorny, I.A.. 2005. Global anthropogenic aerosol
1787 direct forcing derived from satellite and ground-based observations. Journal of
1788 Geophysical Research, 110, D24207, doi: 10.1029/2005JD00635.

1789 Claquin, T., Roelandt, C., Kohfeld, K.E., Harrison, S.P., Tegen, I., Prentice, I.C., Balkanski, Y.,
1790 Bergametti, G., Hansson, M., Mahowald, N., Rodhe, H. and Schulz, M., 2003. Radiative
1791 forcing of climate by ice-age atmospheric dust. Climate Dynamics, 20(2-3): 193-202.

1792 Claquin, T., Schulz, M. and Balkanski, Y.J., 1999. Modeling the mineralogy of atmospheric dust
1793 sources. Journal Of Geophysical Research-Atmospheres, 104(D18): 22243-22256.

1794 Coale, K.H., Johnson, K.S., Chavez, F.P., Buesseler, K.O., Barber, R.T., Brzezinski, M.A.,
1795 Cochlan, W.P., Millero, F.J., Falkowski, P.G., Bauer, J.E., Wanninkhof, R.H., Kudela,
1796 R.M., Altabet, M.A., Hales, B.E., Takahashi, T., Landry, M.R., Bidigare, R.R., Wang,
1797 X.J., Chase, Z., Strutton, P.G., Friederich, G.E., Gorbunov, M.Y., Lance, V.P., Hilting,
1798 A.K., Hiscock, M.R., Demarest, M., Hiscock, W.T., Sullivan, K.F., Tanner, S.J., Gordon,
1799 R.M., Hunter, C.N., Elrod, V.A., Fitzwater, S.E., Jones, J.L., Tozzi, S., Koblizek, M.,
1800 Roberts, A.E., Herndon, J., Brewster, J., Ladizinsky, N., Smith, G., Cooper, D., Timothy,
1801 D., Brown, S.L., Selph, K.E., Sheridan, C.C., Twining, B.S. and Johnson, Z.I., 2004.
1802 Southern ocean iron enrichment experiment: Carbon cycling in high- and low-Si waters.
1803 Science, 304(5669): 408-414.

1804 Coale, K.H., Johnson, K.S., Fitzwater, S.E., Gordon, R.M., Tanner, S., Chavez, F.P., Ferioli, L.,
1805 Sakamoto, C., Rogers, P., Millero, F., Steinberg, P., Nightingale, P., Cooper, D.,
1806 Cochlan, W.P., Landry, M.R., Constantinou, J., Rollwagen, G., Trasvina, A. and Kudela,
1807 R., 1996. A massive phytoplankton bloom induced by an ecosystem-scale iron
1808 fertilization experiment in the equatorial Pacific Ocean. *Nature*, 383(6600): 495-501.

1809 Cornell, R.M. and Schwertmann, U., 2003. *The Iron Oxides: Structure, properties, reactions,*
1810 *occurrences and uses.* Wiley-VCH, Weinheim, 664 pp.

1811 Cwiertny, D.M., Young, M.A. and Grassian, V.H., 2008. Chemistry and photochemistry of
1812 mineral dust aerosol. *Annual Review of Physical Chemistry*, 59: 27-51.

1813 Darwin, C., 1846. An account of the fine dust which often falls on vessels in the Atlantic Ocean.
1814 *Quarterly Journal of the Geological Society of London*, 1846(1): 26-30.

1815 de Baar, H.J.W., Boyd, P.W., Coale, K.H., Landry, M.R., Tsuda, A., Assmy, P., Bakker, D.C.E.,
1816 Bozec, Y., Barber, R.T., Brzezinski, M.A., Buesseler, K.O., Boye, M., Croot, P.L.,
1817 Gervais, F., Gorbunov, M.Y., Harrison, P.J., Hiscock, W.T., Laan, P., Lancelot, C., Law,
1818 C.S., Levasseur, M., Marchetti, A., Millero, F.J., Nishioka, J., Nojiri, Y., van Oijen, T.,
1819 Riebesell, U., Rijkenberg, M.J.A., Saito, H., Takeda, S., Timmermans, K.R., Veldhuis,
1820 M.J.W., Waite, A.M. and Wong, C.S., 2005. Synthesis of iron fertilization experiments:
1821 From the iron age in the age of enlightenment. *Journal of Geophysical Research-Oceans*,
1822 110(C9): C09s16.

1823 de Baar, H.J.W., Gerringa, L.J.A., Laan, P. and Timmermans, K.R., 2008. Efficiency of carbon
1824 removal per added iron in ocean iron fertilization. *Marine Ecology-Progress Series*, 364:
1825 269-282.

1826 de Menocal, P.B., Ruddiman, W.F. and Pokras, E.M., 1993. Influences of high-latitude and low-
1827 latitude processes on African terrestrial climate - Pleistocene eolian records from
1828 equatorial Atlantic Ocean Drilling Program Site-663. *Paleoceanography*, 8(2): 209-242.

1829 Delmonte, B., Andersson, P.S., Schöberg, H., Hansson, M., Petit, J.R., Delmas, R., Gaiero,
1830 D.M., Maggi, V. and Frezzotti, M., 2009. Geographic provenance of aeolian dust in East
1831 Antarctica during Pleistocene glaciations: preliminary results from Talos Dome and
1832 comparison with East Antarctic and new Andean ice core data. *Quaternary Science*
1833 *Reviews*, In Press.

1834 Delmonte, B., Basile-Doelsch, I., Petit, J.R., Maggi, V., Revel-Rolland, M., Michard, A.,
1835 Jagoutz, E. and Grousset, F., 2004. Comparing the Epica and Vostok dust records during
1836 the last 220,000 years: stratigraphical correlation and provenance in glacial periods.
1837 *Earth-Science Reviews*, 66(1-2): 63-87.

1838 Delmonte, B., Delmas, R.J. and Petit, J.R., 2008. Comment on "Dust provenance in Antarctic ice
1839 during glacial periods: From where in southern South America?" by D. M. Gaiero.
1840 *Geophysical Research Letters*, 35(8): L08707.

1841 Desboeufs, K.V., Sofikitis, A., Losno, R., Colin, J.L. and Ausset, P., 2005. Dissolution and
1842 solubility of trace metals from natural and anthropogenic aerosol particulate matter.
1843 *Chemosphere*, 58(2): 195-203.

1844 Dezileau, L., Bareille, B. and Reyss, J.L., 2003. The Pa-231/Th-230 ratio as a proxy for past
1845 changes in opal fluxes in the Indian sector of the Southern Ocean. *Marine Chemistry*,
1846 81(3-4): 105-117.

1847 Diekmann, B., 2007. Sedimentary patterns in the late Quaternary Southern Ocean. *Deep-Sea*
1848 *Research Part II*, 54(21-22): 2350-2366.

1849 Diekmann, B. and Kuhn, G., 2002. Sedimentary record of the mid-Pleistocene climate transition
1850 in the southeastern South Atlantic (ODP Site 1090). *Palaeogeography Palaeoclimatology*
1851 *Palaeoecology*, 182(3-4): 241-258.

1852 Ding, Z.L., Ranov, V., Yang, S.L., Finaev, A., Han, J.M. and Wang, G.A., 2002. The loess
1853 record in southern Tajikistan and correlation with Chinese loess. *Earth And Planetary*
1854 *Science Letters*, 200(3-4): 387-400.

1855 Dubovik, O., Lapyonok, T., Kaufman, Y.J., Chin, M., Ginoux, P., Kahn, R.A. and Sinyuk, A.,
1856 2008. Retrieving global aerosol sources from satellites using inverse modeling.
1857 *Atmospheric Chemistry and Physics*, 8(2): 209-250.

1858 Duce, R.A., Liss, P.S., Merrill, J.T., Atlas, E.L., Buat-Menard, P., Hicks, B.B., Miller, J.M.,
1859 Prospero, J.M., Arimoto, R., Church, T.M., Ellis, W., Galloway, J.N., Hansen, L.,
1860 Jickells, T.D., Knap, A.H., Reinhardt, K.H., Schneider, B., Soudine, A., Tokos, J.J.,
1861 Tsunogai, S., Wollast, R. and Zhou, M., 1991. The atmospheric input of trace species to
1862 the world ocean. *Global Biogeochemical Cycles*, 5(3): 193-259.

1863 Duce, R.A., Unni, C.K., Ray, B.J., Prospero, J.M. and Merrill, J.T., 1980. Long-range
1864 atmospheric transport of soil dust from Asia to the tropical North Pacific: temporal
1865 variability. *Science*, 209(4464): 1522-4.

1866 Dulhunty, J.A., 1982. Holocene sedimentary environments in Lake Eyre, South-Australia.
1867 *Journal of the Geological Society of Australia*, 29(3-4): 437-442.

1868 Eden, D.N. and Hammond, A.P., 2003. Dust accumulation in the New Zealand region since the
1869 last glacial maximum. *Quaternary Science Reviews*, 22(18-19): 2037-2052.

1870 Engelstaedter, S., Kohfeld, K.E., Tegen, I. and Harrison, S.P., 2003. Controls of dust emissions
1871 by vegetation and topographic depressions: An evaluation using dust storm frequency
1872 data. *Geophysical Research Letters*, 30(6): L1294.

1873 Engelstaedter, S., Tegen, I. and Washington, R., 2006. North African dust emissions and
1874 transport. *Earth-Science Reviews*, 79(1-2): 73-100.

1875 Engelstaedter, S. and Washington, R., 2007. Atmospheric controls on the annual cycle of North
1876 African dust. *Journal of Geophysical Research-Atmospheres*, 112(D3): D03103.

1877 EPICA Community Members, 2004. Eight glacial cycles from an Antarctic ice core. *Nature*,
1878 429(6992): 623-628.

1879 Falkowski, P.G., 1997. Evolution of the nitrogen cycle and its influence on the biological
1880 sequestration of CO₂ in the ocean. *Nature*, 387(6630): 272-275.

1881 Field, C.B., Behrenfeld, M.J., Randerson, J.T. and Falkowski, P., 1998. Primary production of
1882 the biosphere: Integrating terrestrial and oceanic components. *Science*, 281(5374): 237-
1883 240.

1884 Fischer, H., Fundel, F., Ruth, U., Twarloh, B., Wegner, A., Udisti, R., Becagli, S., Castellano, E.,
1885 Morganti, A., Severi, M., Wolff, E., Littot, G., Rothlisberger, R., Mulvaney, R., Hutterli,
1886 M.A., Kaufmann, P., Federer, U., Lambert, F., Bigler, M., Hansson, M., Jonsell, U., de
1887 Angelis, M., Boutron, C., Siggaard-Andersen, M.L., Steffensen, J.P., Barbante, C.,
1888 Gaspari, V., Gabrielli, P. and Wagenbach, D., 2007a. Reconstruction of millennial
1889 changes in dust emission, transport and regional sea ice coverage using the deep EPICA
1890 ice cores from the Atlantic and Indian Ocean sector of Antarctica. *Earth And Planetary
1891 Science Letters*, 260(1-2): 340-354.

1892 Fischer, H., Siggaard-Andersen, M.L., Ruth, U., Rothlisberger, R. and Wolff, E., 2007b.
1893 Glacial/interglacial changes in mineral dust and sea-salt records in polar ice cores:
1894 Sources, transport, and deposition. *Reviews of Geophysics*, 45(1): RG1002.

1895 Francois, R. and Bacon, M.P., 1991. Variations in terrigenous input into the deep equatorial
1896 Atlantic during the past 24,000 years. *Science*, 251(5000): 1473-1476.

1897 Francois, R., Frank, M., van der Loeff, M.M.R. and Bacon, M.P., 2004. Th-230 normalization:
1898 An essential tool for interpreting sedimentary fluxes during the late Quaternary.
1899 *Paleoceanography*, 19(1): PA1018.

1900 Frechen, M. and Dodonov, A.E., 1998. Loess chronology of the Middle and Upper Pleistocene in
1901 Tadjikistan. *Geologische Rundschau*, 87(1): 2-20.

1902 Frechen, M., Horvath, E. and Gabris, G., 1997. Geochronology of Middle and Upper Pleistocene
1903 Loess sections in Hungary. *Quaternary Research*, 48(3): 291-312.

1904 Fung, I.Y., Meyn, S.K., Tegen, I., Doney, S.C., John, J.G. and Bishop, J.K.B., 2000. Iron supply
1905 and demand in the upper ocean. *Global Biogeochemical Cycles*, 14(1): 281-295.

1906 Gabric, A.J., Cropp, R., Ayers, G.P., McTainsh, G. and Braddock, R., 2002. Coupling between
1907 cycles of phytoplankton biomass and aerosol optical depth as derived from SeaWiFS time
1908 series in the Subantarctic Southern Ocean. *Geophysical Research Letters*, 29(7): 1112.

1909 Gaiero, D.M., 2007. Dust provenance in Antarctic ice during glacial periods:
1910 From where in southern South America? *Geophysical Research Letters* 34,
1911 L17707.

1912 Gaiero, D.M., Brunet, F., Probst, J.L. and Depetris, P.J., 2007. A uniform isotopic and chemical
1913 signature of dust exported from Patagonia: Rock sources and occurrence in southern
1914 environments. *Chemical Geology*, 238(1-2): 107-120.

1915 Gaiero, D.M., Depetris, P.J., Probst, J.L., Bidart, S.M. and Leleyter, L., 2004. The signature of
1916 river- and wind-borne materials exported from Patagonia to the southern latitudes: a view
1917 from REEs and implications for paleoclimatic interpretations. *Earth And Planetary
1918 Science Letters*, 219(3-4): 357-376.

1919 Gaiero, D.M., Probst, J.L., Depetris, P.J., Bidart, S.M. and Leleyter, L., 2003. Iron and other
1920 transition metals in Patagonian riverborne and windborne materials: Geochemical control
1921 and transport to the southern South Atlantic Ocean. *Geochimica Et Cosmochimica Acta*,
1922 67(19): 3603-3623.

1923 Gao, Y., Arimoto, R., Duce, R.A., Zhang, X.Y., Zhang, G.Y., An, Z.S., Chen, L.Q., Zhou, M.Y.
1924 and Gu, D.Y., 1997. Temporal and spatial distributions of dust and its deposition to the
1925 China Sea. *Tellus Series B-Chemical and Physical Meteorology*, 49(2): 172-189.

1926 Gao, Y., Arimoto, R., Zhou, M.Y., Merrill, J.T. and Duce, R.A., 1992. Relationships between the
1927 dust concentrations over eastern Asia and the remote North Pacific. *Journal Of*
1928 *Geophysical Research-Atmospheres*, 97(D9): 9867-9872.

1929 Garstang, M., Tyson, P.D., Swap, R., Edwards, M., Kallberg, P. and Lindsay, J.A., 1996.
1930 Horizontal and vertical transport of air over southern Africa. *Journal Of Geophysical*
1931 *Research-Atmospheres*, 101(D19): 23721-23736.

1932 Gasso, S. and Stein, A.F., 2007. Does dust from Patagonia reach the sub-Antarctic Atlantic
1933 ocean? *Geophysical Research Letters*, 34(1): L01801.

1934 Gebhardt, H., Sarnthein, M., Grootes, P.M., Kiefer, T., Kuehn, H., Schmieder, F. and Rohl, U.,
1935 2008. Paleonutrient and productivity records from the subarctic North Pacific for
1936 Pleistocene glacial terminations I to V. *Paleoceanography*, 23(4): 21.

1937 Gillette, D., 1978. Wind-tunnel simulation of erosion of soil - effect of soil texture, sandblasting,
1938 wind speed, and soil consolidation on dust production. *Atmospheric Environment*, 12(8):
1939 1735-1743.

1940 Ginoux, P., Chin, M., Tegen, I., Prospero, J.M., Holben, B., Dubovik, O. and Lin, S.J., 2001.
1941 Sources and distributions of dust aerosols simulated with the GOCART model. *Journal of*
1942 *Geophysical Research-Atmospheres*, 106(D17): 20255-20273.

1943 Ginoux, P., Prospero, J.M., Torres, O. and Chin, M., 2004. Long-term simulation of global dust
1944 distribution with the GOCART model: correlation with North Atlantic Oscillation.
1945 Environmental Modelling & Software, 19(2): 113-128.

1946 Gomes, L. and Gillette, D.A., 1993. A comparison of characteristics of aerosol from dust storms
1947 in central-asia with soil-derived dust from other regions. Atmospheric Environment Part
1948 a-General Topics, 27(16): 2539-2544.

1949 Grini, A. and Zender, C.S., 2004. Roles of saltation, sandblasting, and wind speed variability on
1950 mineral dust aerosol size distribution during the Puerto Rican Dust Experiment (PRIDE).
1951 Journal of Geophysical Research-Atmospheres, 109(D7): D07202.

1952 Grousset, F.E., Biscaye, P.E., Revel, M., Petit, J.R., Pye, K., Joussaume, S. and Jouzel, J., 1992.
1953 Antarctic (Dome C) Ice-Core Dust At 18 Ky Bp - Isotopic Constraints On Origins. Earth
1954 And Planetary Science Letters, 111(1): 175-182.

1955 Han, Q., Moore, J.K., Zender, C., Measures, C. and Hydes, D., 2008. Constraining oceanic dust
1956 deposition using surface ocean dissolved Al. Global Biogeochemical Cycles, 22(2):
1957 GB2003.

1958 Harrison, S.P., Kohfeld, K.E., Roelandt, C. and Claquin, T., 1999. The role of dust in climate
1959 changes today, at the last glacial maximum and in the future, International Conference of
1960 Loessfest 99. Elsevier Science Bv, Bonn, Germany, pp. 43-80.

1961 Hays, J.D. and Morley, J.J., 2003. The Sea of Okhotsk: A window on the ice age ocean. Deep-
1962 Sea Research Part I, 50(12): 1481-1506.

1963 Haywood, J.M., Allan, R.P., Culverwell, I., Slingo, T., Milton, S., Edwards, J. and Clerbaux, N.,
1964 2005. Can desert dust explain the outgoing longwave radiation anomaly over the Sahara
1965 during July 2003? *Journal of Geophysical Research-Atmospheres*, 110(D5): D05105.

1966 Herman, J.R., Bhartia, P.K., Torres, O., Hsu, C., Seftor, C. and Celarier, E., 1997. Global
1967 distribution of UV-absorbing aerosols from Nimbus 7/TOMS data. *Journal Of*
1968 *Geophysical Research-Atmospheres*, 102(D14): 16911-16922.

1969 Herman, J.R. and Celarier, E.A., 1997. Earth surface reflectivity climatology at 340-380 nm
1970 from TOMS data. *Journal of Geophysical Research-Atmospheres*, 102(D23): 28003-
1971 28011.

1972 Hesse, P.P., 1994. The Record of Continental Dust from Australia in Tasman Sea Sediments.
1973 *Quaternary Science Reviews*, 13(3): 257-272.

1974 Hesse, P.P., 1997. Mineral magnetic 'tracing' of aeolian dust in southwest Pacific sediments.
1975 *Palaeogeography Palaeoclimatology Palaeoecology*, 131(3-4): 327-353.

1976 Hesse, P.P., Humphreys, G.S., Smith, B.L., Campbell, J. and Peterson, E.K., 2003.
1977 Accumulation and preservation of loess deposits in the Central Tablelands of New South
1978 Wales. In: I.C. Roach (Editor), *Advances in Regolith*. CRC LEME, Canberra, pp. 170-
1979 173.

1980 Hesse, P.P. and McTainsh, G.H., 1999. Last glacial maximum to early holocene wind strength in
1981 the mid-latitudes of the Southern Hemisphere from aeolian dust in the Tasman Sea.
1982 *Quaternary Research*, 52(3): 343-349.

- 1983 Hesse, P.P. and McTainsh, G.H., 2003. Australian dust deposits: modern processes and the
1984 Quaternary record. *Quaternary Science Reviews*, 22(18-19): 2007-2035.
- 1985 Honda, M.C., Kawakami, H., Sasaoka, K., Watanabe, S. and Dickey, T., 2006. Quick transport
1986 of primary produced organic carbon to the ocean interior. *Geophysical Research Letters*,
1987 33(16): L16603.
- 1988 Honjo, S., Dymond, J., Collier, R. and Manganini, S.J., 1995. Export production of particles to
1989 the interior of the equatorial Pacific Ocean during the 1992 EQPAC experiment. *Deep-
1990 Sea Research Part II*, 42(2-3): 831-870.
- 1991 Hovan, S.A., Rea, D.K. and Pisias, N., 1991. Late Pleistocene Continental Climate and Oceanic
1992 Variability Recorded in Northwest Pacific Sediments. *Paleoceanography*, 6(3): 349-370.
- 1993 Hovan, S.A., Rea, D.K., Pisias, N.G. and Shackleton, N.J., 1989. A direct link between the China
1994 loess and marine delta-O-18 records - aeolian flux to the North Pacific. *Nature*,
1995 340(6231): 296-298.
- 1996 Hughes, T., 1992. Abrupt climatic change related to unstable ice-sheet dynamics: toward a new
1997 paradigm. *Palaeogeography Palaeoclimatology Palaeoecology*, 97(3): 203-234.
- 1998 Husar, R.B., Prospero, J.M. and Stowe, L.L., 1997. Characterization of tropospheric aerosols
1999 over the oceans with the NOAA advanced very high resolution radiometer optical
2000 thickness operational product. *Journal Of Geophysical Research-Atmospheres*, 102(D14):
2001 16889-16909.

2002 IPCC, 2001a. Penner, J., Andreae, M., Annegarn, H., Barrie, L., Feichter, J., Hegg, D.,
2003 Jayaraman, A., Leaitch, R., Murphy, D., Nganga, J., Pitari, G., 2001: Aerosols, their
2004 Direct and Indirect Effects. In: Climate Change 2001: The Scientific Basis. Contribution
2005 of Working Group I to the Third Assessment Report of the Intergovernmental Panel on
2006 Climate Change [Houghton, J.T., Y. Ding, D.J. Griggs, M. Noguer, P.J. van der Linden,
2007 X. Dai, K. Maskell, and C.A. Johnson (eds.)]. Cambridge University Press, Cambridge,
2008 United Kingdom and New York, NY, USA.

2009 IPCC, 2001b. V. Ramaswamy, V., Boucher, O., Haigh, J., Hauglustaine, D., Haywood, J.,
2010 Myhre, G., Nakajima, T., Shi, G.Y., Solomon, S., 2001: Radiative Forcing of Climate
2011 Change. In: Climate Change 2001: The Scientific Basis. Contribution of Working Group
2012 I to the Third Assessment Report of the Intergovernmental Panel on Climate Change
2013 [Houghton, J.T., Y. Ding, D.J. Griggs, M. Noguer, P.J. van der Linden, X. Dai, K.
2014 Maskell, and C.A. Johnson (eds.)]. Cambridge University Press, Cambridge, United
2015 Kingdom and New York, NY, USA.

2016 IPCC, 2007. Forster, P., V. Ramaswamy, P. Artaxo, T. Berntsen, R. Betts, D.W. Fahey, J.
2017 Haywood, J. Lean, D.C. Lowe, G. Myhre, J. Nganga, R. Prinn, G. Raga, M. Schulz and
2018 R. Van Dorland, 2007: Changes in Atmospheric Constituents and in Radiative Forcing.
2019 In: Climate Change 2007: The Physical Science Basis. Contribution of Working Group I
2020 to the Fourth Assessment Report of the Intergovernmental Panel on Climate Change
2021 [Solomon, S., D. Qin, M. Manning, Z. Chen, M. Marquis, K.B. Averyt, M. Tignor and
2022 H.L. Miller (eds.)]. Cambridge University Press, Cambridge, United Kingdom and New
2023 York, NY, USA.

- 2024 Iriondo, M., 2000. Patagonian dust in Antarctica. *Quaternary International*, 68: 83-86.
- 2025 Ivanochko, T.S., Ganeshram, R.S., Brummer, G.J.A., Ganssen, G., Jung, S.J.A., Moreton, S.G.
2026 and Kroon, D., 2005. Variations in tropical convection as an amplifier of global climate
2027 change at the millennial scale. *Earth And Planetary Science Letters*, 235(1-2): 302-314.
- 2028 Jaccard, S.L., Haug, G.H., Sigman, D.M., Pedersen, T.F., Thierstein, H.R. and Rohl, U., 2005.
2029 Glacial/interglacial changes in subarctic North Pacific stratification. *Science*, 308(5724):
2030 1003-1006.
- 2031 Janecek, T.R., 1985. Eolian sedimentation in the northwest Pacific Ocean - a preliminary
2032 examination of the data from Deep-Sea Drilling Project Site-576 and Site-578. Initial
2033 Reports of the Deep Sea Drilling Project, 86(NOV): 589-603.
- 2034 Jeong, G.Y., Hillier, S. and Kemp, R.A., 2008. Quantitative bulk and single-particle mineralogy
2035 of a thick Chinese loess-paleosol section: implications for loess provenance and
2036 weathering. *Quaternary Science Reviews*, 27(11-12): 1271-1287.
- 2037 Ji, J.F., Chen, J., Balsam, W., Lu, H.Y., Sun, Y.B. and Xu, H.F., 2004. High resolution
2038 hematite/goethite records from Chinese loess sequences for the last glacial-interglacial
2039 cycle: Rapid climatic response of the East Asian Monsoon to the tropical Pacific.
2040 *Geophysical Research Letters*, 31(3): L03207.
- 2041 Jickells, T.D., An, Z.S., Andersen, K.K., Baker, A.R., Bergametti, G., Brooks, N., Cao, J.J.,
2042 Boyd, P.W., Duce, R.A., Hunter, K.A., Kawahata, H., Kubilay, N., laRoche, J., Liss, P.S.,
2043 Mahowald, N., Prospero, J.M., Ridgwell, A.J., Tegen, I. and Torres, R., 2005. Global iron

2044 connections between desert dust, ocean biogeochemistry, and climate. *Science*,
2045 308(5718): 67-71.

2046 Jin, X., Gruber, N., Frenzel, H., Doney, S.C. and McWilliams, J.C., 2008. The impact on
2047 atmospheric CO₂ of iron fertilization induced changes in the ocean's biological pump.
2048 *Biogeosciences*, 5(2): 385-406.

2049 Johansen, A.M. and Key, J.M., 2006. Photoreductive dissolution of ferrihydrite by
2050 methanesulfonic acid: Evidence of a direct link between dimethylsulfide and iron-
2051 bioavailability. *Geophysical Research Letters*, 33(14): L14818.

2052 Johansen, A.M., Siefert, R.L. and Hoffmann, M.R., 2000. Chemical composition of aerosols
2053 collected over the tropical North Atlantic Ocean. *Journal of Geophysical Research-
2054 Atmospheres*, 105(D12): 15277-15312.

2055 Johnson, K.S., Gordon, R.M. and Coale, K.H., 1997. What controls dissolved iron concentrations
2056 in the world ocean? *Marine Chemistry*, 57(3-4): 137-161.

2057 Journet, E., Desboeufs, K.V., Caquineau, S. and Colin, J.L., 2008. Mineralogy as a critical factor
2058 of dust iron solubility. *Geophysical Research Letters*, 35(7): L07805.

2059 Jouzel, J., Masson-Delmotte, V., Cattani, O., Dreyfus, G., Falourd, S., Hoffmann, G., Minster,
2060 B., Nouet, J., Barnola, J.M., Chappellaz, J., Fischer, H., Gallet, J.C., Johnsen, S.,
2061 Leuenberger, M., Loulergue, L., Luethi, D., Oerter, H., Parrenin, F., Raisbeck, G.,
2062 Raynaud, D., Schilt, A., Schwander, J., Selmo, E., Souchez, R., Spahni, R., Stauffer, B.,
2063 Steffensen, J.P., Stenni, B., Stocker, T.F., Tison, J.L., Werner, M. and Wolff, E.W., 2007.

2064 Orbital and millennial Antarctic climate variability over the past 800,000 years. *Science*,
2065 317(5839): 793-796.

2066 Kahnert, M., Nousiainen, T. and Raisanen, P., 2007. Mie simulations as an error source in
2067 mineral aerosol radiative forcing calculations. *Quarterly Journal of the Royal*
2068 *Meteorological Society*, 133(623): 299-307.

2069 Kaufman, Y.J., Tanre, D. and Boucher, O., 2002. A satellite view of aerosols in the climate
2070 system. *Nature*, 419(6903): 215-223.

2071 Kawahata, H., Okamoto, T., Matsumoto, E. and Ujiie, H., 2000. Fluctuations of eolian flux and
2072 ocean productivity in the mid-latitude North Pacific during the last 200 kyr. *Quaternary*
2073 *Science Reviews*, 19(13): 1279-1291.

2074 Kemp, R.A., Toms, P.S., King, M. and Krohling, D.M., 2004. The pedosedimentary evolution
2075 and chronology of Tortugas, a Late Quaternary type-site of the northern Pampa,
2076 Argentina. *Quaternary International*, 114: 101-112.

2077 Kohfeld, K.E. and Harrison, S.P., 2001. DIRTMAP: the geological record of dust. *Earth-Science*
2078 *Reviews*, 54(1-3): 81-114.

2079 Kohfeld, K.E. and Harrison, S.P., 2003. Glacial-interglacial changes in dust deposition on the
2080 Chinese Loess Plateau. *Quaternary Science Reviews*, 22(18-19): 1859-1878.

2081 Kohfeld, K.E., Le Quere, C., Harrison, S.P. and Anderson, R.F., 2005. Role of marine biology in
2082 glacial-interglacial CO₂ cycles. *Science*, 308(5718): 74-78.

2083 Koren, I., Kaufman, Y.J., Washington, R., Todd, M., Rudich, Y., Martins, J.V. and Rosenfeld,
2084 D., 2007. The Bodele depression: a single spot in the Sahara that provides most of the
2085 mineral dust to the Amazon forest. *Environmental Research Letters*, 1: 014005.

2086 Krinner, G. and Genthon, C., 2003. Tropospheric transport of continental tracers towards
2087 Antarctica under varying climatic conditions. *Tellus Series B-Chemical and Physical*
2088 *Meteorology*, 55(1): 54-70.

2089 Krinner G., Boucher, O. and Balkanski, Y.. 2006. Reduced glacial ice sheet extent in Northern
2090 Asia and Alaska owing to deposition of mineral dust on snow, *Geophysical Research*
2091 *Letters*, 10.1007/s00382-006-0159-z.

2092 Krohling, D.M. and Iriondo, M., 1999. Upper Quaternary Palaeoclimates of the Mar Chiquita
2093 area, North Pampa, Argentina. *Quaternary International*, 57-8: 149-163.

2094 Kubilay, N., Oguz, T., Kocak, M. and Torres, O., 2005. Ground-based assessment of Total
2095 Ozone Mapping Spectrometer (TOMS) data for dust transport over the northeastern
2096 Mediterranean. *Global Biogeochemical Cycles*, 19(1): GB1022.

2097 Kukla, G., 1987. Loess stratigraphy in central China. *Quaternary Science Reviews*, 6(3-4): 191-
2098 219.

2099 Kumar, N., Anderson, R.F., Mortlock, R.A., Froelich, P.N., Kubik, P., Dittrichhannen, B. and
2100 Suter, M., 1995. Increased biological productivity and export production in the glacial
2101 Southern Ocean. *Nature*, 378(6558): 675-680.

2102 Lafon, S., Sokolik, I.N., Rajot, J.L., Caquineau, S. and Gaudichet, A., 2006. Characterization of
2103 iron oxides in mineral dust aerosols: Implications for light absorption. *Journal Of*
2104 *Geophysical Research-Atmospheres*, 111(D21): D21207.

2105 Lambert, F., Delmonte, B., Petit, J.R., Bigler, M., Kaufmann, P., Hutterli, M.A., Stocker, T.F.,
2106 Ruth, U., Steffensen, J.P. and Maggi, V., 2008. Dust-climate couplings over the past
2107 800,000 years from the EPICA Dome C ice core. *Nature*, 452(7187): 616-619.

2108 Latimer, J.C. and Filippelli, G.M., 2001. Terrigenous input and paleoproductivity in the Southern
2109 Ocean. *Paleoceanography*, 16(6): 627-643.

2110 Lee, C.H., Park, C.B. and Kim, J.H., 2004. Asian dust measurement with Mie-scattering Lidar at
2111 Suwon, Korea in the Spring of 2000-2004. In: G.G. Matvienko (Editor), *Conference on*
2112 *Optical Technologies for Atmospheric, Ocean, and Environmental Studies*. Spie-Int Soc
2113 *Optical Engineering*, Beijing, PEOPLES R CHINA, pp. 99-109.

2114 Lefevre, N. and Watson, A.J., 1999. Modeling the geochemical cycle of iron in the oceans and
2115 its impact on atmospheric CO₂ concentrations. *Global Biogeochemical Cycles*, 13(3):
2116 727-736.

2117 Lehmkuhl, F. and Owen, L.A., 2005. Late Quaternary glaciation of Tibet and the bordering
2118 mountains: a review. *Boreas*, 34(2): 87-100.

2119 Li, F., Ginoux, P. and Ramaswamy, V., 2008. Distribution, transport, and deposition of mineral
2120 dust in the Southern Ocean and Antarctica: Contribution of major sources. *Journal of*
2121 *Geophysical Research-Atmospheres*, 113(D10): D10207.

2122 Lim, J. and Matsumoto, E., 2008. Fine aeolian quartz records in Cheju Island, Korea, during the
2123 last 6500 years and pathway change of the westerlies over east Asia. *Journal Of*
2124 *Geophysical Research-Atmospheres*, 113(D8): D08106.

2125 Lisiecki, L.E. and Raymo, M.E., 2005. A Pliocene-Pleistocene stack of 57 globally distributed
2126 benthic delta O-18 records. *Paleoceanography*, 20(1): PA1003.

2127 Loubere, P., Mekik, F., Francois, R. and Pichat, S., 2004. Export fluxes of calcite in the eastern
2128 equatorial Pacific from the Last Glacial Maximum to present. *Paleoceanography*, 19(2).

2129 Lunt, D.J. and Valdes, P.J., 2002. Dust deposition and provenance at the Last Glacial Maximum
2130 and present day. *Geophysical Research Letters*, 29(22): L2085.

2131 Luo, C., Mahowald, N., Bond, T., Chuang, P.Y., Artaxo, P., Siefert, R., Chen, Y. and Schauer, J.,
2132 2008. Combustion iron distribution and deposition. *Global Biogeochemical Cycles*,
2133 22(1): GB1012.

2134 Luo, C., Mahowald, N.M. and del Corral, J., 2003. Sensitivity study of meteorological
2135 parameters on mineral aerosol mobilization, transport, and distribution. *Journal Of*
2136 *Geophysical Research-Atmospheres*, 108(D15): D154447.

2137 Luthi, D., Le Floch, M., Bereiter, B., Blunier, T., Barnola, J.M., Siegenthaler, U., Raynaud, D.,
2138 Jouzel, J., Fischer, H., Kawamura, K. and Stocker, T.F., 2008. High-resolution carbon
2139 dioxide concentration record 650,000-800,000 years before present. *Nature*, 453(7193):
2140 379-382.

2141 Lyle, M., Pisias, N., Paytan, A., Martinez, J.I. and Mix, A., 2007. Reply to comment by R.
2142 Francois et al. on "Do geochemical estimates of sediment focusing pass the sediment test
2143 in the equatorial Pacific?": Further explorations of Th-230 normalization.
2144 *Paleoceanography*, 22(1): PA1217.

2145 Machalett, B., Oches, E.A., Frechen, M., Zoller, L., Hambach, U., Mavlyanova, N.G., Markovic,
2146 S.B. and Endlicher, W., 2008. Aeolian dust dynamics in central Asia during the
2147 Pleistocene: Driven by the long-term migration, seasonality, and permanency of the
2148 Asiatic polar front. *Geochemistry Geophysics Geosystems*, 9: Q08q09.

2149 Mackie, D.S., Boyd, P.W., Hunter, K.A. and McTainsh, G.H., 2005. Simulating the cloud
2150 processing of iron in Australian dust: pH and dust concentration. *Geophysical Research*
2151 *Letters*, 32(6): L06809.

2152 Mackie, D.S., Boyd, P.W., McTainsh, G.H., Tindale, N.W., Westberry, T.K. and Hunter, K.A.,
2153 2008. Biogeochemistry of iron in Australian dust: From eolian uplift to marine uptake.
2154 *Geochemistry Geophysics Geosystems*, 9: Q03Q08.

2155 Maher, B.A., 2007. Environmental magnetism and climate change. *Contemporary Physics*,
2156 48(5): 247-274.

2157 Maher, B.A., 2009. Sourcing and quantifying aeolian dust in the Quaternary sedimentary record,
2158 Southern Ocean, EGU General Assembly 2009, pp. EGU2009-12531.

2159 Maher, B.A., Alekseev, A. and Alekseeva, T., 2003. Magnetic mineralogy of soils across the
2160 Russian Steppe: climatic dependence of pedogenic magnetite formation.
2161 *Palaeogeography Palaeoclimatology Palaeoecology*, 201(3-4): 321-341.

2162 Maher, B.A. and Dennis, P.F., 2001. Evidence against dust-mediated control of glacial-
2163 interglacial changes in atmospheric CO₂. *Nature*, 411(6834): 176-180.

2164 Maher, B.A. and Hu, M.Y., 2006. A high-resolution record of Holocene rainfall variations from
2165 the western Chinese Loess Plateau: antiphase behaviour of the African/Indian and East
2166 Asian summer monsoons. *Holocene*, 16(3): 309-319.

2167 Maher, B.A., Karloukovski, V., Sarah Watkins, S. and Mutch, T., 2007. New magnetic methods
2168 and data on deep-sea sediment dust fluxes, mineralogy and provenance., XVII INQUA
2169 Congress 2007, pp. <http://www.icms.com.au/inqua2007/abstract/475.htm>.

2170 Maher, B.A., Mutch, T.J. and Cunningham, D., 2009. Magnetic and geochemical characteristics
2171 of Gobi Desert surface sediments: Implications for provenance of the Chinese Loess
2172 Plateau. *Geology*, 37(3): 279-282.

2173 Mahowald, N., Kohfeld, K., Hansson, M., Balkanski, Y., Harrison, S.P., Prentice, I.C., Schulz,
2174 M. and Rodhe, H., 1999. Dust sources and deposition during the last glacial maximum
2175 and current climate: A comparison of model results with paleodata from ice cores and
2176 marine sediments. *Journal Of Geophysical Research-Atmospheres*, 104(D13): 15895-
2177 15916.

2178 Mahowald, N.M., Baker, A.R., Bergametti, G., Brooks, N., Duce, R.A., Jickells, T.D., Kubilay,
2179 N., Prospero, J.M. and Tegen, I., 2005. Atmospheric global dust cycle and iron inputs to
2180 the ocean. *Global Biogeochemical Cycles*, 19(4): GB4025.

2181 Mahowald, N.M., Muhs, D.R., Levis, S., Rasch, P.J., Yoshioka, M., Zender, C.S. and Luo, C.,
2182 2006a. Change in atmospheric mineral aerosols in response to climate: Last glacial

2183 period, preindustrial, modern, and doubled carbon dioxide climates. Journal Of
2184 Geophysical Research-Atmospheres, 111(D10): D10202.

2185 Mahowald, N.M., Rivera, G.D.R. and Luo, C., 2004. Comment on "Relative importance of
2186 climate and land use in determining present and future global soil dust emission" by I.
2187 Tegen et al. Geophysical Research Letters, 31(24): L24105.

2188 Mahowald, N.M., Yoshioka, M., Collins, W.D., Conley, A.J., Fillmore, D.W. and Coleman,
2189 D.B., 2006b. Climate response and radiative forcing from mineral aerosols during the last
2190 glacial maximum, pre-industrial, current and doubled-carbon dioxide climates.
2191 Geophysical Research Letters, 33(20): L20705.

2192 Maring, H., Savoie, D.L., Izaguirre, M.A., Custals, L. and Reid, J.S., 2003. Mineral dust aerosol
2193 size distribution change during atmospheric transport. Journal of Geophysical Research-
2194 Atmospheres, 108(D19): D8592.

2195 Marino, F., Castellano, E., Ceccato, D., De Deckker, P., Delmonte, B., Ghermandi, G., Maggi,
2196 V., Petit, J.R., Revel-Rolland, M. and Udisti, R., 2008. Defining the geochemical
2197 composition of the EPICA Dome C ice core dust during the last glacial-interglacial cycle.
2198 Geochemistry Geophysics Geosystems, 9: Q10018.

2199 Marshall, S.J., Tarasov, L., Clarke, G.K.C. and Peltier, W.R., 2000. Glaciological reconstruction
2200 of the Laurentide Ice Sheet: physical processes and modelling challenges. Canadian
2201 Journal of Earth Sciences, 37(5): 769-793.

2202 Marticorena, B. and Bergametti, G., 1995. Modeling the atmospheric dust cycle .1. Design of a
2203 soil-derived dust emission scheme. Journal of Geophysical Research-Atmospheres,
2204 100(D8): 16415-16430.

2205 Marticorena, B., Bergametti, G., Aumont, B., Callot, Y., Ndoume, C. and Legrand, M., 1997.
2206 Modeling the atmospheric dust cycle .2. Simulation of Saharan dust sources. Journal of
2207 Geophysical Research-Atmospheres, 102(D4): 4387-4404.

2208 Martin, J.H., 1990. Glacial-interglacial CO2 change: the iron hypothesis. Paleocyanography,
2209 5(1): 1-13.

2210 Martin, J.H., Gordon, R.M. and Fitzwater, S.E., 1991. The Case for Iron. Limnology and
2211 Oceanography, 36(8): 1793-1802.

2212 Martinez-Garcia, A., Rosell-Mele, A., Geibert, W., Gersonde, R., Masque, P., Gaspari, V. and
2213 Barbante, C., 2009. Links between iron supply, marine productivity, sea surface
2214 temperature, and CO2 over the last 1.1 Ma. Paleocyanography, 24: PA1207.

2215 Marx, S.K., Kamber, B.S. and McGowan, H., 2005a. Provenance of long-travelled dust
2216 determined with ultra-trace-element composition: a pilot study with samples from New
2217 Zealand glaciers. Earth Surface Processes and Landforms, 30(6): 699-716.

2218 Marx, S.K., Kamber, B.S. and McGowan, H.A., 2005b. Estimates of Australian dust flux into
2219 New Zealand: Quantifying the eastern Australian dust plume pathway using trace
2220 element calibrated Pb-210 as a monitor. Earth And Planetary Science Letters, 239(3-4):
2221 336-351.

- 2222 Mason, B.G., Pyle, D.M. and Oppenheimer, C., 2004. The size and frequency of the largest
2223 explosive eruptions on Earth. *Bulletin Of Volcanology*, 66(8): 735-748.
- 2224 McConnell, J.R., Aristarain, A.J., Banta, J.R., Edwards, P.R. and Simoes, J.C., 2007. 20th-
2225 Century doubling in dust archived in an Antarctic Peninsula ice core parallels climate
2226 change and desertification in South America. *Proceedings Of The National Academy Of
2227 Sciences Of The United States Of America*, 104(14): 5743-5748.
- 2228 McGee, D., Marcantonio, F. and Lynch-Stieglitz, J., 2007. Deglacial changes in dust flux in the
2229 eastern equatorial Pacific. *Earth And Planetary Science Letters*, 257(1-2): 215-230.
- 2230 McGowan, H. and Clark, A., 2008. Identification of dust transport pathways from Lake Eyre,
2231 Australia using Hysplit. *Atmospheric Environment*, 42(29): 6915-6925.
- 2232 McGowan, H.A., Kamber, B., McTainsh, G.H. and Marx, S.K., 2005. High resolution
2233 provenancing of long travelled dust deposited on the Southern Alps, New Zealand.
2234 *Geomorphology*, 69(1-4): 208-221.
- 2235 McGowan, H.A., McTainsh, G.H., Zawar-Reza, P. and Sturman, A.P., 2000. Identifying regional
2236 dust transport pathways: Application of kinematic trajectory modelling to a trans-Tasman
2237 case. *Earth Surface Processes and Landforms*, 25(6): 633-647.
- 2238 McTainsh, G., Chan, Y.C., McGowan, H., Leys, J. and Tews, K., 2005. The 23rd October 2002
2239 dust storm in eastern Australia: characteristics and meteorological conditions.
2240 *Atmospheric Environment*, 39(7): 1227-1236.

2241 McTainsh, G.H., 1989. Quaternary Aeolian Dust Processes and Sediments in the Australian
2242 Region. *Quaternary Science Reviews*, 8(3): 235-253.

2243 McTainsh, G.H. and Lynch, A.W., 1996. Quantitative estimates of the effect of climate change
2244 on dust storm activity in Australia during the Last Glacial Maximum. *Geomorphology*,
2245 17(1-3): 263-271.

2246 Measures, C.I., Landing, W.M., Brown, M.T. and Buck, C.S., 2008. High-resolution Al and Fe
2247 data from the Atlantic Ocean CLIVAR-CO2 repeat hydrography A16N transect:
2248 Extensive linkages between atmospheric dust and upper ocean geochemistry. *Global*
2249 *Biogeochemical Cycles*, 22(1): GB1005.

2250 Middleton, N.J., Betzer, P.R. and Bull, P.A., 2001. Long-range transport of 'giant' aeolian quartz
2251 grains: linkage with discrete sedimentary sources and implications for protective particle
2252 transfer. *Marine Geology*, 177(3-4): 411-417.

2253 Miller, R.L., Cakmur, R.V., Perlwitz, J., Geogdzhayev, I.V., Ginoux, P., Koch, D., Kohfeld,
2254 K.E., Prigent, C., Ruedy, R., Schmidt, G.A. and Tegen, I., 2006. Mineral dust aerosols in
2255 the NASA Goddard institute for Space Sciences ModelE atmospheric general circulation
2256 model. *Journal Of Geophysical Research-Atmospheres*, 111(D6): D06208.

2257 Miller, R.L. and Tegen, I., 1998. Climate response to soil dust aerosols. *Journal of Climate*,
2258 11(12): 3247-3267.

2259 Miller, R.L., Tegen, I. and Perlwitz, J., 2004. Surface radiative forcing by soil dust aerosols and
2260 the hydrologic cycle. *Journal of Geophysical Research-Atmospheres*, 109(D4): D04203.

2261 Mitchell, N.C. and Lyle, M.W., 2005. Patchy deposits of Cenozoic pelagic sediments in the
2262 central Pacific. *Geology*, 33(1): 49-52.

2263 Moore, J.K. and Braucher, O., 2008. Sedimentary and mineral dust sources of dissolved iron to
2264 the world ocean. *Biogeosciences*, 5(3): 631-656.

2265 Moore, J.K. and Doney, S.C., 2007. Iron availability limits the ocean nitrogen inventory
2266 stabilizing feedbacks between marine denitrification and nitrogen fixation. *Global
2267 Biogeochemical Cycles*, 21(2): GB2001.

2268 Moore, J.K., Doney, S.C., Glover, D.M. and Fung, I.Y., 2002. Iron cycling and nutrient-
2269 limitation patterns in surface waters of the World Ocean. *Deep-Sea Research Part II*,
2270 49(1-3): 463-507.

2271 Moore, J.K., Doney, S.C. and Lindsay, K., 2004a. Upper ocean ecosystem dynamics and iron
2272 cycling in a global three-dimensional model. *Global Biogeochemical Cycles*, 18(4):
2273 4028.

2274 Moore, J.K., Doney, S.C., Lindsay, K., Mahowald, N. and Michaels, A.F., 2006. Nitrogen
2275 fixation amplifies the ocean biogeochemical response to decadal timescale variations in
2276 mineral dust deposition. *Tellus Series B-Chemical and Physical Meteorology*, 58(5): 560-
2277 572.

2278 Moore, K.G., Clarke, A.D., Kapustin, V.N., McNaughton, C., Anderson, B.E., Winstead, E.L.,
2279 Weber, R., Ma, Y., Lee, Y.N., Talbot, R., Dibb, J., Anderson, T., Doherty, S., Covert, D.
2280 and Rogers, D., 2004b. A comparison of similar aerosol measurements made on the

2281 NASA P3-B, DC-8, and NSFC-130 aircraft during TRACE-P and ACE-Asia. *Journal of*
2282 *Geophysical Research-Atmospheres*, 109(D15): D15s15.

2283 Moorthy, K.K., Babu, S.S., Satheesh, S.K., Srinivasan, J. and Dutt, C.B.S., 2007. Dust
2284 absorption over the "Great Indian Desert" inferred using ground-based and satellite
2285 remote sensing. *Journal of Geophysical Research-Atmospheres*, 112(D9): D09206.

2286 Moreno, T., Querol, X., Castillo, S., Alastuey, A., Cuevas, E., Herrmann, L., Mounkaila, M.,
2287 Elvira, J. and Gibbons, W., 2006. Geochemical variations in aeolian mineral particles
2288 from the Sahara-Sahel Dust Corridor. *Chemosphere*, 65(2): 261-270.

2289 Moulin, C., Lambert, C.E., Dulac, F. and Dayan, U., 1997. Control of atmospheric export of dust
2290 from North Africa by the North Atlantic oscillation. *Nature*, 387(6634): 691-694.

2291 Murray, R.W., Leinen, M., Murray, D.W., Mix, A.C. and Knowlton, C.W., 1995. Terrigenous Fe
2292 input and biogenic sedimentation in the glacial and interglacial equatorial Pacific Ocean.
2293 *Global Biogeochemical Cycles*, 9(4): 667-684.

2294 Myhre, G., 2009. Consistency Between Satellite-Derived and Modelled Estimates of the Direct
2295 Aerosol Effect. *Science*, 325(5937): 187-190.

2296 Narcisi, B., Petit, J.R., Delmonte, B., Basile-Doelsch, I. and Maggi, V., 2005. Characteristics and
2297 sources of tephra layers in the EPICA-Dome C ice record (East Antarctica): Implications
2298 for past atmospheric circulation and ice core stratigraphic correlations. *Earth And*
2299 *Planetary Science Letters*, 239(3-4): 253-265.

2300 Nilson, E. and Lehmkuhl, F., 1999. Interpreting temporal patterns in the late Quaternary dust
2301 flux from Asia to the North Pacific, International Conference on Loess and Palaeosols -
2302 Characteristics, Stratigraphy, Chronology and Climate. Pergamon-Elsevier Science Ltd,
2303 Bonn, Germany, pp. 67-76.

2304 Nousiainen, T., 2009. Optical modeling of mineral dust particles: A review. *Journal of*
2305 *Quantitative Spectroscopy and Radiative Transfer*, 110(14-16): 1261-1279.

2306 Nousiainen, T., Zubko, E., Niemi, J.V., Kupiainen, K., Lehtinen, M., Muinonen, K. and Videen,
2307 G., 2009. Single-scattering modeling of thin, birefringent mineral-dust flakes using the
2308 discrete-dipole approximation. *Journal of Geophysical Research-Atmospheres*, 114:
2309 D07207.

2310 Olivarez, A.M., Owen, R.M. and Rea, D.K., 1991. Geochemistry Of Eolian Dust In Pacific
2311 Pelagic Sediments - Implications For Paleoclimatic Interpretations. *Geochimica Et*
2312 *Cosmochimica Acta*, 55(8): 2147-2158.

2313 Orgeira, M.J., Vasquez, C.A., Compagnucci, R.H., Raposo, I. and Pereyra, F.X., 2009. Rock
2314 magnetism in soils of the Pampean plain. Buenos Aires province, Argentina. Linking
2315 climate and magnetic behaviour. *Revista Mexicana De Ciencias Geologicas*, 26(1): 65-
2316 78.

2317 Overpeck, J., Rind, D., Lacs, A. and Healy, R., 1996. Possible role of dust-induced regional
2318 warming in abrupt climate change during the last glacial period. *Nature*, 384(6608): 447-
2319 449.

2320 Park, C.B., Lee, C.H., Kim, J.H. and Ieee, 2005. Remote sensing and statistical analysis of Asian
2321 dust measured by 532/1064 nm Lidar during 2002-2005, Pacific Rim Conference on
2322 Lasers and Electro-Optics. Ieee, Tokyo, JAPAN, pp. 736-738.

2323 Patterson, E.M. and Gillette, D.A., 1976. Measurements of visible and infrared imagery index of
2324 refraction and of size distribution for Saharan dust aerosols over Atlantic. Bulletin of the
2325 American Meteorological Society, 57(1): 146-146.

2326 Patterson, E.M. and Gillette, D.A., 1977. Measurements of visibility vs. mass-concentration for
2327 airborne soil particles. Atmospheric Environment, 11(2): 193-196.

2328 Paytan, A., Kastner, M. and Chavez, F.P., 1996. Glacial to interglacial fluctuations in
2329 productivity in the equatorial Pacific as indicated by marine barite. Science, 274(5291):
2330 1355-1357.

2331 Paytan, A., Lyle, M., Mix, A. and Chase, Z., 2004. Climatically driven changes in oceanic
2332 processes throughout the equatorial Pacific. Paleoceanography, 19(4): PA4017.

2333 Pedersen, T.F., 1983. Increased productivity in the eastern equatorial Pacific during the last
2334 glacial maximum (19,000 to 14,000 yr BP). Geology, 11(1): 16-19.

2335 Peltier, W.R., 1994. Ice Age Paleotopography. Science, 265(5169): 195-201.

2336 Peltier, W.R. and Marshall, S., 1995. Coupled energy-balance ice-sheet model simulations of the
2337 glacial cycle - a possible connection between terminations and terrigenous dust. Journal
2338 Of Geophysical Research-Atmospheres, 100(D7): 14269-14289.

2339 Perlwitz, J., Tegen, I. and Miller, R.L., 2001. Interactive soil dust aerosol model in the GISS
2340 GCM 1. Sensitivity of the soil dust cycle to radiative properties of soil dust aerosols.
2341 Journal Of Geophysical Research-Atmospheres, 106(D16): 18167-18192.

2342 Perlwitz, J., and R.L. Miller, 2009. Cloud cover increase with increasing aerosol absorptivity - A
2343 counterexample to the conventional semi-direct aerosol effect. Journal Of Geophysical
2344 Research-Atmospheres, submitted.

2345 Perry, K.D., Cahill, T.A., Eldred, R.A., Dutcher, D.D. and Gill, T.E., 1997. Long-range transport
2346 of North African dust to the eastern United States. Journal Of Geophysical Research-
2347 Atmospheres, 102(D10): 11225-11238.

2348 Petit, J.R., Briat, M. and Royer, A., 1981. Ice-age aerosol content from east antarctic ice core
2349 samples and past wind strength. Nature, 293(5831): 391-394.

2350 Petit, J.R., Jouzel, J., Raynaud, D., Barkov, N.I., Barnola, J.M., Basile, I., Bender, M.,
2351 Chappellaz, J., Davis, M., Delaygue, G., Delmotte, M., Kotlyakov, V.M., Legrand, M.,
2352 Lipenkov, V.Y., Lorius, C., Pepin, L., Ritz, C., Saltzman, E. and Stievenard, M., 1999.
2353 Climate and atmospheric history of the past 420,000 years from the Vostok ice core,
2354 Antarctica. Nature, 399(6735): 429-436.

2355 Piketh, S.J., Tyson, P.D. and Steffen, W., 2000. Aeolian transport from southern Africa and iron
2356 fertilization of marine biota in the South Indian Ocean. South African Journal of Science,
2357 96(5): 244-246.

2358 Pitty, A.F., 1968. Particle Size Of Saharan Dust Which Fell In Britain In July 1968. Nature,
2359 220(5165): 364-365.

- 2360 Pondaven, P., Ruiz-Pino, D., Druon, J.N., Fravallo, C. and Treguer, P., 1999. Factors controlling
2361 silicon and nitrogen biogeochemical cycles in high nutrient, low chlorophyll systems (the
2362 Southern Ocean and the North Pacific): Comparison with a mesotrophic system (the
2363 North Atlantic). *Deep-Sea Research Part I*, 46(11): 1923-1968.
- 2364 Pondaven, P., Ruiz-Pino, D., Fravallo, C., Treguer, P. and Jeandel, C., 2000. Interannual
2365 variability of Si and N cycles at the time-series station KERFIX between 1990 and 1995 -
2366 A 1-D modelling study. *Deep-Sea Research Part I*, 47(2): 223-257.
- 2367 Prins, M.A., Beets, C.J., Dijkstra, N., Vriend, M., Zheng, H.B. and Weltje, G.J., 2008.
2368 Unravelling the geologic dust record, 8th Annual V M Goldschmidt Conference.
2369 Pergamon-Elsevier Science Ltd, Vancouver, CANADA, pp. A762-A762.
- 2370 Prins, M.A., Vriend, M., Nugteren, G., Vandenberghe, J., Lu, H.Y., Zheng, H.B. and Weltje,
2371 G.J., 2007. Late Quaternary aeolian dust input variability on the Chinese Loess Plateau:
2372 inferences from unmixing of loess grain-size records. *Quaternary Science Reviews*, 26(1-
2373 2): 230-242.
- 2374 Prospero, J.M., 1981. Eolian transport to the World Ocean. In: C. Emiliani (Editor), *The Oceanic*
2375 *Lithosphere*. Wiley Interscience, New York, pp. 801-874.
- 2376 Prospero, J.M., 1996a. The Atmospheric Transport of Particles to the Ocean. In: V. Ittekkot, P.
2377 Schafer, S. Honjo and P.J. Depetris (Editors), *Particle Flux in the Ocean*. John Wiley &
2378 Sons Ltd, New York, pp. 372.

2379 Prospero, J.M., 1996b. Saharan dust transport over the North Atlantic Ocean and Mediterranean:
2380 an overview. Environmental Science and Technology Library, 11(Impact of Desert Dust
2381 Across the Mediterranean): 133-151.

2382 Prospero, J.M., 1999. Long-term measurements of the transport of African mineral dust to the
2383 southeastern United States: Implications for regional air quality. Journal Of Geophysical
2384 Research-Atmospheres, 104(D13): 15917-15927.

2385 Prospero, J.M. and Carlson, T.N., 1972. Vertical and areal distribution of Saharan dust over
2386 western equatorial North Atlantic Ocean. Journal of Geophysical Research, 77(27): 5255-
2387 5265.

2388 Prospero, J.M., Ginoux, P., Torres, O., Nicholson, S.E. and Gill, T.E., 2002. Environmental
2389 characterization of global sources of atmospheric soil dust identified with the Nimbus 7
2390 Total Ozone Mapping Spectrometer (TOMS) absorbing aerosol product. Reviews of
2391 Geophysics, 40(1): RG1002.

2392 Prospero, J.M. and Lamb, P.J., 2003. African droughts and dust transport to the Caribbean:
2393 Climate change implications. Science, 302(5647): 1024-1027.

2394 Prospero, J.M. and Nees, R.T., 1986. Impact of the North African drought and El Niño on
2395 mineral dust in the Barbados trade winds. Nature, 320(6064): 735-738.

2396 Prospero, J.M., Uematsu, M. and Savoie, D., 1989. Mineral aerosol transport to the Pacific
2397 Ocean. In: J.P. Riley, R. Chester and R. Duce (Editors), Chemical Oceanography.
2398 Academic Press, New York, pp. 187-218.

2399 Pye, K., 1989. Processes of fine particle formation, dust source regions, and climatic changes. .
2400 In: M. Leinen and M. Sarnthein (Editors), Paleoclimatology and Paleometeorology:
2401 Modern and Past Patterns of Global Atmospheric Transport Kluwer Academic Pubs,
2402 Dordrecht, pp. 3-30.

2403 Raiswell, R., Benning, L.G., Tranter, M. and Tulaczyk, S., 2008. Bioavailable iron in the
2404 Southern Ocean: the significance of the iceberg conveyor belt. *Geochemical*
2405 *Transactions*, 9: :7.

2406 Ramsperger, B., Peinemann, N. and Stahr, K., 1998. Deposition rates and characteristics of
2407 aeolian dust in the semi-arid and sub-humid regions of the Argentinean Pampa. *Journal of*
2408 *Arid Environments*, 39(3): 467-476.

2409 Rea, D.K., 1994. The Paleoclimatic Record Provided By Eolian Deposition In The Deep-Sea -
2410 The Geologic History Of Wind. *Reviews Of Geophysics*, 32(2): 159-195.

2411 Rea, D.K. and Hovan, S.A., 1995. Grain-size distribution and depositional processes of the
2412 mineral component of abyssal sediments - lessons from the North Pacific.
2413 *Paleoceanography*, 10(2): 251-258.

2414 Rea, D.K., Leinen, M. and Janecek, T.R., 1985. Geologic approach to the long-term history of
2415 atmospheric circulation. *Science*, 227(4688): 721-725.

2416 Reader, M.C., Fung, I. and McFarlane, N., 1999. The mineral dust aerosol cycle during the Last
2417 Glacial Maximum. *Journal Of Geophysical Research-Atmospheres*, 104(D8): 9381-9398.

2418 Reid, J.S., Jonsson, H.H., Maring, H.B., Smirnov, A., Savoie, D.L., Cliff, S.S., Reid, E.A.,
2419 Livingston, J.M., Meier, M.M., Dubovik, O. and Tsay, S.C., 2003. Comparison of size
2420 and morphological measurements of coarse mode dust particles from Africa. *Journal of*
2421 *Geophysical Research-Atmospheres*, 108(D19): D8593.

2422 Revel-Rolland, M., De Deckker, P., Delmonte, B., Hesse, P.P., Magee, J.W., Basile-Doelsch, I.,
2423 Grousset, F. and Bosch, D., 2006. Eastern Australia: A possible source of dust in East
2424 Antarctica interglacial ice. *Earth and Planetary Science Letters*, 249(1-2): 1-13.

2425 Ridgwell, A.J., 2002. Dust in the Earth system: the biogeochemical linking of land, air and sea.
2426 *Philosophical Transactions Of The Royal Society Of London Series A-Mathematical*
2427 *Physical And Engineering Sciences*, 360(1801): 2905-2924.

2428 Ridgwell, A.J. and Watson, A.J., 2002. Feedback between aeolian dust, climate, and atmospheric
2429 CO₂ in glacial time. *Paleoceanography*, 17(4): PA1059.

2430 Roberts, H.M., 2008. The development and application of luminescence dating to loess deposits:
2431 a perspective on the past, present and future. *Boreas*, 37(4): 483-507.

2432 Roberts, H.M. and Duller, G.A.T., 2004. Standardised growth curves for optical dating of
2433 sediment using multiple-grain aliquots. *Radiation Measurements*, 38(2): 241-252.

2434 Rothlisberger, R., Bigler, M., Wolff, E.W., Joos, F., Monnin, E. and Hutterli, M.A., 2004. Ice
2435 core evidence for the extent of past atmospheric CO₂ change due to iron fertilisation.
2436 *Geophysical Research Letters*, 31(16): L16207.

2437 Rothlisberger, R., Mulvaney, R., Wolff, E.W., Hutterli, M.A., Bigler, M., Sommer, S. and
2438 Jouzel, J., 2002. Dust and sea salt variability in central East Antarctica (Dome C) over the
2439 last 45 kyrs and its implications for southern high-latitude climate. *Geophysical Research*
2440 *Letters*, 29(20): L1963.

2441 Rousseau, D.D., Antoine, P., Hatte, C., Lang, A., Zoller, L., Fontugne, M., Ben Othman, D.,
2442 Luck, J.M., Moine, O., Labonne, M., Bentaleb, I. and Jolly, D., 2002. Abrupt millennial
2443 climatic changes from Nussloch (Germany) Upper Weichselian eolian records during the
2444 Last Glaciation. *Quaternary Science Reviews*, 21(14-15): 1577-1582.

2445 Ruth, U., 2005. Mineral dust records from Greenland ice cores, PAGES newsletter (invited
2446 contribution). PAGES International Project Office, Bernn., pp. 17-18.

2447 Ruth, U., Wagenbach, D., Steffensen, J.P. and Bigler, M., 2003. Continuous record of
2448 microparticle concentration and size distribution in the central Greenland NGRIP ice core
2449 during the last glacial period. *Journal Of Geophysical Research-Atmospheres*, 108(D3):
2450 D4098.

2451 Sarthou, G., Baker, A.R., Blain, S., Achterberg, E.P., Boye, M., Bowie, A.R., Croot, P., Laan, P.,
2452 de Baar, H.J.W., Jickells, T.D. and Worsfold, P.J., 2003. Atmospheric iron deposition
2453 and sea-surface dissolved iron concentrations in the eastern Atlantic Ocean. *Deep-Sea*
2454 *Research Part I*, 50(10-11): 1339-1352.

2455 Sassen, K., DeMott, P. J., Prospero, J.M. and Poellot, M.R.. 2003. Saharan dust storms and
2456 indirect aerosol effects on clouds: CRYSTAL-FACE results, *Geophysical Research*
2457 *Letters*, 30(12), 1633.

2458 Schellenberger, A. and Veit, H., 2006. Pedostratigraphy and pedological and geochemical
2459 characterization of Las Carreras loess-paleosol sequence, Valle de Tafi, NW-Argentina.
2460 Quaternary Science Reviews, 25(7-8): 811-831.

2461 Schroth, A.W., Crusius, J., Sholkovitz, E.R. and Bostick, B.C., 2009. Iron solubility driven by
2462 speciation in dust sources to the ocean. Nature Geoscience, 2(5): 337-340.

2463 Schutz, L. and Jaenicke, R., 1974. Particle number and mass distributions above 10-4 cm radius
2464 in sand and aerosol of Sahara desert. Journal of Applied Meteorology, 13(8): 863-870.

2465 Schwertmann, U. and Taylor, R.M., 1987. Iron oxides. In: J.B. Dixon and S.B. Weed (Editors),
2466 Minerals in Soil Environments, 2nd ed. Soil Science Society of America, Madison.

2467 Schwertmann, U.C., R.M., 1991. Iron Oxides in the Laboratory: Preparation and
2468 Characterization. VCH, Weinheim, 137 pp.

2469 Sedwick, P., Sholkovitz, E.R. and Church, T., 2007. Impact of anthropogenic combustion
2470 emissions on the fractional solubility of aerosol iron: Evidence from the Sargasso Sea.
2471 Geochemistry Geophysics Geosystems, 8(10): Q10Q06.

2472 Sedwick, P.N., Bowie, A.R. and Trull, T.W., 2008. Dissolved iron in the Australian sector of the
2473 Southern Ocean (CLIVAR SR3 section): Meridional and seasonal trends. Deep-Sea
2474 Research Part I-Oceanographic Research Papers, 55(8): 911-925.

2475 Sedwick, P.N., Church, T.M., Bowie, A.R., Marsay, C.M., Ussher, S.J., Achilles, K.M., Lethaby,
2476 P.J., Johnson, R.J., Sarin, M.M. and McGillicuddy, D.J., 2005. Iron in the Sargasso Sea
2477 (Bermuda Atlantic Time-series Study region) during summer: Eolian imprint,

2478 spatiotemporal variability, and ecological implications. *Global Biogeochemical Cycles*,
2479 19(4): GB4006.

2480 Shao, Y. and Raupach, M.R., 1993. Effect of saltation bombardment on the entrainment of dust
2481 by wind. *Journal Of Geophysical Research-Atmospheres*, 98(D7): 12719-12726.

2482 Shao, Y.P., Leys, J.F., McTainsh, G.H. and Tews, K., 2007. Numerical simulation of the October
2483 2002 dust event in Australia. *Journal Of Geophysical Research-Atmospheres*, 112:
2484 D08207.

2485 Shaw, E.C., Gabric, A.J. and McTainsh, G.H., 2008. Impacts of aeolian dust deposition on
2486 phytoplankton dynamics in Queensland coastal waters. *Marine and Freshwater Research*,
2487 59(11): 951-962.

2488 [Schepanski, K., I. Tegen, M. C. Todd, B. Heinold, G. Bönisch, B. Laurent, and A. Macke,](#)
2489 [2009. Meteorological processes forcing Saharan dust emission inferred from MSG-](#)
2490 [SEVIRI observations of subdaily dust source activation and numerical models, *J.*](#)
2491 [Geophys. Res., 114, D10201, doi:10.1029/2008JD010325.](#)

2492 [Schepanski, K., I. Tegen, B. Laurent, B. Heinold, and A. Macke, 2007, A new Saharan dust](#)
2493 [source activation frequency map derived from MSG-SEVIRI IRchannels, *Geophys. Res.*](#)
2494 [Lett., 34, L18803, doi:10.1029/2007GL030168.](#)

2495 Shigemitsu, M., Narita, H., Watanabe, Y.W., Harada, N. and Tsunogai, S., 2007. Ba, Si, U, Al,
2496 Sc, La, Th, C and C-13/C-12 in a sediment core in the western subarctic Pacific as
2497 proxies of past biological production. *Marine Chemistry*, 106(3-4): 442-455.

Formatted: Font: Times New Roman, 12 pt

Formatted: Font: Times New Roman, 12 pt

Formatted: Font: Times New Roman, 12 pt

Formatted: Font: Times New Roman, 12 pt

Formatted: Font: Times New Roman, 12 pt

2498 Shin, S.I., Liu, Z., Otto-Bliesner, B., Brady, E.C., Kutzbach, J.E. and Harrison, S.P., 2003. A
2499 simulation of the last glacial maximum climate using the NCAR-CCSM. *Climate*
2500 *Dynamics*, 20(2-3): 127-151.

2501 Siegenthaler, U., Monnin, E., Kawamura, K., Spahni, R., Schwander, J., Stauffer, B., Stocker,
2502 T.F., Barnola, J.M. and Fischer, H., 2005. Supporting evidence from the EPICA
2503 Dronning Maud Land ice core for atmospheric CO₂ changes during the past millennium.
2504 *Tellus Series B-Chemical and Physical Meteorology*, 57(1): 51-57.

2505 Sokolik, I.N. and Toon, O.B., 1996. Direct radiative forcing by anthropogenic airborne mineral
2506 aerosols. *Nature*, 381(6584): 681-683.

2507 Sokolik, I.N. and Toon, O.B., 1999. Incorporation of mineralogical composition into models of
2508 the radiative properties of mineral aerosol from UV to IR wavelengths. *Journal of*
2509 *Geophysical Research-Atmospheres*, 104(D8): 9423-9444.

2510 Sow, M., Alfaro, S.C., Rajot, J.L. and Marticorena, B., 2009. Size resolved dust emission fluxes
2511 measured in Niger during 3 dust storms of the AMMA experiment. *Atmospheric*
2512 *Chemistry and Physics*, 9(12): 3881-3891.

2513 Spokes, L.J., Jickells, T.D. and Lim, B., 1994. Solubilization of Aerosol Trace-Metals by Cloud
2514 Processing - a Laboratory Study. *Geochimica Et Cosmochimica Acta*, 58(15): 3281-
2515 3287.

2516 Spracklen, D.V., Carslaw, K.S., Kulmala, M., Kerminen, V.M., Sihto, S.L., Riipinen, I.,
2517 Merikanto, J., Mann, G.W., Chipperfield, M.P., Wiedensohler, A., Birmili, W. and

2518 Lihavainen, H., 2008. Contribution of particle formation to global cloud condensation
2519 nuclei concentrations. *Geophysical Research Letters*, 35(6): 5.

2520 Stancin, A.M., Gleason, J.D., Hovan, S.A., Rea, D.K., Owen, R.M., Moore, T.C., Hall, C.M. and
2521 Blum, J.D., 2008. Miocene to recent eolian dust record from the Southwest Pacific Ocean
2522 at 40 degrees S latitude. *Palaeogeography Palaeoclimatology Palaeoecology*, 261(3-4):
2523 218-233.

2524 Stancin, A.M., Gleason, J.D., Rea, D.K., Owen, R.M., Moore, T.C., Blum, J.D. and Hovan, S.A.,
2525 2006. Radiogenic isotopic mapping of late Cenozoic eolian and hemipelagic sediment
2526 distribution in the east-central Pacific. *Earth And Planetary Science Letters*, 248(3-4):
2527 840-850.

2528 Steffensen, J.P., 1985. Microparticles in snow from the South Greenland Ice Sheet. *Tellus Series*
2529 *B-Chemical and Physical Meteorology*, 37(4-5): 286-295.

2530 Steffensen, J.P., 1997. The size distribution of microparticles from selected segments of the
2531 Greenland Ice Core Project ice core representing different climatic periods. *Journal of*
2532 *Geophysical Research-Oceans*, 102(C12): 26755-26763.

2533 Stuut, J.B.W. and Lamy, F., 2004. Climate variability at the southern boundaries of the Namib
2534 (Southwestern Africa) and Atacama (northern Chile) coastal deserts during the last
2535 120,000 yr. *Quaternary Research*, 62(3): 301-309.

2536 Sugden, D.E., McCulloch, R.D., Bory, A.J.M. and Hein, A.S., 2009. Influence of Patagonian
2537 glaciers on Antarctic dust deposition during the last glacial period. *Nature Geoscience*,
2538 2(4): 281-285.

2539 Summerell, G.K., Dowling, T.I., Richardson, D.P., Walker, J. and Lees, B., 2000. Modelling
2540 current parna distribution in a local area. Australian Journal of Soil Research, 38(4): 867-
2541 878.

2542 Sun, Y.B., Tada, R.J., Chen, J.C., Liu, Q.S., Toyoda, S., Tani, A., Ji, J.F. and Isozaki, Y., 2008.
2543 Tracing the provenance of fine-grained dust deposited on the central Chinese Loess
2544 Plateau. Geophysical Research Letters, 35(1): L01804.

2545 Svensson, A., Biscaye, P.E. and Grousset, F.E., 2000. Characterization of late glacial continental
2546 dust in the Greenland Ice Core Project ice core. Journal Of Geophysical Research-
2547 Atmospheres, 105(D4): 4637-4656.

2548 Sviridenkov, M.A., Gillette, D.A., Isakov, A.A., Sokolik, I.N., Smirnov, V.V., Belan, B.D.,
2549 Pachenko, M.V., Andronova, A.V., Kolomiets, S.M., Zhukov, V.M. and Zhukovsky,
2550 D.A., 1993. Size distributions of dust aerosol measured during the Soviet-American
2551 experiment in Tajikistan, 1989. Atmospheric Environment Part a-General Topics, 27(16):
2552 2481-2486.

2553 Swap, R., Garstang, M., Greco, S., Talbot, R. and Kallberg, P., 1992. Saharan Dust in the
2554 Amazon Basin. Tellus Series B: Chemical and Physical Meteorology, 44(2): 133-149.

2555 Tagliabue, A., Bopp, L. and Aumont, O., 2009. Evaluating the importance of atmospheric and
2556 sedimentary iron sources to Southern Ocean biogeochemistry. Geophysical Research
2557 Letters, 36: L13601.

2558 Tanaka, T.Y. and Chiba, M., 2006. A numerical study of the contributions of dust source regions
2559 to the global dust budget. Global And Planetary Change, 52(1-4): 88-104.

2560 Taylor, R.M., McKenzie, R.M., Fordham, A.W. and Gillman, G.P., 1983. Oxide minerals. In:
2561 A.E. Martin (Editor), Soils: an Australian viewpoint. CSIRO/Academic Press,
2562 Melbourne/London, pp. 309-334.

2563 Tegen, I. and Fung, I., 1995. Contribution To The Atmospheric Mineral Aerosol Load From
2564 Land-Surface Modification. *Journal Of Geophysical Research-Atmospheres*, 100(D9):
2565 18707-18726.

2566 Tegen, I., Harrison, S.P., Kohfeld, K., Prentice, I.C., Coe, M. and Heimann, M., 2002. Impact of
2567 vegetation and preferential source areas on global dust aerosol: Results from a model
2568 study. *Journal Of Geophysical Research-Atmospheres*, 107(D21): D4576.

2569 Tegen, I., Werner, M., Harrison, S.P. and Kohfeld, K.E., 2004. Relative importance of climate
2570 and land use in determining present and future global soil dust emission. *Geophysical
2571 Research Letters*, 31(5): L05105.

2572 Textor, C., Schulz, M., Guibert, S., Kinne, S., Balkanski, Y., Bauer, S., Bernsten, T., Berglen, T.,
2573 Boucher, O., Chin, M., Dentener, F., Diehl, T., Easter, R., Feichter, H., Fillmore, D.,
2574 Ghan, S., Ginoux, P., Gong, S., Kristjansson, J.E., Krol, M., Lauer, A., Lamarque, J.F.,
2575 Liu, X., Montanaro, V., Myhre, G., Penner, J., Pitari, G., Reddy, S., Seland, O., Stier, P.,
2576 Takemura, T. and Tie, X., 2006. Analysis and quantification of the diversities of aerosol
2577 life cycles within AeroCom. *Atmospheric Chemistry and Physics*, 6: 1777-1813.

2578 Thompson, R. and Maher, B.A., 1995. Age models, sediment fluxes and paleoclimatic
2579 reconstructions for the Chinese loess and paleosol sequences. *Geophysical Journal
2580 International*, 123(2): 611-622.

2581 Toggweiler, J.R., Russell, J.L. and Carson, S.R., 2006. Midlatitude westerlies, atmospheric CO₂,
2582 and climate change during the ice ages. *Paleoceanography*, 21(2).

2583 Torii, M., Lee, T.Q., Fukuma, K., Mishima, T., Yamazaki, T., Oda, H. and Ishikawa, N., 2001.
2584 Mineral magnetic study of the Taklimakan desert sands and its relevance to the Chinese
2585 loess. *Geophysical Journal International*, 146(2): 416-424.

2586 Tsuda, A., Takeda, S., Saito, H., Nishioka, J., Nojiri, Y., Kudo, I., Kiyosawa, H., Shiimoto, A.,
2587 Imai, K., Ono, T., Shimamoto, A., Tsumune, D., Yoshimura, T., Aono, T., Hinuma, A.,
2588 Kinugasa, M., Suzuki, K., Sohrin, Y., Noiri, Y., Tani, H., Deguchi, Y., Tsurushima, N.,
2589 Ogawa, H., Fukami, K., Kuma, K. and Saino, T., 2003. A mesoscale iron enrichment in
2590 the western Subarctic Pacific induces a large centric diatom bloom. *Science*, 300(5621):
2591 958-961.

2592 Uematsu, M., Duce, R.A., Prospero, J.M., Chen, L., Merrill, J.T. and McDonald, R.L., 1983.
2593 Transport of mineral aerosol from Asia over the north Pacific Ocean. *Journal of*
2594 *Geophysical Research-Oceans and Atmospheres*, 88(NC9): 5343-5352.

2595 Uematsu, M., Wang, Z.F. and Uno, I., 2003. Atmospheric input of mineral dust to the western
2596 North Pacific region based on direct measurements and a regional chemical transport
2597 model. *Geophysical Research Letters*, 30(6): L1342.

2598 VanCuren, R.A. and Cahill, T.A., 2002. Asian aerosols in North America: Frequency and
2599 concentration of fine dust. *Journal of Geophysical Research-Atmospheres*, 107(D24):
2600 D4804.

2601 Visser, F., Gerringa, L.J.A., Van der Gaast, S.J., de Baar, H.J.W. and Timmermans, K.R., 2003.
2602 The role of the reactivity and content of iron of aerosol dust on growth rates of two
2603 Antarctic diatom species. *Journal of Phycology*, 39(6): 1085-1094.

2604 Wagenbach, D. and Geis, K., 1987. The mineral dust record in a high-altitude alpine glacier
2605 (Colle-Gnifetti, Swiss Alps). In: M. Leinen and M. Sarnthein (Editors), *Nato Advanced*
2606 *Research Workshop on Paleoclimatology and Paleometeorology : Modern and Past*
2607 *Patterns of Global Atmospheric Transport*. Kluwer Academic Publ, Oracle, Az, pp. 543-
2608 564.

2609 Wagener, T., Losno, R., Bonnet, S. and Mahowald, N., 2008. Revisiting atmospheric dust export
2610 to the South Hemisphere ocean. *Global Biogeochemical Cycles*, 22(2): GB2006.

2611 Wake, C.P., Mayewski, P.A., Li, Z., Han, J. and Qin, D., 1994. Modern eolian dust deposition in
2612 Central-Asia. *Tellus Series B-Chemical and Physical Meteorology*, 46(3): 220-233.

2613 Walter, H.J., Hegner, E., Diekmann, B., Kuhn, G. and van der Loeff, M.M.R., 2000. Provenance
2614 and transport of terrigenous sediment in the South Atlantic Ocean and their relations to
2615 glacial and interglacial cycles: Nd and Sr isotopic evidence. *Geochimica Et*
2616 *Cosmochimica Acta*, 64(22): 3813-3827.

2617 Wang, H., Mason, J.A. and Balsam, W.L., 2006a. The importance of both geological and
2618 pedological processes in control of grain size and sedimentation rates in Peoria Loess.
2619 *Geoderma*, 136(1-2): 388-400.

2620 Wang, T., Ta, W.Q. and Liu, L.C., 2007. Dust emission from desertified lands in the Heihe River
2621 Basin, Northwest China. *Environmental Geology*, 51(8): 1341-1347.

2622 Wang, X.M., Zhou, Z.J. and Dong, Z.B., 2006b. Control of dust emissions by geomorphic
2623 conditions, wind environments and land use in northern China: An examination based on
2624 dust storm frequency from 1960 to 2003. *Geomorphology*, 81(3-4): 292-308.

2625 Wang, Y.Q., Zhang, X.Y. and Arimoto, R., 2006c. The contribution from distant dust sources to
2626 the atmospheric particulate matter loadings at XiAn, China during spring. *Science of the*
2627 *Total Environment*, 368(2-3): 875-883.

2628 Warren, A., Chappell, A., Todd, M. C., Bristow, C., Drake, N., Engelstaedter, S., Martins, V.,
2629 M'baïnayel, S. and Washington, R., 2007. Dust-raising in the dustiest place on earth,
2630 *Geomorphology*, 92, 25-37.

2631 Washington, R., Todd, M., Middleton, N.J. and Goudie, A.S., 2003. Dust-storm source areas
2632 determined by the total ozone monitoring spectrometer and surface observations. *Annals*
2633 *Of The Association Of American Geographers*, 93(2): 297-313.

2635 Washington, R. and Todd, M.C., 2005. Atmospheric controls on mineral dust emission from the
2636 Bodele Depression, Chad: The role of the low level jet. *Geophysical Research Letters*,
2637 32(17): L17701.

2638 Washington, R., Todd, M.C., Lizcano, G., Tegen, I., Flamant, C., Koren, I., Ginoux, P.,
2639 Engelstaedter, S., Bristow, C.S., Zender, C.S., Goudie, A.S., Warren, A. and Prospero,
2640 J.M., 2006. Links between topography, wind, deflation, lakes and dust: The case of the
2641 Bodele Depression, Chad. *Geophysical Research Letters*, 33(9): L09401.

2642 Watkins, S.J., Maher, B.A. and Bigg, G.R., 2007. Ocean circulation at the Last Glacial
2643 Maximum: A combined modeling and magnetic proxy-based study. *Paleoceanography*,
2644 22(2): PA2204.

2645 Watson, A.J., Bakker, D.C.E., Ridgwell, A.J., Boyd, P.W. and Law, C.S., 2000. Effect of iron
2646 supply on Southern Ocean CO₂ uptake and implications for glacial atmospheric CO₂.
2647 *Nature*, 407(6805): 730-733.

2648 Watson, A.J. and Garabato, A.C.N., 2006. The role of Southern Ocean mixing and upwelling in
2649 glacial-interglacial atmospheric CO₂ change. *Tellus Series B-Chemical and Physical*
2650 *Meteorology*, 58(1): 73-87.

2651 Werner, M., Tegen, I., Harrison, S.P., Kohfeld, K.E., Prentice, I.C., Balkanski, Y., Rodhe, H. and
2652 Roelandt, C., 2002. Seasonal and interannual variability of the mineral dust cycle under
2653 present and glacial climate conditions. *Journal of Geophysical Research-Atmospheres*,
2654 107(D24): 4744.

2655 Williams, E.R., 2008. Comment on "Atmospheric controls on the annual cycle of North African
2656 dust" by S. Engelstaedter and R. Washington. *Journal of Geophysical Research-*
2657 *Atmospheres*, 113(D23): D23109.

2658 Winckler, G., Anderson, R.F., McGee, D., Fleisher, M.Q. and Mahowald, N., 2008. Half a
2659 million years of coherent dust flux variations in the tropical Pacific and Antarctica, 8th
2660 Annual V M Goldschmidt Conference. Pergamon-Elsevier Science Ltd, Vancouver,
2661 CANADA, pp. A1026-A1026.

2662 Wolff, E.W., Fischer, H., Fundel, F., Ruth, U., Twarloh, B., Littot, G.C., Mulvaney, R.,
2663 Rothlisberger, R., de Angelis, M., Boutron, C.F., Hansson, M., Jonsell, U., Hutterli,
2664 M.A., Lambert, F., Kaufmann, P., Stauffer, B., Stocker, T.F., Steffensen, J.P., Bigler, M.,
2665 Siggaard-Andersen, M.L., Udisti, R., Becagli, S., Castellano, E., Severi, M., Wagenbach,
2666 D., Barbante, C., Gabrielli, P. and Gaspari, V., 2006. Southern Ocean sea-ice extent,
2667 productivity and iron flux over the past eight glacial cycles. *Nature*, 440(7083): 491-496.

2668 Xiao, J., Porter, S.C., An, Z.S., Kumai, H. and Yoshikawa, S., 1995. Grain-size of quartz as an
2669 indicator of winter monsoon strength on the loess plateau of central China during the last
2670 130,000-yr. *Quaternary Research*, 43(1): 22-29.

2671 Xiao, J.L., An, Z.S., Liu, T.S., Inouchi, Y., Kumai, H., Yoshikawa, S. and Kondo, Y., 1999. East
2672 Asian monsoon variation during the last 130,000 Years: evidence from the Loess Plateau
2673 of central China and Lake Biwa of Japan. *Quaternary Science Reviews*, 18(1): 147-157.

2674 Yoshioka, M., Mahowald, N., Dufresne, J.L. and Luo, C., 2005. Simulation of absorbing aerosol
2675 indices for African dust. *Journal Of Geophysical Research-Atmospheres*, 110(D18): 22.

2676 Yung, Y.L., Lee, T., Wang, C.H. and Shieh, Y.T. 1996. Dust: A diagnostic of the hydrologic
2677 cycle during the Last Glacial Maximum. *Science*, 271, 962-963, DOI:10.1126/ science.
2678 271.5251.962.

2679 Zarate, M.A., 2003. Loess of southern South America. *Quaternary Science Reviews*, 22(18-19):
2680 1987-2006.

2681 Zender, C.S., Bian, H.S. and Newman, D., 2003. Mineral Dust Entrainment and Deposition
2682 (DEAD) model: Description and 1990s dust climatology. *Journal of Geophysical*
2683 *Research-Atmospheres*, 108(D14): D4416.

2684 Zender, C.S., Miller, R.L. and Tegen, I., 2005. Quantifying Mineral Dust Mass Budgets:
2685 Terminology, Constraints, and Current Estimates. *Eos*, 85(48): 509-512.

2686 Zhang, D.Z. and Iwasaka, Y., 2004. Size change of Asian dust particles caused by sea salt
2687 interaction: Measurements in southwestern Japan. *Geophysical Research Letters*, 31(15):
2688 L15102.

2689 Zhang, J.Y., Wang, P.X., Li, Q.Y., Cheng, X.R., Jin, H.Y. and Zhang, S.Y., 2007. Western
2690 equatorial Pacific productivity and carbonate dissolution over the last 550 kyr:
2691 Foraminiferal and nannofossil evidence from ODP Hole 807A. *Marine*
2692 *Micropaleontology*, 64(3-4): 121-140.

2693 Zhang, X.Y., Arimoto, R. and An, Z.S., 1999. Glacial and interglacial patterns for Asian dust
2694 transport. *Quaternary Science Reviews*, 18(6): 811-819.

2695 Zhang, X.Y., Lu, H.Y., Arimoto, R. and Gong, S.L., 2002. Atmospheric dust loadings and their
2696 relationship to rapid oscillations of the Asian winter monsoon climate: two 250-kyr loess
2697 records. *Earth And Planetary Science Letters*, 202(3-4): 637-643.

2698 Zhao, T.L., Gong, S.L., Zhang, X.Y. and McKendry, I.G., 2003. Modelled size-segregated wet
2699 and dry deposition budgets of soil dust aerosol during ACE-Asia 2001: Implications for
2700 trans-Pacific transport. *Journal of Geophysical Research-Atmospheres*, 108(D23): 8665.

2701 Zhu, A., Ramanathan, V., Li, F. and Kim, D., 2007. Dust plumes over the Pacific, Indian, and
2702 Atlantic oceans: Climatology and radiative impact. *Journal Of Geophysical Research-*
2703 *Atmospheres*, 112(D16): 20.

2704 Ziegler, C.L., Murray, R.W., Hovan, S.A. and Rea, D.K., 2007. Resolving eolian, volcanogenic,
2705 and authigenic components in pelagic sediment from the Pacific Ocean. *Earth and*
2706 *Planetary Science Letters*, 254(3-4): 416-432.

2707 Ziegler, C.L., Murray, R.W., Plank, T. and Hemming, S.R., 2008. Sources of Fe to the equatorial
2708 Pacific Ocean from the Holocene to Miocene. *Earth and Planetary Science Letters*,
2709 270(3-4): 258-270.

2710 Zielinski, G.A., Mayewski, P.A., Meeker, L.D., Whitlow, S. and Twickler, M.S., 1996. A
2711 110,000-yr record of explosive volcanism from the GISP2 (Greenland) ice core.
2712 *Quaternary Research*, 45(2): 109-118.

2713

2714

2715 Figure captions.

2716 Figure 1. Schematic of the hypothetical glacial dust-atmospheric CO₂-climate feedback system.
2717 Different components of the Earth system can directly interact in three possible ways: positive
2718 influences (an increase in one component resulting directly in an increase in a second
2719 component) are indicated by red arrows; negative influences are indicated by black arrows; or no
2720 influence. An even number (including zero) of negative influences within any given closed loop
2721 give rise to a positive feedback, operation of which tends to amplify any initial perturbation (e.g.
2722 the ice-albedo feedback). An odd number of negative influences gives rise to a negative
2723 feedback, which tends to dampen any perturbation. Primary interactions are indicated by solid
2724 lines, additional interactions dotted lines. Four main (positive) dust-atmospheric CO₂-climate
2725 feedback loops exist in this system. 1. Dust supply → ocean export production → xCO₂ →
2726 temperature → ice volume → sea level → dust supply (four negative interactions). 2. Dust
2727 supply → ocean export production → xCO₂ → temperature → hydrological cycle → vegetation
2728 → dust supply (two negative interactions). 3. Dust supply → ocean export production → xCO₂
2729 → temperature → hydrological cycle → dust supply (two negative interactions). 4. Dust supply
2730 → ocean export production → xCO₂ → temperature → ice volume → dust supply (two negative
2731 interactions). From Ridgwell, 2002.

2732

2733 Figure 2. Dust deflation and entrainment processes (modified from Pye, 1987).

2734

2735 Figure 3. a) Remotely sensed aerosol optical depth measurements (Husar et al., 1997); b) The
2736 global distribution of major dust sources and dust transport paths based on the Total Ozone
2737 Mapping Satellite (TOMS) absorbing aerosol index (AAI) (Prospero et al., 2002). The figure is a
2738 composite of monthly mean TOMS AAI frequency of occurrence distributions computed using a
2739 threshold of 1.0 in the North Africa – Middle East – Asian dust belt and 0.7 everywhere else.
2740 The arrows show the main transport paths over the oceans. The arrow size is not indicative of the
2741 magnitude of the transport nor the distance that dust is carried. Some major points of note:

2742 During the late boreal spring, summer and fall, huge quantities of African dust are carried
2743 to the western Atlantic and into the Caribbean and the eastern United States; also, from sources
2744 in the Arabian Peninsula and southwest Asia to the Arabian Sea and Indian Ocean. Dust is also
2745 carried across the Mediterranean to Europe and the Middle East.

2746 Over the Atlantic during the boreal winter and early spring, dust from the Sahara and the
2747 Sahel is carried to South America; large quantities are also carried on occasion to the mid-
2748 latitude Atlantic and into Europe, as indicated by the north-looping arrow.

2749 The large arrow in the North Pacific shows the main direction of large dust storms carried
2750 from Asia every boreal spring, in some cases penetrating to North America; the dust originates
2751 from a variety of sources including arid regions in Inner Mongolia (cross-hatched area) which do
2752 not show up well in the TOMS product.

2753 The dust sources in the Southern Hemisphere are considerably smaller and less active
2754 than those in the Northern Hemisphere. The most active are those in Argentina, southern Africa
2755 and Australia.

2756

2757 Figure 4. a) Normalised size distributions of dust measured on Tenerife, Canary Islands (July,
2758 1995) and in Puerto Rico (July, 2000) using the identical instrument, a TSI APS 3310. The
2759 Tenerife site is ~ 300 km from the N. African coast while Puerto Rico is 5000 km to the west.

2760 The transit time for dust outbreaks is about 5 – 7 days; b) wind tunnel data (Alfaro et al., 1997)
2761 indicating smaller modal particle sizes entrained and transported at higher wind speeds.

2762
2763 Figure 5. Effect of the mass median diameter on dust deposition flux and on optical depth of the
2764 particle size distribution. Optical depth expresses the amount of radiation removed by scattering
2765 or absorption. Values are normalized to a size distribution with a mass median diameter of 4.5
2766 μm and a sigma value of 2.1 (Reid et al., 2003, Table 1). A log-normal distribution with a
2767 constant width is assumed (Balkanski et al., 2007).

2768
2769 Figure 6. Transmission electron micrographs of discrete, pedogenic ‘free iron’ grains, a)
2770 typically acicular particles of goethite (αFeOOH), scale bar = 200 nm, b) more equidimensional
2771 particles of haematite ($\alpha\text{Fe}_2\text{O}_3$) - the smaller, electron-opaque particles -, essentially
2772 unassociated with the larger, clean flakes of kaolinite, scale bar = 1 μm ; c) ultrafine haematite
2773 crystallite, soil sample, Morocco, scale bar = 100 nm. Micrographs from Maher et al. (2003),
2774 Jones (in Schwertmann, 1991), and Lieke (pers. comm.), respectively.

2775
2776 Figure 7. a) Atmospheric warming from absorption of radiation by dust; b) resultant net surface
2777 cooling. Integration of satellite and ground-based data for 2002 (from Chung et al., 2005).

2778
2779 Figure 8. Changes in glacial/interglacial dust concentrations over a pole-to-pole transect,
2780 spanning Greenland (the NGRIP ice core record, dust mass, ppm/10, Ruth, 2005, Svensson et al.,
2781 2000), the northern North Atlantic (Core T88, 48.3 °N, 25.0°W, high-field magnetic dust proxy,
2782 Maher, unpub. data), equatorial Atlantic (ODP Site 633A, 1.28 °N, 11.98 °W, terrigenous %,
2783 deMenocal et al., 1993) and Antarctica (EPICA Dome C, dust mass, EPICA Community
2784 members, 2004).

2785
2786 Figure 9. a) Measured aeolian MARs for the present day (for MAR data, see Appendix 1, and for
2787 MARs, age, site and quality control data, see the updated ‘DIRTMAP3’ database (Maher and
2788 Kohfeld, 2009, http://www.lec.lancs.ac.uk/research/LU_themes/inqua_working_group.php); b)
2789 modelled LGM MARs (Mahowald et al., 2006).

2790
2791 Figure 10. a) Measured aeolian MARs for the LGM (for MAR data, see Appendix 1, and for
2792 MARs, age, site and quality control data, see the updated ‘DIRTMAP3’ database (Maher and
2793 Kohfeld, 2009, http://www.lec.lancs.ac.uk/research/LU_themes/inqua_working_group.php); b)
2794 modelled LGM MARs (Mahowald et al., 2006 and Mahowald, pers. comm).

2795
2796 Figure 11. Typically trimodal particle size distribution of Chinese loess (Wang et al., 2007).

2797
2798 Figure 12. Time series of North Greenland Ice core Project (NGRIP) and Chinese loess data,
2799 synchronized on the NGRIP SS09 age scale (Ruth et al., 2003). Ice core data: $\delta^{18}\text{O}$, dust mass
2800 and mean particle size (diameter, lognormal mode of volume distribution); loess data: quartz
2801 mean diameter, from the central Loess Plateau site, Luochuan (Xiao et al., 1999).

2802
2803 Figure 13. Particle size records for the mid-latitude Pacific over several glacial-interglacial
2804 stages (redrawn from Hovan et al., 1991 and Zhang et al., 2007; ‘v’ in panel 3 = volcanic ash).

2805

2806 Figure 14. Time series of dust flux to the central equatorial Pacific (TTN013-PC72; 0.1°N,
2807 139.4°W) and to the EPICA Dome C Antarctic ice core (from Winckler et al., 2008).
2808
2809 Figure 15. Dust fluxes at the Vostok and EPICA Dome C Antarctic ice cores (redrawn from
2810 Lambert et al., 2008).
2811
2812 Figure 16. The sectors of the Southern Ocean, together with the frontal system of the Antarctic
2813 Circumpolar Current, and the locations of the deep sea sediment and Antarctic ice cores referred
2814 to here (modified from Diekmann, 2007).
2815
2816 Figure 17. Isotopic characterization (Nd:Sr) of Antarctic dusts and suite of potential source
2817 areas, a) as reported for < 5µm potential source samples (Delmonte et al., 2004), and b) a
2818 refinement of plot a; progress definition of the Patagonian isotopic signature and inclusion of
2819 new samples from Australia (Revel-Rolland et al., 2006) and the Puna/Altiplano of South
2820 America (Gaiero, 2007; Delmonte et al., 2009) to explain the non-Patagonian isotopic signature
2821 found in the Antarctic dust.
2822
2823 Figure 18. Comparison of the Southern Ocean and Antarctic ice core records over the last 1.1Ma.
2824 (a) Temperature reconstruction from EPICA ice cores (black) (Jouzel et al., 2007) and alkenone-
2825 based SST from site PS2489-2/ODP1090 (red). Marine Isotope Stages (MIS) are shown for
2826 reference. (b) Atmospheric CO₂ concentrations from the EPICA ice cores. Dashed line indicates
2827 the CO₂ level when productivity starts to increase above the average interglacial value. Filled
2828 area illustrates CO₂ concentrations below 230 ppmv. Glacial terminations are shown for
2829 reference. (c) EPICA Fe flux (blue) and site PS2489-2/ODP1090 Fe flux (red). (d) EPICA
2830 Insoluble dust (light brown) and site PS2489-2/ODP1090 long-chain odd carbon-numbered n-
2831 alkanes (C25-35) mass accumulation rate (MAR) (blue). (e) Site PS2489-2/ODP1090 C37
2832 alkenones MAR (green) and TOC MAR (Diekmann and Kuhn, 2002) (black). Shaded areas
2833 highlight the high-productivity intervals, when alkenone MARs are 3 x the average interglacial
2834 value. (Redrawn from Martinez-Garcia et al., 2009).
2835
2836 Figure 19. Time series of proxy records for palaeo-productivity and dust flux for the equatorial
2837 Pacific through several glacial-interglacial cycles (Redrawn from Anderson et al., 2008).

2838 Figure 20. ²³⁰Th-normalised fluxes of biogenic opal in the three sectors of the Southern Ocean
2839 (from Diekmann, 2007).

2840 Figure 21. a) Global δ¹⁸O stack (Lisiecki & Raymo, 2005) versus n-alkanes concentrations from
2841 Southern Ocean site PS2489-2/ODP1090; marine isotope stages shown; b) Temperature
2842 reconstruction from EPICA ice cores (Jouzel et al., 2007) and alkenone-based SSTs from
2843 PS2489-2/ODP1090; c) atmospheric CO₂ concentration from the EPICA ice cores (Luthi et al.,
2844 2008; Petit et al., 1999; Siegenthaler et al., 2005) versus alkenones concentration, PS2489-
2845 2/ODP1090.
2846
2847 Figure 22. Schematic of the sources, process and impacts of dust on climate, a) at the present
2848 day, and b) at the LGM, with key gaps in data and understanding marked by ‘?’ on the diagrams.
2849
2850

2851 Table captions.

2852

2853 Table 1. Comparison of a range of modelled present day dust fluxes (mean annual, by region).
2854 The unit is Tg/yr, numbers in brackets = the % of the annual mean global emission flux. (From
2855 Tanaka & Chiba, 2006).

2856

2857

2858

2859

